

**CORRELATING MECHANICAL PROPERTIES OF  
CANCELLOUS BONE IN THE RAT WITH VARIOUS  
DENSITY MEASURES**

A Thesis

by

**RAMYA RAMASWAMY**

Submitted to the Office of Graduate Studies of  
Texas A&M University  
in partial fulfillment of the requirements for the degree of

**MASTER OF SCIENCE**

December 2003

Major Subject: Mechanical Engineering

**CORRELATING MECHANICAL PROPERTIES OF  
CANCELLOUS BONE IN THE RAT WITH VARIOUS  
DENSITY MEASURES**

A Thesis

by

RAMYA RAMASWAMY

Submitted to the Texas A&M University  
in partial fulfillment of the requirements  
for the degree of

MASTER OF SCIENCE

Approved as to style and content by:

---

Harry A. Hogan  
(Chair of Committee)

---

Susan A. Bloomfield  
(Member)

---

Arun Srinivasa  
(Member)

---

Dennis L. O'Neal  
(Interim Head of Department)

December 2003

Major Subject: Mechanical Engineering

## ABSTRACT

Correlating Mechanical Properties of Cancellous Bone in the Rat with Various Density Measures. (December 2003)

Ramya Ramaswamy, B.E. Bharathiyar University

Chair of Advisory Committee: Dr. Harry A. Hogan

This study focussed on the reduced platen compression (RPC) testing of the cancellous bone of the proximal tibia. The objective of this study was to improve the current testing methods with an emphasis on the location of the RPC specimens, and to correlate the mechanical properties of the rodent cancellous bone with the various density measures. Analytical studies were made to assess the effect of the size and shape of the platen based on the values from mechanical testing of the cancellous bone.

RPC specimens are made from transverse slices of the proximal tibia metaphysis. Specimen location was determined using planar radiograph method at a distance of 1.75 mm distal to the growth plate. The distance from the top of the proximal tibia to the line at 1.75 mm distal to the growth plate was measured and this distance is termed as the first cut distance. Specimen thickness of 2 mm was then cut for the RPC test. Endocortical method was followed to determine the platen sizing for RPC testing. The cancellous bone was then tested in compression to failure.

Correlations were performed between the mechanical properties of the cancellous bone and the density measures from pQCT and radiographic techniques. SigmaStat and TableCurve 2D were used to perform the correlations and estimate the P value for the correlation. Linear and power law fits were made for all the correlations.

Based on this study, several improvements to the reduced platen compression test were recommended. An improved specimen location method was developed. However, it requires a corrective distance to account for the tissue that cannot be identified in the radiographic analysis. A new method for estimating the

density of the cancellous bone that is directly tested by the platen was developed. Correlations between the density of the cancellous bone and the mechanical properties show that, there is a strong correlation between ultimate stress and aluminum layer intensity. Elastic modulus correlates best with the last batch tested in this study. Recommendations for future study include advanced technology like finite element analysis and custom shaped platens to enhance RPC testing.

## TABLE OF CONTENTS

	Page
ABSTRACT .....	iii
TABLE OF CONTENTS .....	v
LIST OF FIGURES .....	vii
LIST OF TABLES .....	viii
 CHAPTER	
I INTRODUCTION .....	1
1.1 Motivation and Rationale .....	1
1.2 Objectives .....	3
II BACKGROUND .....	5
2.1 Bone Structure and Physiology .....	5
2.2 Mechanical Properties of Bone .....	10
2.3 Anatomy of the Tibia .....	11
2.4 Osteoporosis and Bone Density .....	13
2.5 Relevant Research on Bone Density Measurements .....	13
2.6 Relevant Research on Correlating Bone Density Measures and Mechanical Properties .....	15
III METHODS .....	21
3.1 Overview of the Experimental Design .....	21
3.2 Experimental Animals .....	21
3.3 Bone Removal and Preparation .....	22
3.4 Radiographs .....	23
3.5 RPC Specimen Preparation and Location Determination .....	23
3.6 Platen Sizing Using Image Analysis .....	26

CHAPTER	Page
3.7 Bone Density from pQCT .....	30
3.7 Bone Density from Specimen X - Rays .....	31
3.9 Compression Testing.....	35
3.10 Data Analysis .....	37
3.11 Correlation.....	38
IV RESULTS .....	40
4.1 Introduction .....	40
4.2 Specimen Location, Preparation and Platen Sizing .....	40
4.3 Reduced Platen Compression Test Mechanical Data.....	42
4.4 Radiography Technique Results.....	42
4.5 pQCT Density Results.....	50
4.6 Results from Correlations.....	50
V DISCUSSION .....	65
5.1 Introduction .....	65
5.2 Specimen Location.....	65
5.3 Radiography Technique .....	66
5.4 Correlations .....	67
VI CONCLUSIONS AND RECOMMENDATIONS .....	72
6.1 Conclusions .....	72
6.2 Recommendations .....	73
REFERENCES .....	75
APPENDIX I.....	80
APPENDIX II .....	83
VITA .....	114

## LIST OF FIGURES

FIGURE	Page
2.1 Cancellous and Cortical Bone (after Siegel, 1998).....	6
2.2 Rodent Tibia and Femur .....	7
2.3 Proximal Rodent Tibia.....	12
3.1 Specimen Location Based on Lateral Tubercle Landmarks (Rogers, 2002) .....	24
3.2 New Specimen Location Procedure.....	27
3.3 Specimen Location Showing Saw Blade Kerf.....	28
3.4 Radiograph of RPC Specimen .....	29
3.5 Image Analysis of RPC Specimen.....	32
3.6 Endocortical Circle of RPC Specimen.....	33
3.7 Endocortical Circle and Actual Tested Area (69%) .....	34
3.8 Reduced Platen Compression Test .....	36
4.1 Calibration Curve for Batch I .....	46
4.2 Calibration Curve for Batch II .....	47
4.3 Calibration Curve for Batch III.....	48
4.4 Calibration Curve for Batch IV .....	49
4.5 Correlation Curve for the Last Two Batches (Power Law) Ultimate Stress (MPa) vs. Average Intensity (Al. Layers) .....	59
4.6 Correlation Curve for the Last Two Batches (Power Law) Elastic Modulus (MPa) vs. Average Intensity (Al. Layers).....	60
4.7 Correlation Curve for the Last Two Batches (Power Law) Ultimate Stress (MPa) vs. Trabecular Density pQCT .....	61
4.8 Correlation Curve for the Last Two Batches (Power Law) Elastic Modulus (MPa) vs. Trabecular Density pQCT .....	62
4.9 Correlation Curve for the Last Two Batches, Platen Area Only (Power Law) Ultimate Stress (MPa) vs. Average Intensity (Al. Layers) .....	63
4.10 Correlation Curve for the Last Two Batches, Platen Area Only (Power Law) Elastic Modulus (MPa) vs. Average Intensity (Al. Layers) .....	64

## LIST OF TABLES

TABLE	Page
2.1 List of Correlations from Previous Compression Test Studies .....	20
3.1 Summary of Experimental Design for the Bone Muscle Recovery Study .....	22
4.1 Specimens of Each Tested Group in Respective Batches .....	41
4.2 Specimen Preparation Evaluation – Values Presented are Mean $\pm$ SD for Each Treatment Group of BMR Study .....	43
4.3 Based on the Testing Schedule Followed, Specimen Preparation Results for the Four Batches are Given Below. Values Presented are Mean $\pm$ SD.....	44
4.4 Results from Mechanical Testing - Reduced Platen Compression Test. Values Presented are Mean $\pm$ SD.....	44
4.5 Results from Radiographic Techniques. Values Presented are Mean $\pm$ SD with the Minimum and Maximum Values Included in Parenthesis.....	45
4.6 Results from Radiographic Techniques for Only the Platen Area, for the Batch III and Batch IV. Values Presented are Means $\pm$ SD for Each Batch.....	45
4.7 Results from pQCT for Bone Mineral Density (BMD) Values.....	50
4.8 List of $r_2$ Values and P Values for Correlation Between Average Intensity and Ultimate Stress (b = power law exponent) .....	54
4.9 List of $r_2$ Values and P Values for Correlation Between Average Intensity and Elastic Modulus (b = power law exponent).....	55
4.10 List of $r_2$ Values and P Values for Correlations Between pQCT - Trabecular Density and Ultimate Stress (b = power law exponent) .....	56
4.11 List of $r_2$ Values and P Values for Correlations Between pQCT - Trabecular Density and Elastic Modulus (b = power law exponent) .....	57
4.12 List of $r_2$ Values and P Values for Platen Area Only for Correlation Between Average Intensity and Ultimate Stress (b = power law exponent) .....	58
4.13 List of $r_2$ Values and P Values for Platen Area Only for Correlation Between Average Intensity and Elastic Modulus (b = power law exponent) .....	58



TABLE	Page
5.1 Ranges of Exponent b.....	70

# CHAPTER I

## INTRODUCTION

### 1.1 Motivation and Rationale

Bone is a vital, dynamic connective tissue, which has evolved to reflect a balance between its two major functions – provision of mechanical integrity for locomotion and protection, and involvement in the metabolic pathways associated with mineral homeostasis (Marcus et al., 1996). Principal responsibility of the skeleton is to support the loads and moments, which arise during activity, a responsibility that results in mechanical strain in the bone tissue. Structural function of the skeletal system is to provide support for the body against gravity and to act as a rigid lever system for muscular action. It also serves as a protective covering for internal organs. One of the primary metabolic functions of bone is its ability to serve as a repository for calcium which is necessary for nerve conduction, muscle contraction, clot formation and cell secretion (Weiss, 1983). Mechanical stresses associated with normal function plays an important role on the inherent architecture of the bone. There is a very high correlation between the trabecular alignment in bone and the principal stress directions that are estimated to occur during the normal skeletal function. Hence, the structure/function relationships coupled with its role in maintaining mineral homeostasis strongly suggest that bone is a system of optimum structural design. Bone strives towards an optimized structure, in that an individual's level of activity tunes the mass and morphology of the skeleton such that it is sufficient to withstand the extremes of functional loading, but not so much as to make transportation a functional liability.

Macroscopically, bone is classified into two types in a mature skeleton: cortical and cancellous bone. Cortical bone, also known as compact bone, is hard (porosity of 5%-10%) and is found largely in the shafts of the long bones, which

---

This thesis follows the style of the Journal of Biomechanics.

surround the marrow cavity. Cancellous, or spongy, bone is made up of a network of fine interlacing rod- and plate-like components called the trabeculae that enclose the cavities containing either the red or the fatty marrow. Cancellous bone (porosity 75%-90%) is found in the vertebrae, the majority of the flat bones, and in the ends of the long bones.

Traditional mechanical testing has long been used as a method for determining the mechanical properties of bone tissue (Engesaeter et al., 1978). Initially these studies were conducted to understand better the mechanisms of bone fracture and the loads at which these occur. In recent years, mechanical properties of the bones have been measured through a variety of testing procedures such as three-point bending, compression and torsion. The rat model has been used very frequently in recent times, owing to the ease and cost-effectiveness in acquiring and testing large number of animals. Hence, significant attention has been given to the testing of the whole bone properties of the femur and tibia of the rat, but most of these tests have been performed on the cortical shell rather than the cancellous core of the bones. Reduced platen compression (RPC) testing, a recently developed method of testing, utilizes reduced platen size so as to load only the cancellous core of the cross-sectional slices taken from the metaphysis of long bones such as the tibia and femur. Challenges with this test include selecting platens that test as much cancellous bone as possible without loading any cortical tissue. Also, appropriate specimen location in the bone must be selected so as to maximize the availability of cancellous bone (Rogers, 2002).

In addition to mechanical testing, many different density measures are characterized because the density of the bone plays a major role in determining its strength and other mechanical properties. It has been identified that the apparent density (mineralized bone mass/ bulk volume) and the ash apparent density (ash mass/ bulk volume) are reasonably effective predictors of bone strength and stiffness (Hernandez et al., 2001). These measurements were made on laboratory specimens, however, whereas clinically available density measures are much less direct parameters. The most widely available clinical bone density measure is the bone mineral density (BMD), as

determined by dual-energy X-ray absorptiometry (DEXA). In fact, BMD is used to screen patients for osteoporosis. Osteoporosis, one of the major diseases affecting over a million Americans today, is characterized by a reduction in the density of the bone. Osteoporosis is a serious concern because this reduced BMD predisposes to fractures that cause pain, disability and, occasionally, premature death (Cummings et al., 2002).

The National Institutes of Health (2000) defines osteoporosis as “a skeletal disorder characterized by compromised bone strength that results in an increased risk of fracture”. The operational definition is based on a commonly measured surrogate of bone strength – bone mineral density (BMD). A person with a spinal BMD T-score between -2.5 and -1.0 is classified as osteopenic, and a T-score less than -2.5 is classified as osteoporotic. Normal bone has a T-score higher than -1. T-score is the number of standard deviations from the mean (average) value. Reliance on BMD as an indicator of bone strength has deflected attention from size, shape, and internal structure of the bone, which are also major factors in determining the load bearing capacity and resistance to fracture of the bone. Nevertheless, at present, BMD measurement is the best surrogate clinical marker of bone properties, and considerable interest remains in investigating the relationships between density and mechanical properties.

## **1.2 Objectives**

The focus of this thesis is on the relationship between the mechanical properties of cancellous bone in the rat and various measures of bone density. Such studies have not been possible previously because of a lack of methods for measuring mechanical properties of cancellous bone in the rat. In this study, the recently developed reduced platen compression (RPC) test method will be used. The RPC test was first developed by Ruhmann (1998) and was further modified by Rogers (2002). Currently, density of the bone is measured in  $\text{mg}/\text{cm}^3$  using peripheral quantitative computed tomography (pQCT). Other density measures are also available, however, based upon x-rays that are made of RPC specimens. Comparing the mechanical properties of bone with the density measures gives us a better understanding and insight on what it means

functionally if a bone has high or low density. This thesis also aims at fine-tuning the RPC specimen location and cutting methods. A study by the National Space Biomedical Research Institute (NSBRI) is seeking to define the effect of prolonged exposure to microgravity on the skeletal system, and the animals from this study provide the source for bone specimens. One tibia from each animal was made available for this thesis research.

The objectives of this thesis can be summarized as:

1. To improve the current procedures for reduced platen compression testing of the proximal tibia of the rodent with an emphasis on specimen location.
2. To correlate the various density measures with the mechanical properties of rat cancellous bone using statistical methods.
3. To compare and evaluate the different density measures as predictors, or correlates, of mechanical properties.

## CHAPTER II

### BACKGROUND

#### 2.1 Bone Structure and Physiology

The human body consists of 206 bones, which are of all shapes and sizes. It is a connective tissue composed of cells, fiber and ground substance. This ground substance calcifies to form a rigid structure. Bone also serves as an attachment for muscles and ligaments, protects the vital organs of the thorax and the central nervous system, acts as a blood-forming organ and is a storehouse for calcium and phosphorus. On a micro-scale level, bone is a highly dynamic tissue, which continually adjusts to its physiological and mechanical environment by changing its composition and microscopic architecture (Martin et al., 1998).

The structure of bone is very similar to reinforced concrete that is used to make a building or a bridge. The steel rods that support the buildings are replaced by collagen fibers in the bone. The cement that surrounds and supports the rods is formed by minerals (including calcium and phosphorous) from the blood that crystallize and surround the rods. These minerals give the bones strength while the collagen rods provide resiliency. (Osteogenesis Imperfecta Foundation)

Macroscopically, bone is of two types: (1) hard compact cortical bone, found in long bones; and (2) spongy cancellous bone found in vertebrae and at the ends of the long bones (Fig 2.1). The relative quality and quantity of these two kinds of tissue varies in different bones. The exact composition of the bones varies depending upon a large number of factors including: the age and sex of the animal, the specific bone in question, and the location of the sample (Bronzino et al., 1995).

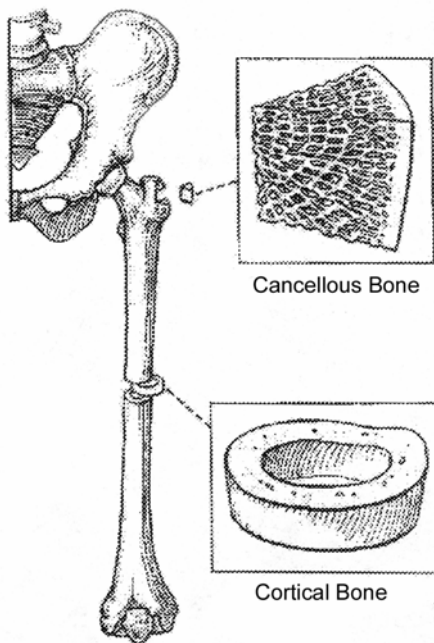


Fig 2.1 Cancellous and Cortical Bone (after Siegel, 1998)

The simple skeletal tissue includes lamellar bone, woven bone, hyaline cartilage, fibrocartilage, fibrous tissue and bone marrow. Lamellar bone or the mature bone is a highly organized and regularly oriented. Woven bone or primary bone has the same composition of the lamellar bone, but it lacks the order and oriented mechanical properties. The trabeculae are deposited as a disorganized clump that conforms to the geometry of the capillary loops that precede and nourish their osteoblasts. The first hard tissue in many anatomical areas is the hyaline cartilage and similar to woven bone, hyaline cartilage forms soft tissues. Fibrous tissue is embedded in collagen.

Embryologically, bone may be detected by 8 weeks in a developing human (Patten et al., 1974). Bone development proceeds along two paths – intramembranous and endochondral bone formation (Cowin, 1989). Bone formation takes place directly on a scaffold of condensed primary connective tissue in intramembranous bone formation. In the endochondral bone formation, bone formation takes place indirectly on the condensed primary connective tissue via an intermediate

model composed of cartilage (Cowin, 1989). This is the kind of bone formation that produces long bones. Chondroblasts are formed by the differentiation of the mesenchymal cells. These chondroblasts proliferate and secrete the characteristic matrix of cartilage, which shape up into miniature models of long bones (Cowin, 1989). The end of a long bone is called the epiphysis, the central portion is called the diaphysis, and the transition region in between both is called the metaphysis (Fig 2.2). All of these sites undergo extensive bone modeling to maintain the shape of bone during growth (Cowin, 1989). Furthermore, the diaphysis is composed of solely cortical bone, whereas the metaphysis and epiphysis regions also contain significant amounts of cancellous bone within the interiors.

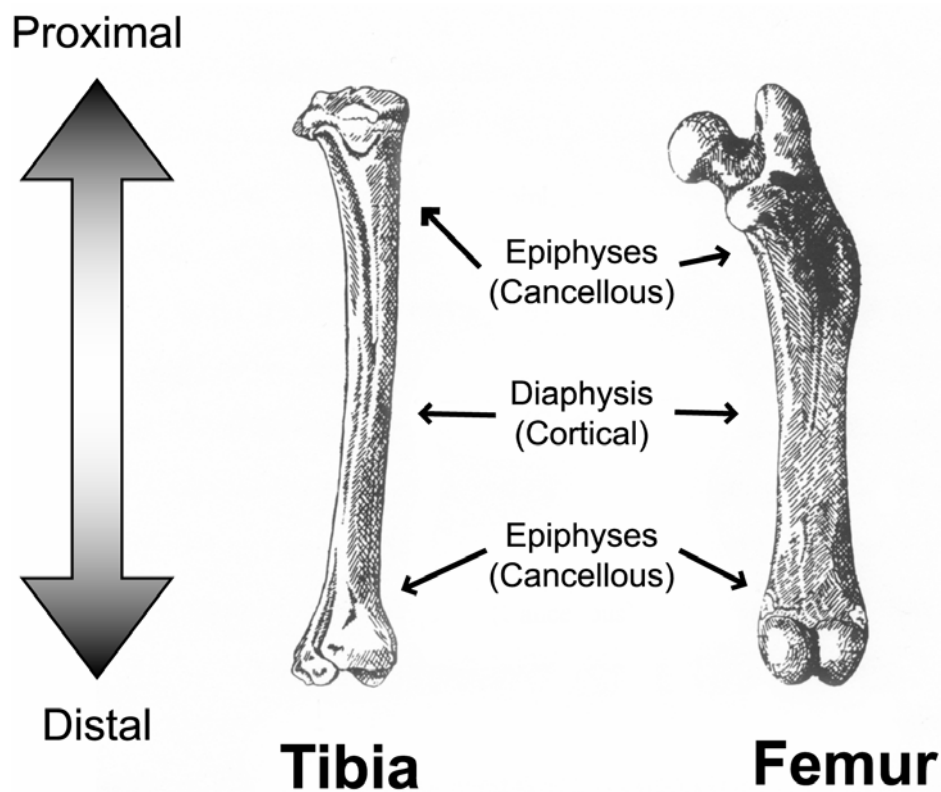


Fig. 2.2 Rodent Tibia and Femur



Bone is subjected to constant remodeling. Remodeling helps in the maintenance of the mechanical and physiological properties of the bone. Bones have the power of healing and also isolating and/or confining a variety of local threats like infection, foreign bodies and tumors. In humans and larger mammals, remodeling takes place with the help of osteons also called haversian systems. Bones are first destroyed/eaten away by bone destroying cells called osteoclasts. Osteoclasts erode the bone and form cavities called cutting cones in cancellous and resorption cavities on cortical bones (Cowin, 2001). Osteoblasts are bone forming cells that synthesize and secrete unmineralized bone matrix called the osteoid.

Generally, cortical bone is found on the outer layers of the bone, forming an outer covering over the spongy bones and spinal chord. The quantity of the two types varies according to functional requirements at different bones and at different places of the same bone. Cortical bone is very dense and porosity is very high in the cancellous bones.

Cortical bone is a hard compact bone found largely in the shafts of long bones, which surround marrow cavity. Cortical bone is highly calcified and contains osteocytes and few small Haversian canals. Cortical bones are highly organized, slow forming and have mineral content more than that of cancellous bones. About 80% of the skeletal mass in adult human skeleton is cortical bone, which is largely responsible for the supportive and protective function of the skeleton (Cowin, 2001).

Cancellous bone is highly porous and is more randomly organized than cortical bone. The porosity of the cancellous bone is the proportion of the total volume that is not occupied by bone tissue (Currey, 2002). In humans, it is filled with marrow and in birds, it is filled with air. It is found in high concentrations in the ends of the long bones, at metaphyseal regions, and along the lining of the marrow cavity at the diaphyseal region. Cancellous bone structure contains a lattice of plates and rods, three-dimensional branches called trabeculae, which are interspersed by bone marrow.

Mammalian cortical bone tissue can be of two main types – woven or lamellar (Cowin, 2001). Woven bone is the first bone that is formed during the

embryonic development or during repair of fractures. It is mostly cellular in nature, and the lacunae in which the osteocytes reside is not flattened as in mature bones (Vaughan, 1975). Woven bones have lower mineral content and are generally replaced, except in certain areas like tooth sockets and at cranial sutures (Cowin, 1989).

Lamellar bone is highly oriented and regularly organized. Lamellar bone is made up of unit layers on top of each other. Each layer consists of fine fibers that run along the same direction but adjacent layers can have difference of up to  $90^\circ$  between axes (Cowin, 2001). Lamellae of the adult cortical bone are of three major patterns – concentric lamellae, circumferential lamellae and interstitial lamellae. In the rat, cortical bone is primarily composed of circumferential lamellar bone. Also, there are no osteons or haversian systems in rats. In the cancellous bones, there are two types called trabecular packets or hemiosteon shaped shallow crescents and interstitial lamellae (Cowin, 2001).

Primary bone is formed where no bone has existed before. Based on the way bone is deposited, the two types of primary bone are circumferential lamellar and plexiform. Circumferential lamellar bone has a good mechanical strength, is dense and contains blood vessels. Plexiform bone is very similar to woven bone, but has better mechanical properties (Vaughan, 1975). Plexiform bone is found in rapidly growing animals like cows and is structurally similar to dense, well-oriented cancellous bone. Plexiform bone contains rectilinear residual vascular spaces, which often produce a brick wall appearance (Martin et al., 1998).

Secondary bone results from the resorption of existing bones and is more or less replaced by new lamellar bone. This process is known as remodeling. In adult humans, most compact bone is entirely composed of secondary bone, which may include whole osteons and the remnants of older osteons that have been partially resorbed (Martin et al., 1998). Trabeculae in most adult bones are also made up of secondary bone, and it's turned over more frequently than compact bone. However, remodeling rarely produces osteons, as they usually do not fit inside individual trabeculae (Martin et al., 1998).

Primary bone is resorbed by osteoclasts and secondary bone is formed by osteoblasts. There is a higher rate of remodeling on the bones that carry greater loads. Higher rate of remodeling increases the porosity of the bone tissue and decreases mineralization.

Four main physiological functions of the bone are protection of vital structures, hematopoiesis, mineral homeostasis and structural support. The skull, rib cage, vertebral column, etc. carry out the protection of the vital structures. The fabrication of cancellous core and cortical shell allows bone to be both stiff and resistive to damage. In addition to the external load, muscle and ligament forces act on the bones as well as gravitational forces (Rogers, 2002). Hematopoiesis is a metabolic function, which involves the production of red blood cells, white blood cells and platelets. The skeletal system contains 99% of the body's total calcium and phosphorous and thus it is the major reservoir for these minerals (Vaughan, 1981).

## **2.2 Mechanical Properties of Bone**

Mechanical properties of the bone are governed by the same principles as those of the manmade load-bearing structures (Martin et al., 1998). The ability of the vertebrae to adapt their bone structure to the imposed loading results in a highly complex, and when healthy, exquisitely efficient structure (Martin et al., 1998).

To be exact in defining the material properties of the bone, it is an anisotropic, heterogeneous, inhomogeneous, nonlinear, thermorheologically complex viscoelastic material (Bronzino et al., 1995). There are three main loading conditions which have considerable effect on the mechanical properties of the bone – orientation of the specimen in relation to the bone it came from, whether the specimen is wet or dry, and the strain rate on the bone (Currey, 2002). Bone also exhibits electromechanical effects both in vivo and in vitro when wet, and when dry, it exhibits piezoelectric properties (Bronzino et al., 1995).

Certain assumptions are done for the testing of bones so as to reduce the mathematical complexity. For most part, bones are assumed as linear elastic solid.

Mechanical properties vary significantly around the periphery and along the length of the bone, vary between cancellous and cortical bones and also between location of the bone. In the cancellous bone, it is important to distinguish the differences in structural property of the cancellous bone and the material properties of the trabeculae that comprises the cancellous structure (Ruhmann, 1998). Trabecular properties are the properties of the individual trabecular struts and branches that comprise the cancellous structure as a whole. Compared to cortical bone, cancellous bone can sustain strains 75% before failing in vivo, but cortical bone fractures when strain exceeds 2% (Rogers, 2002).

Bone is a smart material, it adapts to the force acting on it. Bones at locations which are subjected to higher loads, remodel or experience increased growth rate and changes in cross-sectional geometry to provide better load bearing support (Park et al., 1992). This reaction of bone reshaping itself over time in response to the forces acting on it is known as Wolff's law. Bones subjected to disuse, lack of exercise or old age result in resorption of bone, decrease of bone mineral density, and loss of bone strength. It is to be noted that loss of strength necessarily doesn't mean a change in the size of the bone. But Martin and Burr (1989) have noted that bone that receives little exercise is actually likely to increase in cross-section in an attempt to maintain strength.

### **2.3 Anatomy of the Tibia**

The tibia is a large medial bone of the lower leg, which transmits weight between the femur and the foot. It is the major weight bearing bone of the lower leg (Gray, 1977;White, 2000). The tibia articulates proximally with the femur, distally with the talus and laterally with the fibula.

The tibial plateau is the surface on the proximal tibia on which the femur rests. The tibial plateau is separated into two surfaces – the lateral and medial menisci (Rogers, 2002). The shaft of the tibia is prismatic and almost triangular in section. There are two ridges on the superior end of the proximal tibia called the lateral and medial intercondylar tubercles (Rogers, 2002) (Fig 2.3).

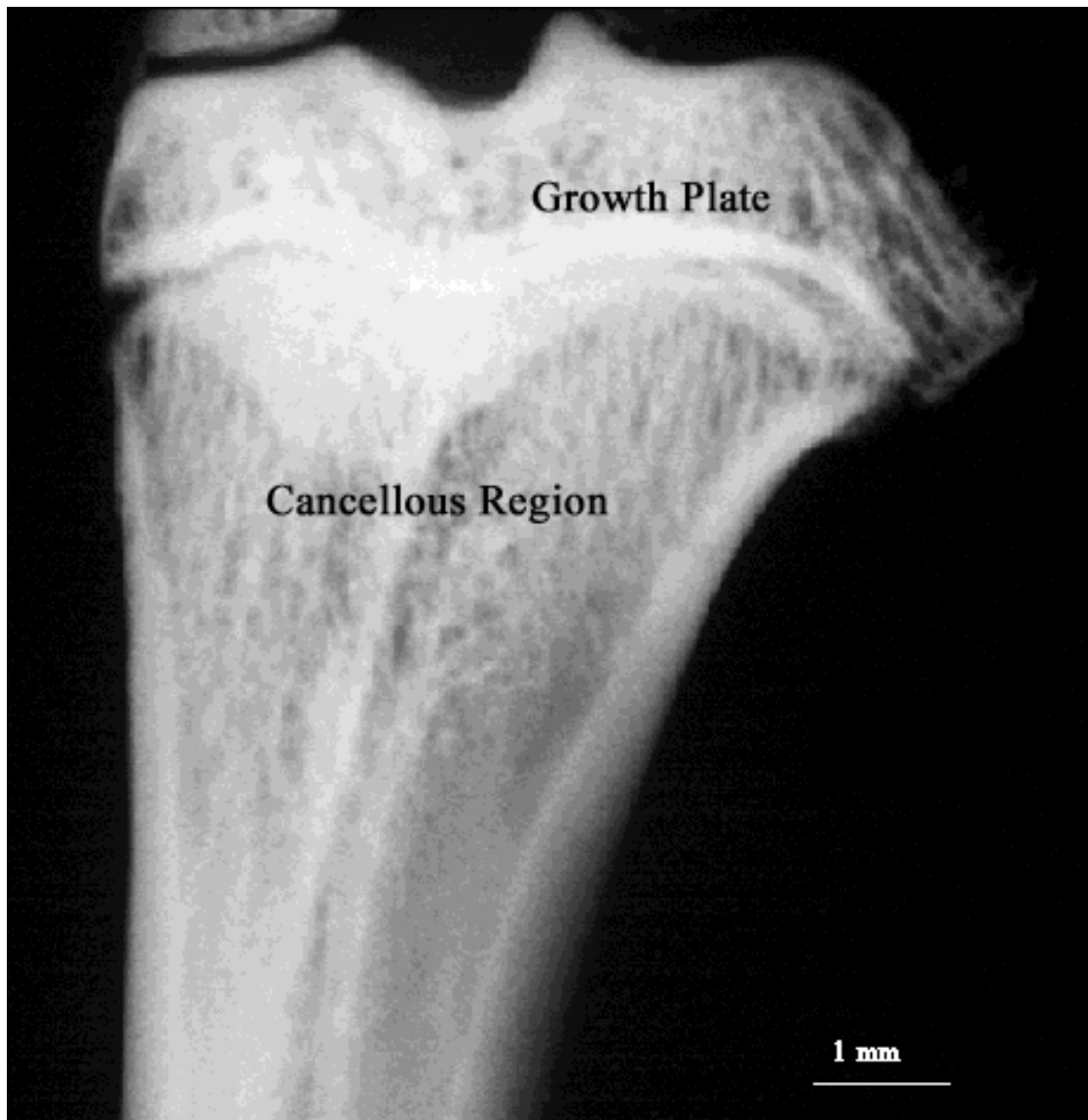


Fig. 2.3 Proximal Rodent Tibia

## **2.4 Osteoporosis and Bone Density**

Osteoporosis is a common clinical problem associated with substantial disability and fracture of bones (Cummings, 2002). Two common features of osteoporotic fractures are bone loss and falls. Until recently, it was typically diagnosed only after a serious complication arose. Currently, however, non-invasive tests are performed to estimate bone mass and predict fracture rate. The most commonly used predictor of fracture is based on the density of bone, defined as bone mineral density (BMD). Bone mass (BMD) is a measure of the amount of bone mineral, the distribution of bone mass and bone geometry are related to bone strength and stiffness. Further, stiffness and strength of the bone are a function of density of the bone. Stiffness is generally defined as the amount of force required to deform a structure.

Osteoporosis is a progressive bone disease in which the bone mineral is normally mineralized but the amount of bone is decreased and the structural integrity of the trabecular bone is impaired, making it more brittle. Bone strength reflects the integration of bone quality and bone density. Bone density is generally expressed in terms of grams of mineral per volume or area. In any given individual, it is determined by peak bone mass.

Some of the most common methods of determining the BMD of bones are described in the following pages. The most common method currently for measuring BMD at hips for humans is DEXA (Cummings, 2002), at wrist or forearms are pQCT or radiographic absorptiometry (Yates et al., 1995). Generally, DEXA is the most preferred method, as bone mass is highly correlated with it. DEXA assesses the amount of mineral or BMC in a two-dimensional projection and divides it by the area. Thus, BMD by DEXA is not a true density but rather an “area density” or mass per unit area.

## **2.5 Relevant Research on Bone Density Measurements**

A number of methods are available to measure the BMD values and assess the risk to fracture. Currently the most popular noninvasive method is dual energy X-ray absorptiometry (DEXA). There are also single energy X-ray absorptiometry

(SEXA), quantitative computer tomography (QCT), radiogrammetry ultrasound and radiographic absorptiometry (RA). Some of the methods used for measuring bone density of peripheral areas for humans and animal models are peripheral quantitative computer tomography (pQCT), micro-computer tomography ( $\mu$ -CT), radiographic densities measured using aluminum step-wedge radiographic techniques, etc. This thesis deals with density measures from pQCT and aluminum step-wedge radiographic techniques.

The pQCT bone densitometer measures volumetric bone mineral density at peripheral skeletal sites. pQCT allows for selective measurement of bone cortical and trabecular bone mineral density and cross-sectional areas at sites on the radius and tibia. Using planar measurements such as DEXA, changes in density may be obscured by changes in skeletal size. The precision error (%CV) calculated from duplicate measurements in pre-menopausal women is 1.4% for trabecular bone measured at a site 4% from the radial endplate and for cortical bone density measured at the 20% radial site (Children's Hospital Medical Center of Cincinnati). pQCT is widely used to measure density and area in mouse long bones because it has excellent precision and can be used nondestructively both ex-vivo and in-vivo (Brodt et al., 2001). It is typically used for areas like wrist, forearm, heel, etc. pQCT is more widely used in Europe than the United States (Mayo Foundation for Medical Education and Research).

Radiographic absorptiometry is a method of photo densitometry, developed during the late 1980s, in which radiographs of the specimen are taken along with an aluminum step-wedge. The films are then digitized, the soft tissue effects subtracted from the image and the intensities of the bone are compared with that of the aluminum step-wedge, to determine the bone density and bone mineral content. According to the American Academy of Orthopedic Surgeons (AAOS), the correlation between radiographic absorptiometry values and the actual bone density is excellent. The radiographic absorptiometry has relatively good accuracy and good precision and is inexpensive. Radiographic absorptiometry is typically used for measuring the bone density of smaller sites like wrist and arm.

## **2.6 Relevant Research on Correlating Bone Density Measures and Mechanical Properties**

Correlations between bone mineral density and mechanical properties continue to be of interest from research and clinical perspectives because of the extensive use of BMD as surrogate measures of bone stiffness and strength. Correlations for rat models are extremely important, as rodents are used mainly in both skeletal research and drug development. Generally, correlations are performed using linear and power law models for skeletal research. But, Currey (1986) has shown that power law model correlations are best for the mechanical properties of cancellous bone.

Ebbesen et al. (1999) have shown that bone density measured by DEXA, QCT, pQCT and ashing correlates highly with the vertebral compressive stress. The objective of this study was to evaluate the ability of DEXA and QCT to predict vertebral compressive strength and to investigate whether pQCT was suitable for ex situ evaluation of the vertebral bone density and strength. The study also aims at describing the correlations between mass or density and load or stress by both linear and power relations. The specimens were obtained from 101 human lumbar vertebral bodies' (L3) without posterior elements. The L3 samples were scanned using DEXA, QCT and pQCT. After the removal of the end plates, the whole vertebrae were compressed at the rate of 5 mm/min between two loading plates to estimate the maximum load and stress. The specimens were then ashed to determine the ash density. The main findings from this study are – mass and area density (DEXA BMD) measures have higher correlation to compressive load ( $r^2 = 0.86$ ) values than to compressive stress ( $r^2 = 0.75$ ) values and trabecular bone volumetric density (QCT) has a higher correlation to compressive stress ( $r^2 = 0.75$ ) than to compressive load ( $r^2 = 0.61$ ). It was also shown that linear and power law relations revealed similar ability to describe the relation between mass or density with load or stress.

Hernandez et al. (2001) have identified that apparent density and ash apparent density are effective predictors of bone strength and stiffness. The objective of



this study was to determine the relative influence of bone volume fraction and ash fraction on the ultimate stress and elastic modulus of cancellous and cortical human bone with a large variation in ash fraction. Specimens obtained from human vertebrae and femur, tested by Keller (1994) were used for this study. The specimens were mechanically tested using uniaxial compression and then ashed in a muffled furnace at 650°C. A two-parameter power law function of the form shown below was used to explain in a better fashion the variance in data.

$$y = a(BV/TV)^b \alpha^c \quad (2.1)$$

Ulrich et al. (1999) determined the elastic constants using finite element analysis and 3D structural indices from various skeletal sites. The objective was to calculate the 3D structural indices and elastic constants of the human cancellous bone from different skeletal sites and to investigate its predictive value for bone in a “critical” density range, where it cannot be identified as osteoporotic or normal from measurement of BMD alone. High resolution  $\mu$ CT was used to assess the structural indices like bone surface, bone volume, trabecular thickness. Using linear multivariable regression analysis, it has been shown that by supplementing BV/TV with single structural indices the  $R^2$  values of the predicted elastic constants can be increased from 53% (BV/TV alone) to as much as 82% (BV/TV and mean intercept length (MIL)). They have showed that due to the clear improvements in the prediction of elastic constants for bone samples, detection of osteoporosis could be improved by supplementing BMD measurements with assessment of bone micro-architecture in vivo.

VanAusdal et al. (2001) determined the apparent density, ash densities and volume fraction using dry weight, ash weight, bone volume and total volume. The objective is to determine the relationship of measured apparent density and the strength of cancellous bone in the proximal tibia to the radiographic densities measured using aluminum step-wedge radiographic techniques. Thirteen-step aluminum step-wedge was calibrated to a range of known densities. The known area density of each step was

correlated to the gray level or optical density of the corresponding step on the radiograph. This was used as a predictor of trabecular density and bone strength of the human proximal tibia. They showed that the radiographic technique could be used to predict the mechanical strength, apparent density and ash density of the trabecular bone in the proximal tibia.

Morgan et al. (2003) determined the site dependence of the relationship between the apparent density of the human trabecular bone and its elastic modulus. Bones from vertebra, proximal tibia and proximal femur were used for this study. Uniaxial mechanical tests were conducted to determine the elastic moduli. Polished unlubricated stainless-steel platens and end-caps were used to reduce errors due to end artifacts. Apparent density was calculated as a ratio of wet mass of the specimen and bulk volume. Apparent density of the specimen was also determined using finite element analysis. The relationships between elastic modulus and apparent density did not show any dependence on anatomic site. Although there was difference in the power law exponents for correlations, significant differences were found among the leading coefficients. Hence, the observed site-specificity in apparent modulus-density relationship may be attributed to inter-site variations in architecture.

Goulet et al. (1994) studied the relationship between density of the cancellous bone to its strength and modulus. The main purpose of this study was to investigate the relations between the structural parameters of the cancellous bone and its correlations. Also, to evaluate the important parameters for maintaining the strength of the bone and its integrity. Cubes of cancellous bone from the human tibia and 6 other sites were studied using  $\mu$ CT to produce complete three-dimensional digitization from which morphological and architectural parameters could be measured in a nondestructive manner. The cubes were then mechanically tested in uniaxial compression in three orthogonal directions and to failure in one direction to find the orthogonal tangent elastic moduli and ultimate strengths. Ash density and apparent densities were also determined. A high correlation between the basic stereologic measurements was found, indicating that there is a relationship between the amount of

bone and number of trabeculae in cancellous bone. Regression analysis was used to estimate the modulus and ultimate strength, using morphology and architecture as the independent variable; these regressions accounted for 68-90% of the variance in these measures. These relationships were dependent on the metaphyseal type and donor, with the modulus also dependent on the direction of testing. This indicates that the properties of the individual trabeculae, as well as their amount and organization, may be important in predicting the mechanical properties of cancellous bone.

J. C. Rice et al. (1988) made a study of previously conducted experiments on human and bovine bone tissue. This study includes by Carter and Hayes (1976, 1977), Currey (1969), McElhaney (1966), Galante et al. (1970) to draw the conclusions that Young's modulus and strength of the bone are proportional to the square of the apparent density and hence proportional to one another. Carter and Hayes (1977) concluded that elastic modulus is proportional to the strain rate to 0.06 power. Previous studies have shown that elastic modulus varies with the way cross-sectional area was determined. Estimates for the elastic modulus for human cancellous bone varies from 1 to 20 GPa. This study shows that elastic modulus proportional to the square of apparent density gave a better representation of the data than did a proportionality to the cube and did as well as that square plus the cube. Also, strength of the cancellous bone is proportional to the square of the apparent density and, elastic modulus is directly proportional to the ultimate strength. Fyhrie and Vashishth (2000) showed similar results regarding the proportionality between ultimate strength and stiffness.

Luthringer, K. (2001) recently conducted a study to determine the correlation between the mechanical properties found from the RPC test on the cancellous bones of femurs of rodents and the pixel intensity density. She developed a procedure to calibrate the pixel intensity and layers of aluminum from step-wedges, and also analyzed the scanning and imaging software. The density of the cancellous bone compartment of each RPC specimen was determined in terms of layers of aluminum and then compared with the stiffness, maximum load, elastic modulus and ultimate stress of the specimen. RPC image data showed smaller average intensities for the alcohol sub-group for both

10 week and OVX main group. The intensity for the non-OVX (sham) was higher than the chow fed or pair fed subgroups. The trends in the values for stiffness, maximum load, elastic modulus and ultimate stress showed smaller values for alcohol fed subgroup. She recommended smaller step-wedges, to facilitate easier scanning, and to make new ones with fewer layers.

Table 2.1 shows a comparison of the various correlations done in previous studies. Different methods for estimating the apparent density were followed in each study. Specimens are all from human studies but from various locations. All specimens were tested to failure by compression.

Table 2.1 List of Correlations from Previous Compression Test Studies

Authors	Type of Bone	Correlation	$r^2$	P (or) b	Comments
Ebbesen et al. (1999)	Lumbar Vertebral bodies (L3) – Human	pQCT Vs. Stress – Power & Linear	0.81 ( $y = ax^b$ ) 0.82 ( $y = a+bx$ )	$P < 0.00001$	End-plates removed
Hernandez et al. (2001)	Vertebrae and Femur – Human	Bone volume fraction Vs. Compressive strength – Power Law	0.91 ( $y = ax^b$ )	$b = 1.9$	End-plates used $BV/TV = \frac{\rho}{1.41 + 1.29\alpha}$
Keller (1994)	Vertebrae and Femur – Human	Ash Density Vs. Elastic Modulus – Power Law	0.97 ( $y = ax^b$ )		Using End-plates One parameter model
Fyhrie et al. (2000)	Vertebral cancellous bone – Human	Ultimate Strength Vs. Stiffness – Pearson's Correlation	0.90 ( $y = a+bx$ )	$P < 0.001$	Brass end-caps glued
Hodgskinson et al. (1990)	Vertebral Cancellous bone – Human	Ultimate Strength Vs. Stiffness - Linear	0.89 ( $y = a+bx$ )	$P < 0.001$	
Morgan et al. (2003)	Proximal Tibia – Human	Elastic Modulus Vs. Apparent Density – Power Law	0.84 ( $y = ax^b$ )	$b = 1.93$ $P < 0.001$	End artifacts minimized
Nicholson et al. (1997)	Lumbar Spine – Human	Elastic Modulus Vs. Apparent Density – Linear & Power Law	0.81 ( $y = a+bx$ ) 0.85 ( $y = ax^b$ )	$b = 2.70$ $P < 0.001$	Negative Correlation Ultrasonic technique

## CHAPTER III

### METHODS

#### 3.1 Overview of the Experimental Design

This section will discuss the procedures used to accomplish the objectives of this study. The rodent tibiae used in this study came from bone loss experiments conducted in association with the National Space Biomedical Research Institute (NSBRI). The study describes the temporal course of recovery in bone and muscle strength following an extended exposure to simulated microgravity. The tibiae from this study provided an opportunity to understand better the correlation of mechanical properties to various bone density measures.

The reduced platen compression testing procedures studied herein continue the earlier work of Harms (2000) and Rogers (2002) by improving the imaging techniques and specimen location. This thesis also seeks to improve testing conditions and preparation of the specimen for reduced platen compression testing. In this study

#### 3.2 Experimental Animals

Six-month old Sprague-Dawley rats were used for the bone muscle recovery (BMR) study. After a week of acclimatization, the rats were separated into 3 broad groups: baseline control (N =10), aging control (N = 60) and hindlimb unloading recovery (N=60) (Table 3.1). The baseline control group was sacrificed before the start of the suspension period to determine an initial baseline for the outcome variables. All experimental hindlimb unloaded (HU) rats were subjected to 28 days of hindlimb unloading by tail suspension. The aging controls were not suspended but were pair-fed to HU rats to control for any effects of reduced energy intake. In this study

The hindlimbs were unloaded by tail suspension of the rats (Morey-Holton and Globus, 1998). Unloading of the hindlimbs was achieved by tail suspension. The tail was harnessed to a swivel apparatus on the wire spanning the top of the cage.

The height of the animal's hindlimb was adjusted to prevent any contact with the cage bottom, resulting in approximately 30° head-down tilt (Bloomfield et al., 2002). The forelimbs of the animal maintained contact with the cage bottom, allowing the rat full access to the entire cage. This was done for a period of 28 days. This was followed by recovery periods of 7, 14 or 28 days. The animals were sacrificed at the end of recovery, as summarized in Table 3.1. Aging controls were also sacrificed at each time point. The tibias were harvested for mechanical testing.

Table 3.1 Summary of Experimental Design for the Bone Muscle Recovery Study

Treatment Group	Recovery Period (after 28d HU)				
	28-d	0-dR	7-dR	14-dR	28-dR
Baseline Control (BC)	13				
Control (CON)		10	12	12	15
HU-Recovery		16	14	13	9
Age (months)	6	7	7.25	7.5	8

dR = days recovery

HU = Hindlimb Unloaded

### 3.3 Bone Removal and Preparation

In order to get a better understanding of the cancellous bone, the focus of this study was the proximal tibial metaphysis, for this is the region of the tibia with maximum cancellous bone tissue. The soft tissue of the tibia were removed and the tibias were separately wrapped in gauze wetted with phosphate buffered saline solution, sealed in plastic capsules and frozen at -80°C. Freezing has been shown not to affect the mechanical properties of the bone (Pelker et al., 1984). Although this project deals with cancellous bone only, a brief description will be provided for the three-point bending procedure followed for each bone.

### **3.4 Radiographs**

The bones were radiographed with the anterior side facing upward (anterior-posterior (A-P), or coronal view). X-rays were developed on Kodak X-Omat TL Film (Eastman Kodak Company, Rochester, NY) and radiated with a General Electric Industrial Radiograph Machine (General Electric, Lexington, MA) set at 25 kilovolts and 1 milliamperere. Focal film distance was fixed at 30 inches with an exposure time of 60, 80 and 100 seconds. For the first batch of bones, 60-sec exposure was better suited for identifying the first cut distance. For all the other groups, 80-sec exposure was used. This exposure time was chosen because of clarity and ease in recognition between the cancellous and cortical bone. Also, the calibration curves were best for this exposure time.

### **3.5 RPC Specimen Preparation and Location Determination**

One of the first steps for the preparation of specimens for reduced platen compression (RPC) testing is to determine the precise specimen location. Generally, the thickness of the specimen for RPC testing is 2 mm. As mentioned earlier, the specimen is taken from the metaphysis of the proximal tibia, so as to isolate the cancellous bone tissue. The ideal specimen location would be parallel and distal to the growth plate. Prior to this study, the tibia was sliced longitudinally along the sagittal and coronal plane to study the growth plate (Rogers, 2002). Rogers (2002) studied the tibia for prominent landmarks to determine approximate specimen location, as shown in Fig 3.1. Rogers (2002) used the two ridges of the lateral meniscus, one of them being the lateral intercondylar tubercle, as a reference to determine the first cut distance.





Fig 3.1 Specimen Location Based on Lateral Tubercle Landmarks (Rogers, 2002)

The cancellous bone content of the metaphysis can be observed from the radiographs of the proximal tibia, although the level of detail is imperfect since it is a planar projection technique. The target location for each specimen was located by studying the radiographs. The radiographs were digitized using Polaroid SprintScan 35-slide scanner (Polaroid Corporation, Cambridge, MA) at 2700 dpi (dots/pixel per inch) as a TIF file. The TIF file was then imported into SigmaScan Image (Version 1.20, Jandel Scientific Software, San Rafael, CA) for image analysis. A calibration factor was then calculated for the imported images to translate pixels into standard units. No magnification was involved, as the specimens were placed directly on the x-ray film. The calibration factor was based on the scanning resolution and is as follows:

$$(2700dpi)^{-1} \times \left( 25.4 \frac{mm}{in} \right) = 9.407 \times 10^{-3} \frac{mm}{pixel} \quad (3.1)$$

Previously, the first cut distance was measured from the proximal end of the tibia to the distal extent of the growth plate. During this study, it was noted from the radiographs that the growth plate of the specimen was not a straight line, but the growth plate has two peaks with a dip between them. As shown in Fig 3.1, the first cut distance was determined to be from a line through the ridges of the lateral meniscus to another line drawn below the growth plate. In order to devise better and easier methods for specimen location, there were a few changes incorporated during the course of this thesis.

As before, lines were drawn and distances measured using SigmaScan. In this case, however, a line was drawn tangent to the highest point (i.e., most proximal) of the two “ridges” (or highest points) on the growth plate, as depicted by line A in Fig 3.2. Another line (labeled B) was sketched tangent to the two highest points on the tibial plateau and parallel to line A. In order to determine the target specimen location, lines were drawn parallel to the line through the growth plate (line A) at distances of 1.5, 1.75 and 2mm (labeled C). By trial and error, the best distance was determined to be 1.75 mm

from the growth plate (line A). The first cut distance was then determined to be the distance from line B to the specified line C (1.75 mm from line A). This process was followed for each individual specimen. Using this measurement, a transverse cut was made using an Isomet low-speed diamond blade-wafering saw (Buehler LTD, Lake Bluff, IL), under constant irrigation with tap water.

The specimen was gripped with special grippers fabricated so as to ensure no movement during cutting. Care was taken to ensure that the blade and the highest ridges of the tibial plateau were aligned in order to replicate the line drawn at the top (line B). The blade was then moved the prescribed first cut distance using the built-in micrometer on the saw, and the first cut was made. Fig 3.3 shows the saw blade kerf. After the first cut, the thickness of the epiphysis piece was measured using digital calipers (Mitutoyo Corporation, Japan) and recorded. The specimen was then visually inspected to make sure that the cut specimen did not include any growth plate. A second transverse cut was made at a distance of 2.4 mm from the initial cut, to produce a specimen with a thickness of 2 mm. The extra 0.4-mm accounts for the kerf of the saw blade (Fig 3.3). The thickness of the RPC specimen was then measured using digital calipers and the values were recorded. The specimen was also inspected visually to observe any structural defects or other notable features. Care was taken to ensure that the specimen was kept wet and not allowed to dry during the entire specimen preparation process.

### **3.6 Platen Sizing Using Image Analysis**

The RPC specimen was then radiographed in a cross-sectional (or axial) view for computer aided image analysis (Fig. 3.4). The specimen was radiographed distal side facing upwards. X-rays were made on the same machine as before with settings at 20 kilovolts and 1 milliamperere. Focal film distance was fixed at 30 inches with an exposure time of 80 seconds. These were then digitized as TIF files and imported into SigmaScan Image and Adobe Photoshop (Version 6.0, Adobe Systems Inc., San Jose, CA).

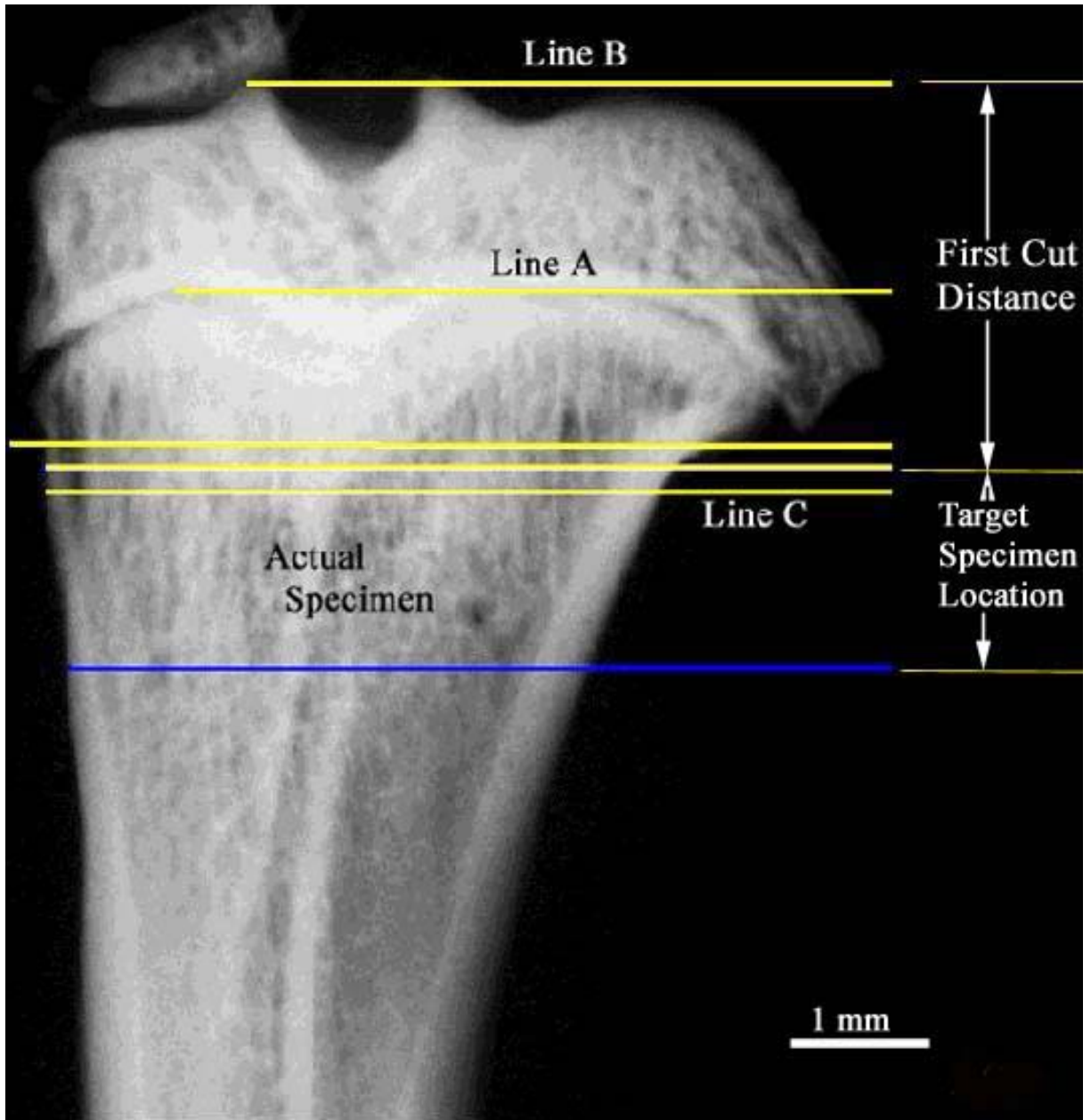


Fig. 3.2 New Specimen Location Procedure

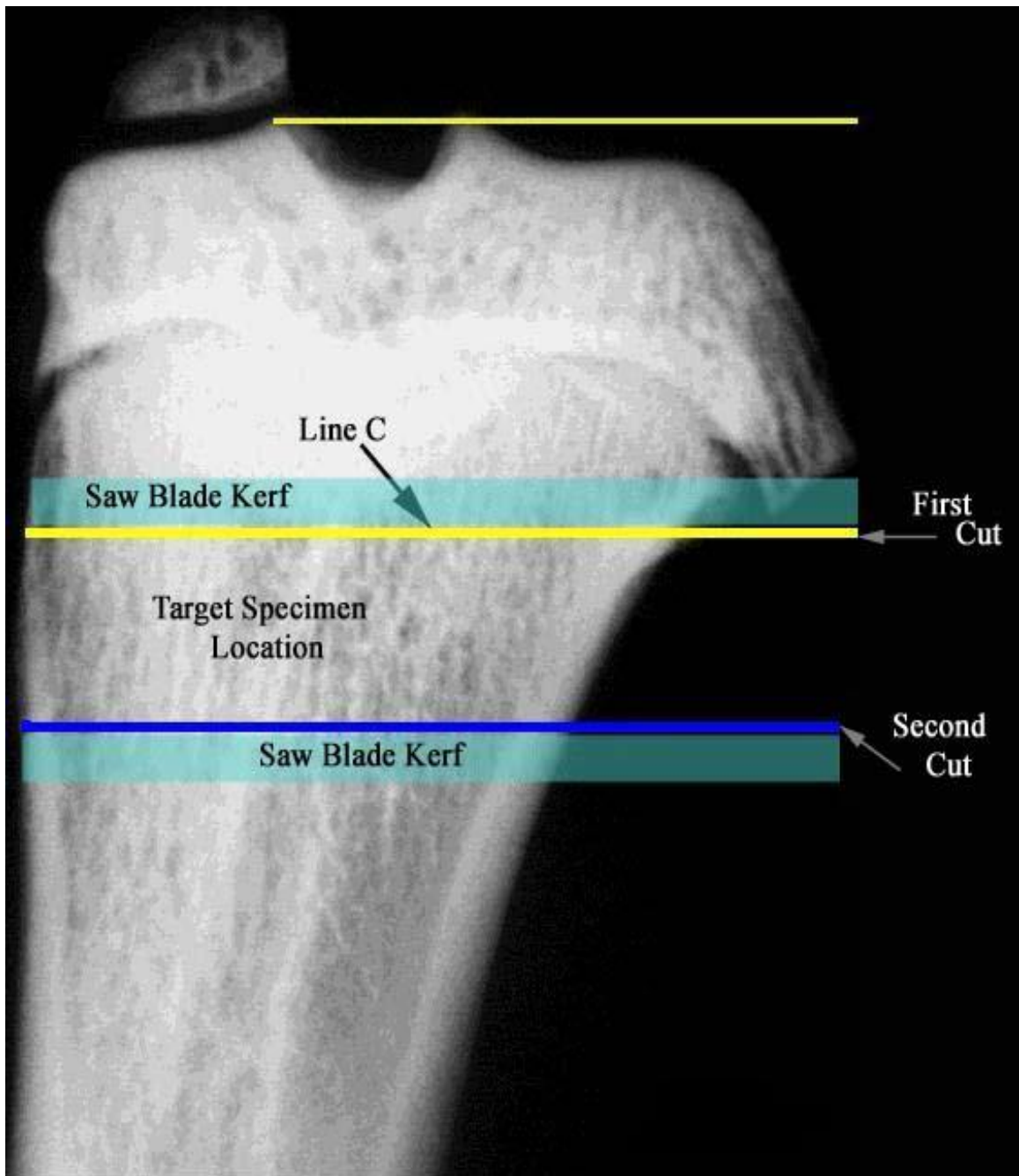


Fig 3.3 Specimen Location Showing Saw Blade Kerf

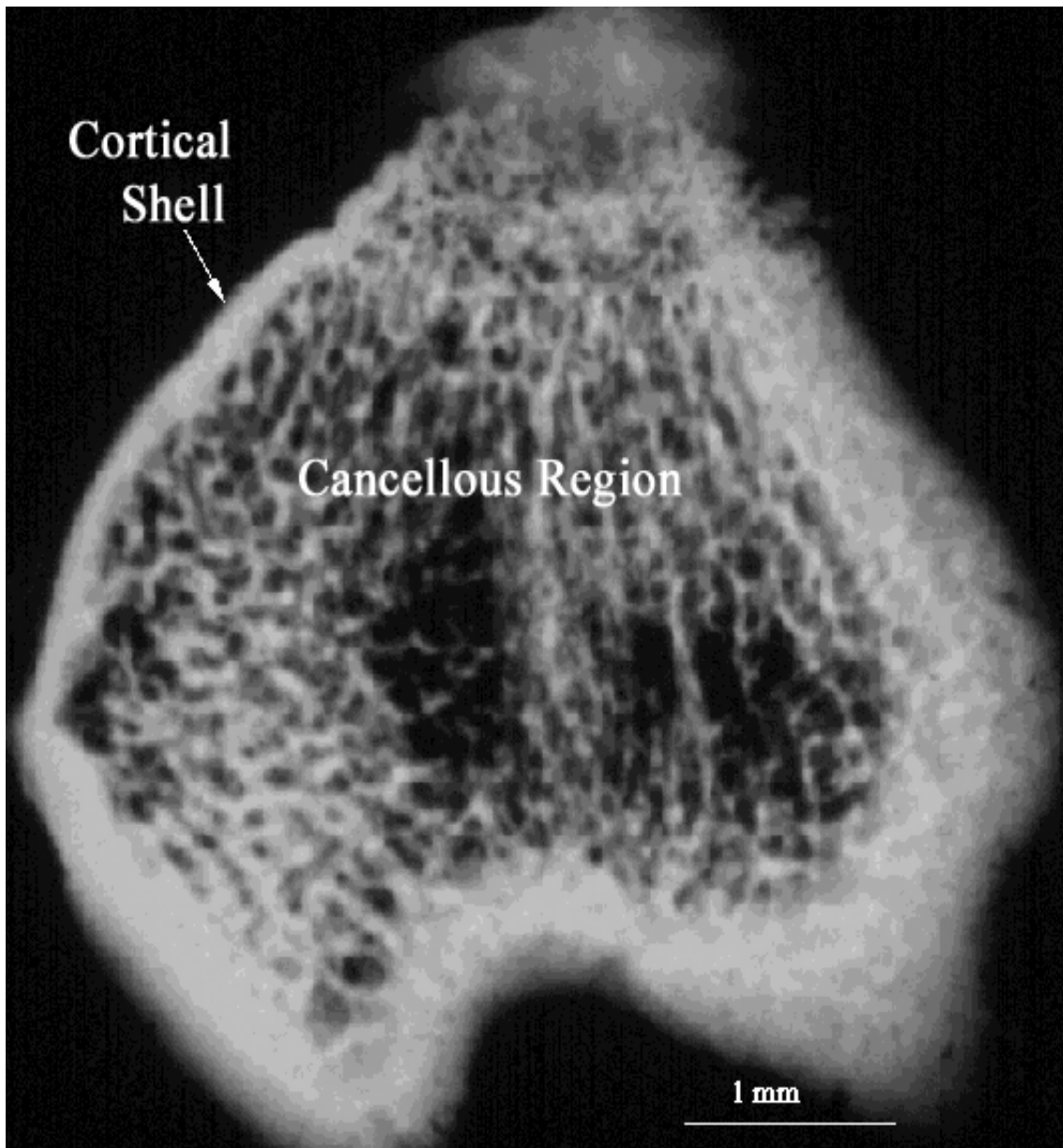


Fig. 3.4 Radiograph of RPC Specimen

Using SigmaScan Image, the interior region of the specimen was traced to outline the region of the cancellous bone only. Fig 3.5 shows the outline trace with the cancellous region shaded. Quantitative analysis of the shaded region determined the properties of interest like area, major and minor axis lengths, shape factor and pixel intensity. Using the major and the minor axis lengths, Rogers (2002) used a target range of platen sizes to specify the size of the platen used for RPC testing. The size was determined as a percent of the minor axis lengths.

A revised process was also developed. The first step of the process was to use Adobe Photoshop to draw the endocortical circle on the specimens, as indicated in Fig 3.6. Using 69% of the endocortical circle, as decided by Rogers (2002), another circle was drawn concentric to the endocortical to determine the platen diameter and platen area. The rationale behind this tracing is to encompass the maximum cancellous area as possible without getting too close to the cortical shell. If the platens are too large, excessive load sharing by the cortical shell could occur. Once the platen diameter was found using this method, the platen was placed directly on the specimen to make a visual inspection and determine if any adjustments were required. Some of the specimens needed a size that was bigger or smaller than the one prescribed by the endocortical method. The platen was then used as the actual platen size for each specimen, which was then used to test the specimen.

### **3.7 Bone Density from pQCT**

Bone scans of tibiae were obtained by peripheral quantitative computed tomography (pQCT) using a XCT Research M (Stratec; Norland Corp., Fort Atkinson, WI). Scans were made in vivo as part of the experimental protocol for the BMR study sponsored by the NSBRI. Being able to make such scans in vivo is a major advantage of this technique because it permits longitudinal measurements (repeated in time) on each animal. The locations of the in vivo scans were at the proximal tibia metaphysis at 5.0, 5.5 and 6.0 mm distal to the proximal plateau and also at the mid-diaphysis (50% overall length). Each scan slice was centered at each of these locations, and 0.5 mm thick. All

scans were obtained at a CT speed of 2.5 mm/sec with a voxel resolution of 0.10 x 0.10 x 0.50 mm. These details were established at the beginning of the BMR study and were being followed before this thesis research began.

Using standard Stratec software (version 5.40B), values of total, cortical and cancellous bone mineral density (BMD); and total cross-sectional, cortical bone and marrow area were obtained for each slice. Data for the three slices taken at each bone region were averaged to get a mean value for each site. In addition, the polar cross-sectional moment of inertia ( $CSMI_p$ ) was obtained at the tibial mid-diaphyses for use in intrinsic property calculations for three-point bending tests. These measurements were done at Dr. Bloomfield's laboratory at the Department of Health and Kinesiology. Coefficients of variation for pQCT measurements at this lab are 1.24%, 2.13% and 1.95% for in vivo proximal tibia total BMD, cancellous BMD and total area, respectively.

### **3.7 Bone Density from Specimen X - Rays**

As alternate density measures to the BMD values from pQCT, image analysis was conducted based on x-rays of each RPC specimen. As described previously, the cancellous boundary of the RPC specimen was traced for each x-ray using SigmaScan Image software. One of the built-in image analysis features is determination of average pixel intensity of the cancellous region traced. Pixel values range from 0 to 255, with 0 being black and 255 being white. In addition, aluminum step-wedges were radiographed along with the specimens on the same film in order to allow for calibration to factor out any radiographic discrepancies due to exposure time or film processing. Based on a study made by Luthringer (2001), step-wedges with 3, 4, 5, 6, 7 layers were made. The material used was Reynolds Extra Heavy-Duty aluminum foil. The radiographed images of the step-wedges were digitally imaged and traced to determine the intensities, using the same process as for the specimens. The densities so obtained were then plotted against aluminum layers. Sixth order polynomials were fitted to these plots with coefficient of determination ( $R^2$ ) values greater than 0.99 for most batches.



Thirty-three discrete pairs of values were then generated from the fit equation and input into SigmaScan Image software to calibrate the intensity output in terms of aluminum layers. The actual values calibrated for each batch are in the Appendix I (pg. 75). The cancellous areas and the total area of the specimens were traced and the aluminum layer intensities of the cancellous areas were obtained. Hence, the cancellous compartment of the specimen was calibrated in terms of pixel intensities and aluminum layers.

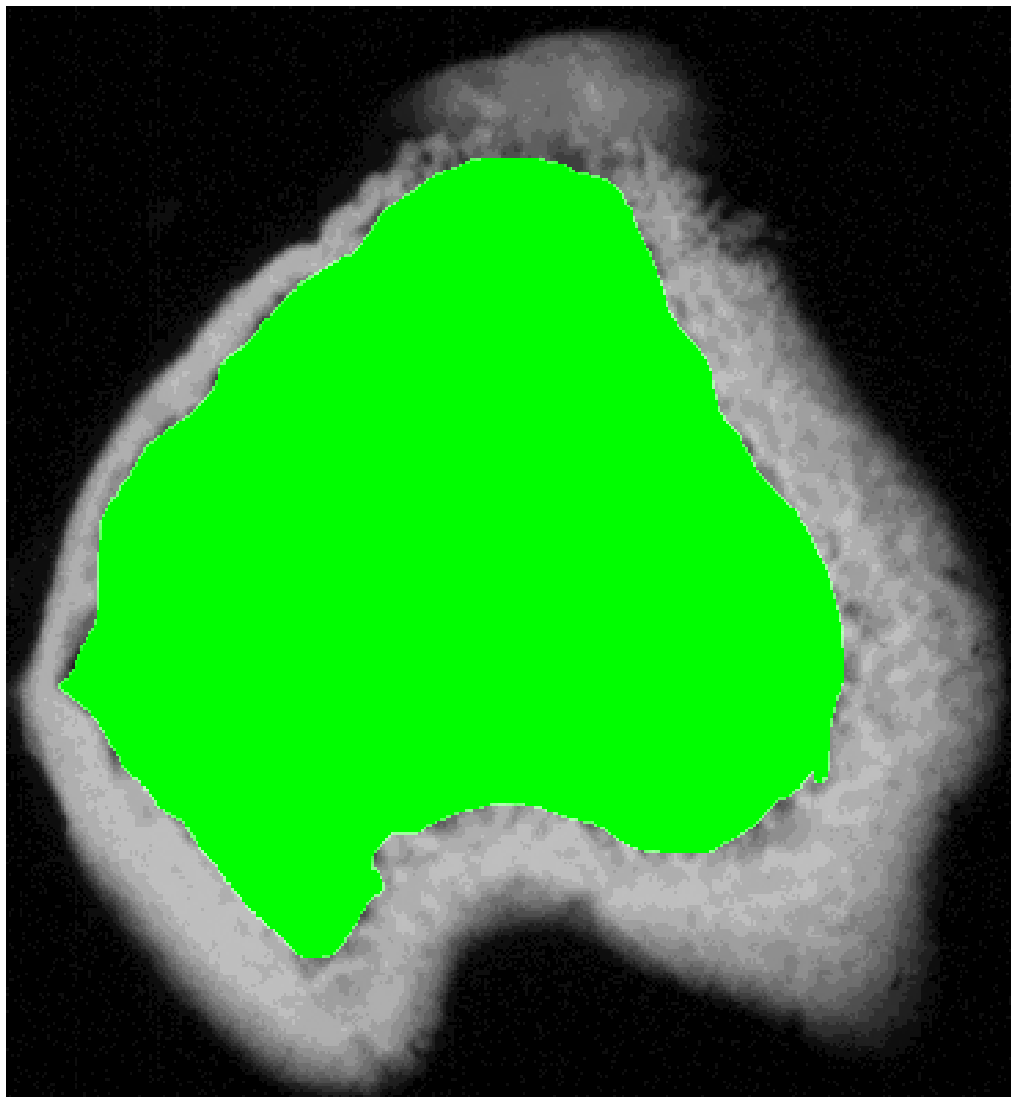


Fig. 3.5 Image Analysis of RPC Specimen

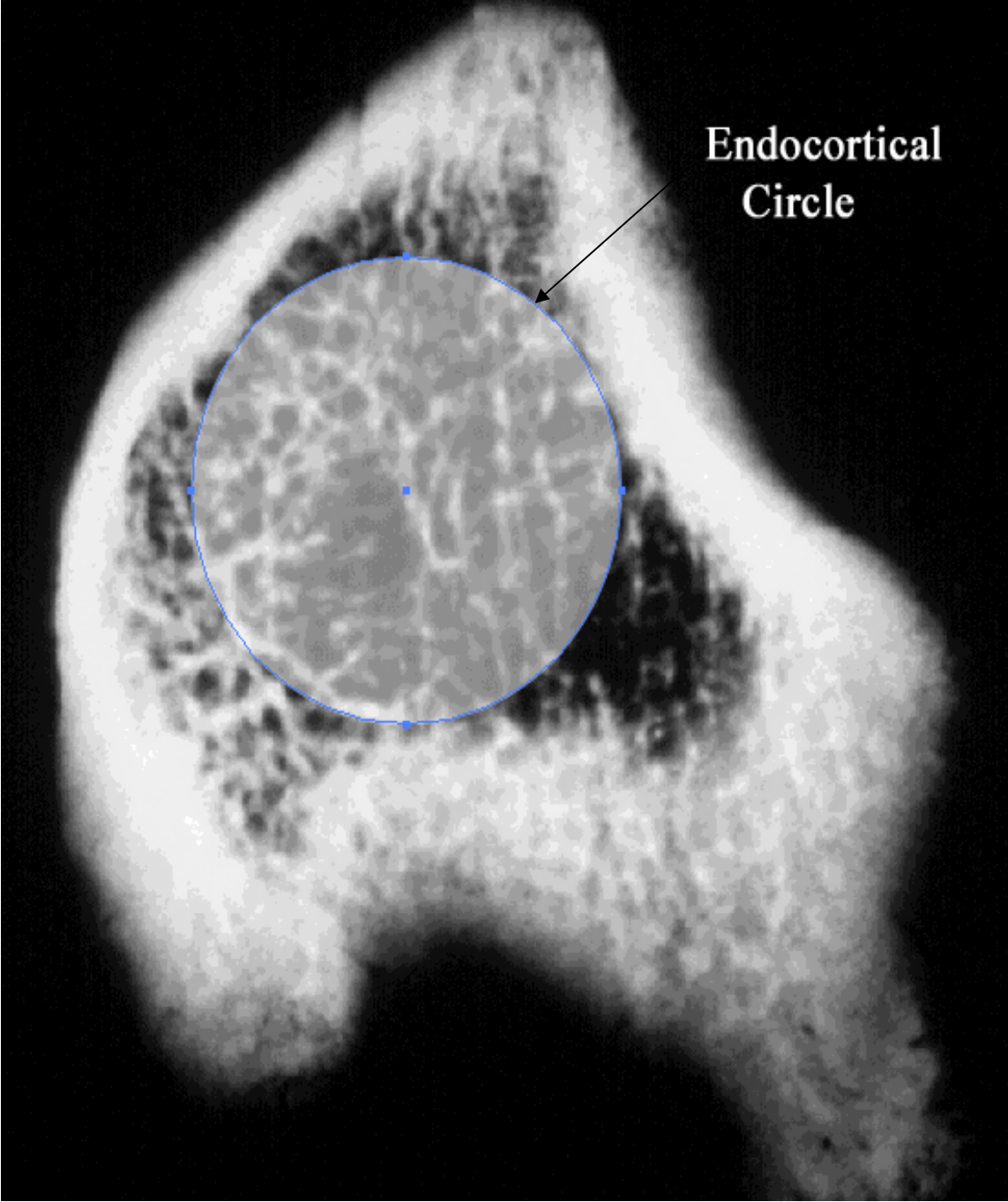


Fig. 3.6 Endocortical Circle of RPC Specimen

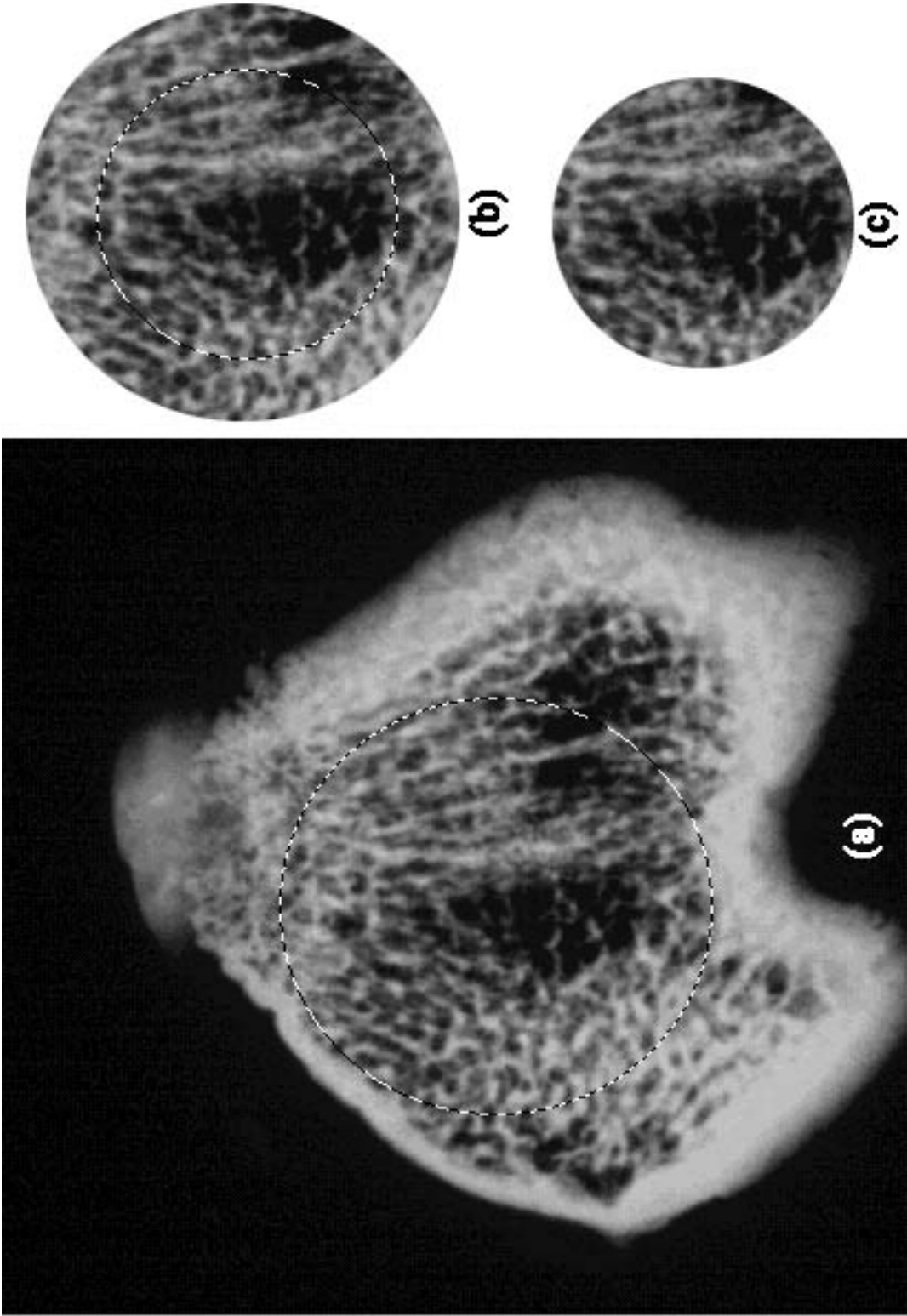


Fig. 3.7 Endocortical Circle and Actual Tested Area (69%)

In order to understand and to get a density determination of the cancellous area tested under the platen, a new procedure was also followed. After determining the diameter of the platen required for the test, the area enclosed by the endocortical circle was selected (see Fig 3.7 (a)). Using Adobe Photoshop (Version 6.0, Adobe Systems Inc., San Jose, CA), the cortical shell and the rest of the specimen were removed from the selected endocortical region (Fig 3.7 (b)). Then, an inner circle of the same diameter as that of the platen was drawn. This area was then removed from the bigger circle (Fig 3.7 (c)). Thus, the actual test area of the cancellous compartment was isolated from the whole RPC specimen for analysis. This region was then traced using SigmaScan following the same procedure as described above to determine the average intensities in terms of both pixel intensity and aluminum layers.

### **3.9 Compression Testing**

After the selection of platens, the bones were grouped according to platen size and each group was tested in random order. Compression testing was done on Instron model 1125 mechanical testing machine, as indicated schematically in Fig. 3.8. Quasi-static loading was applied at a rate of 0.2 in/mm on the upper platen, while the lower platen was stationary. Displacement was measured using a linear variable differential transformer (LVDT) mounted on the cross-head of the Instron machine. The LVDT was calibrated to have a stroke of  $\pm 0.025$  in between  $-10$  V and  $10$  V. Load-displacement data were collected digitally at a rate of 10 Hz using Labtech Notebook Pro Software Version 8.01 (Laboratory Technologies Corporation, Wilmington, MA) on a desktop IBM compatible personal computer. The specimens were thawed before RPC testing, but were wrapped in wet gauze until testing. During testing, the specimens were not allowed to dry.

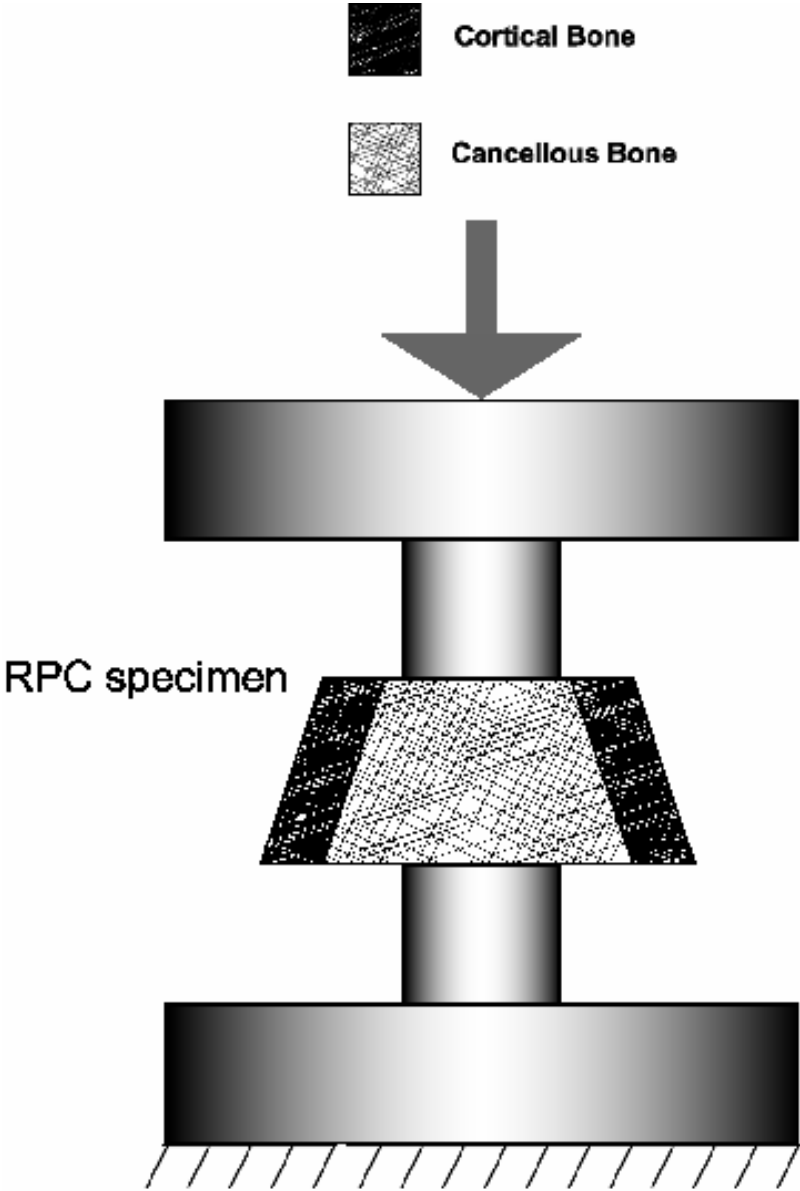


Fig 3.8 Reduced Platen Compression Test

### 3.10 Data Analysis

The raw data from RPC testing was analyzed using Microsoft Excel 97 and TableCurve 2D v. 2.03 (Jandel Scientific, San Rafael, CA). The raw data from the compression test consisted of test time in seconds, displacement in inches, and loads in pounds. These data were then converted such that displacements were in millimeters and load in Newton and analyzed to obtain the mechanical properties of interest.

Based on the assumption of uni-axial compression of the cancellous bone compressed between the platens, the volume of the material comprising the loaded specimen was taken to be the product of the specimen thickness ( $t$ ) and the cross-sectional area of the platen ( $A_{\text{platen}}$ ). The following parameters were then determined from the force-displacement data recorded during each test:

- Maximum Force ( $F_M$ )  $\Rightarrow$  {N}
- Displacement at Maximum Force ( $D_m$ )  $\Rightarrow$  {mm}
- Stiffness ( $k$ )  $\Rightarrow$  {N/mm}

The stiffness is defined as the slope of the force-displacement curve in the elastic region. This was determined by using a best-fit linear regression in TableCurve 2D. The y-intercept was also calculated in the linear regression. Maximum force during compression is actually a crushing force, since the specimen undergoes confined compression.

The displacements were corrected so that the initial load occurs at zero displacement on the force-displacement graph. The corrected displacement accounts for the initial absence of loading at the beginning of the compression test. The following equation was used to correct the displacement:

$$\text{Corrected } D_x = D_x - \left( \frac{b}{k} \right) \quad (3.2)$$

where,  $D_x$  is the initial displacement value,  $b$  is the y-intercept and  $k$  is the stiffness.

Since, a purely uni-axial stress state was assumed, the following intrinsic properties for the RPC specimen were found:

- Ultimate Stress ( $\sigma_{\max}$ ) {MPa} – Ultimate stress is the strength of the cancellous bone at the maximum force. It is determined by:

$$\sigma_{\max} = \frac{F_M}{A_{\text{platen}}} \quad (3.3)$$

where,  $F_M$  is the maximum force and  $A_{\text{platen}}$  is the cross-sectional area of the platen used for compression of the cancellous bone

- Elastic Modulus (E) {MPa} – Elastic modulus is the stiffness of the cancellous core that was compressed and is determined by:

$$E = \frac{\sigma_{zz}}{\varepsilon_{zz}} = \frac{t \cdot F_M}{\Delta t \cdot A_{\text{platen}}} = \frac{k \cdot t}{A_{\text{platen}}} \quad (3.4)$$

where,  $k$  is the stiffness of the specimen,  $t$  is the thickness, and  $A_{\text{platen}}$  is the cross-sectional area of the platens used,  $\Delta t$  is the displacement, and  $\varepsilon_{zz}$  is the normal strain.

Thus, the elastic modulus and ultimate stress were estimated from the stiffness, maximum force, thickness and area of the RPC specimen. The tracing of the cancellous core and the cortical shell from SigmaScan provided data on the geometric properties of the specimens like cancellous, cortical and total area of the specimen and average intensities in terms of pixels and aluminum layers. The average intensity in terms of aluminum layers and pixel intensity were compared with the mechanical properties determined from the compression testing data.

### 3.11 Correlation

Correlation measures the strength of association between two variables, which can be used as a gauge of the certainty of prediction. The two variables need not be related to one another. The coefficient of correlation  $r$  varies from  $-1$  to  $+1$ , with  $-1$  meaning that there is a perfect negative relationship between the variables,  $+1$  indicates that there is a perfect positive relationship between the variables. A value of  $0$  means that the two variables are completely independent of each other.

Generally, correlation is expressed in terms of  $r^2$ , the coefficient of determination. The advantage of the coefficient of determination is that it provides an equal interval and ratio scale measure of the strength of the correlation. In effect, the correlation coefficient,  $r$ , gives the true direction of the correlation (+ or -) but only the square root of the strength of the correlation; while the coefficient of determination,  $r^2$ , gives the true strength of the correlation but without an indication its direction. Both of them together give the most complete information.

Correlations were performed using two commercial softwares – SigmaStat and TableCurve 2D. SigmaStat was used to provide the P value for the correlation, for P value gives the probability of incorrectly rejecting the null hypothesis. TableCurve 2D software was used to generate the correlation graphs showing the linear and power law curve fit, with confidence intervals. TableCurve 2D software also provides the value for the power exponent  $b$  for the power law fit.

After obtaining the mechanical properties, the pQCT densities and radiographic densities were correlated using SigmaStat (Version 2.03, Jandel Scientific Software, San Rafael, CA), TableCurve 2D (Version 2.03 Jandel Scientific, San Rafael, CA) and Microsoft Excel 97. Two types of correlation curves were fitted to the data – linear correlation ( $y = a + bx$ ) and power law ( $y = ax^b$ ). The graphs were plotted using all three-software programs for the mechanical properties estimated from the reduced platen compression testing and the various density measures. These graphs help to determine the relationship between the mechanical properties and the density, and also provide us with the strength of this relation.



## CHAPTER IV

### RESULTS

#### 4.1 Introduction

In this section, the results from mechanical testing of the rat bone specimens are reported. Data from specimen location, densities and correlations are also presented.

All values are given as averages for the treatment group, along with the standard error of the mean (SEM) or standard deviation (SD) as noted. Differences were considered statistically significant if the p-value was less than 0.05. Statistical analysis was conducted using SigmaStat (Version 2.0, SPSS Science, Chicago, IL), TableCurve 2D (v 2.03, Jandel Scientific, San Rafael, CA), and Microsoft Excel 97.

The bone muscle recovery (BMR) study consisted of 120 specimens. The experimental design of the BMR study required staggering of the number of animals tested at any one time due to limitations of resources. Thus, RPC tests were conducted in a series of batches. Batch I consists of 19 specimens, Batch II consists of 39 specimens, Batch III consists 21 specimens and Batch IV 29 specimens. One specimen in the third batch shattered during the RPC preparation process and hence was not tested. Fifteen specimens were not used in Batch I and one specimen of Batch II is yet to be tested. Table 4.1 shows the number of specimens of each tested group in all the batches. Study group designations were presented previously in Table 3.1 (pg. 22).

#### 4.2 Specimen Location, Preparation and Platen Sizing

A brief description of the geometric properties of the RPC specimen is provided next. Consistency in the specimen location was desired so as to maintain uniform testing conditions and this was assessed by comparing the “first cut distance” (determined as previously described) with the “actual cut distance”.

Table 4.1 Specimens of Each Tested Group in Respective Batches

	Batch I	Batch II	Batch III	Batch IV
28-d BC	2	5	2	3
0-dR CON	3	6	0	1
7-dR CON	2	6	1	2
14-dR CON	2	6	4	0
28-dR CON	2	0	5	8
0-dR HU	2	6	2	5
7-dR HU	2	6	4	0
14-dR HU	4	4	0	5
28-dR HU	0	0	3	5
Total	19	39	21	29

dR – Days Recovery

HU - HindlimbUnloaded

The “actual cut distance” was defined to be the thickness of the epiphysis piece plus 0.40 mm, which must be added in order to account for the width of the material the saw blade removed. Table 4.2 presents these results in terms of treatment groups used in the BMR study. Also, Table 4.3 summarizes the same results by testing batches. This thesis aims at understanding the correlations between mechanical properties and various density measures irrespective of the animal group. Hence, results are presented in terms of tested batches. As seen from Tables 4.2 and 4.3, there were no significant differences between the values of the first cut distance and the actual cut distance.

#### **4.3 Reduced Platen Compression Test Mechanical Data**

This section reports the mechanical properties results obtained from the reduced platen compression testing performed on the specimens. Extrinsic and intrinsic properties are presented in Table 4.4.

#### **4.4 Radiography Technique Results**

The first step in performing the calibrations of the aluminum layer step wedges was to radiograph each step-wedge along with the specimens. The radiograph was then calibrated in terms of pixel intensity using SigmaScan Image Software. Calibration curves were plotted using pixel intensity to the layers of aluminum. Figs. 4.1 to 4.4 show the calibration curves for each group tested in the BMR study. Recall that the actual calibration values for each batch are provided in the Appendix I (pg. 75).

Average intensity of the specimen in terms of aluminum layers was calibrated using SigmaScan Image as described in Chapter III. Table 4.5 shows the average aluminum layer intensity for the whole cancellous region of the specimen, for every batch. Similarly, Table 4.6 shows the average aluminum layer intensity for only the cancellous region tested under the platen, for Batch III and Batch IV.

Table 4.2 Specimen Preparation Evaluation – Values Presented are Mean  $\pm$  SD for Each Treatment Group of BMR Study

	0-dR	28-dR CON
N	10	2
First Cut Distance (mm)	3.51 $\pm$ 0.32	3.05 $\pm$ 0.40
Actual Cut Distance (mm)	3.28 $\pm$ 0.31	2.98 $\pm$ 0.32
Specimen Thickness (mm)	1.99 $\pm$ 0.06	2.01 $\pm$ 0.02

dR – Days Recovery

	28-d BC	7-dR CON	14-dR CON	28-dR CON
N	12	11	12	13
First Cut Distance (mm)	3.62 $\pm$ 0.30	3.52 $\pm$ 0.23	3.43 $\pm$ 0.33	3.77 $\pm$ 0.22
Actual Cut Distance (mm)	3.38 $\pm$ 0.40	3.24 $\pm$ 0.25	3.25 $\pm$ 0.28	3.66 $\pm$ 0.18
Specimen Thickness (mm)	1.99 $\pm$ 0.04	1.99 $\pm$ 0.04	1.99 $\pm$ 0.05	1.97 $\pm$ 0.05

dR – Days Recovery

	28-d HU	7-dR HU	14-dR HU	28-dR HU
N	15	12	13	8
First Cut Distance (mm)	3.63 $\pm$ 0.49	3.35 $\pm$ 0.30	3.72 $\pm$ 0.22	3.62 $\pm$ 0.22
Actual Cut Distance (mm)	3.34 $\pm$ 0.58	3.17 $\pm$ 0.29	3.51 $\pm$ 0.22	3.62 $\pm$ 0.32
Specimen Thickness (mm)	2.01 $\pm$ 0.04	1.99 $\pm$ 0.08	1.99 $\pm$ 0.04	2.05 $\pm$ 0.20

dR – Days Recovery

HU – Hindlimb Unloaded

Table 4.3 Based on the Testing Schedule Followed, Specimen Preparation Results for the Four Batches are Given Below. Values Presented are Mean  $\pm$  SD

	Total Group	Batch I	Batch II	Batch III	Batch IV
N	108	19	39	21	29
First Cut Distance (mm)	$3.57 \pm 0.33$	$3.46 \pm 0.33$	$3.44 \pm 0.28$	$3.53 \pm 0.37$	$3.84 \pm 0.20$
Actual Cut Distance (mm)	$3.67 \pm 0.35$	$3.48 \pm 0.31$	$3.57 \pm 0.32$	$3.64 \pm 0.37$	$3.98 \pm 0.15$
Specimen Thickness (mm)	$1.99 \pm 0.07$	$2.01 \pm 0.02$	$1.99 \pm 0.05$	$1.98 \pm 0.06$	$2.00 \pm 0.11$

Table 4.4 Results from Mechanical Testing - Reduced Platen Compression Test. Values Presented are Mean  $\pm$  SD

Extrinsic Properties	N	Extrinsic Properties		Extrinsic Properties	
		Max Load (N)	Stiffness (N)	Ultimate Stress (MPa)	Elastic Modulus (MPa)
Total Group	108	$5.80 \pm 5.57$	$127.02 \pm 130.81$	$1.37 \pm 1.29$	$60.39 \pm 62.56$
Batch I	19	$7.37 \pm 6.11$	$129.99 \pm 83.10$	$1.60 \pm 1.29$	$57.52 \pm 36.43$
Batch II	39	$6.84 \pm 6.85$	$179.53 \pm 177.35$	$1.63 \pm 1.67$	$84.42 \pm 85.87$
Batch III	21	$4.13 \pm 2.45$	$82.36 \pm 68.38$	$1.03 \pm 0.63$	$40.19 \pm 34.93$
Batch IV	29	$4.57 \pm 4.45$	$86.81 \pm 88.93$	$1.14 \pm 1.00$	$44.58 \pm 42.98$

Table 4.5 Results from Radiographic Techniques. Values Presented are Mean  $\pm$  SD with the Minimum and Maximum Values Included in Parenthesis

	N	Cancellous Region
		Average Intensity (Al. Layers)
Total Group	108	7.11 $\pm$ 5.71 (4.6-20.17)
Batch I	19	14.25 $\pm$ 1.95 (11.18-20.17)
Batch II	39	12.71 $\pm$ 2.51 (8.51-18.84)
Batch III	21	7.90 $\pm$ 1.46 (4.6-10.53)
Batch IV	29	9.37 $\pm$ 1.58 (7.09-13.5)

Table 4.6 Results from Radiographic Techniques for Only the Platen Area, for the Batch III and Batch IV. Values Presented are Means  $\pm$  SD for Each Batch

	N	Cancellous Region
		Average Intensity (Al. Layers)
Batch III	21	5.50 $\pm$ 1.42 (2.53-8.18)
Batch IV	29	6.98 $\pm$ 1.62 (4.79-11.16)
Last Two Batches	50	6.36 $\pm$ 1.69 (2.53-11.16)

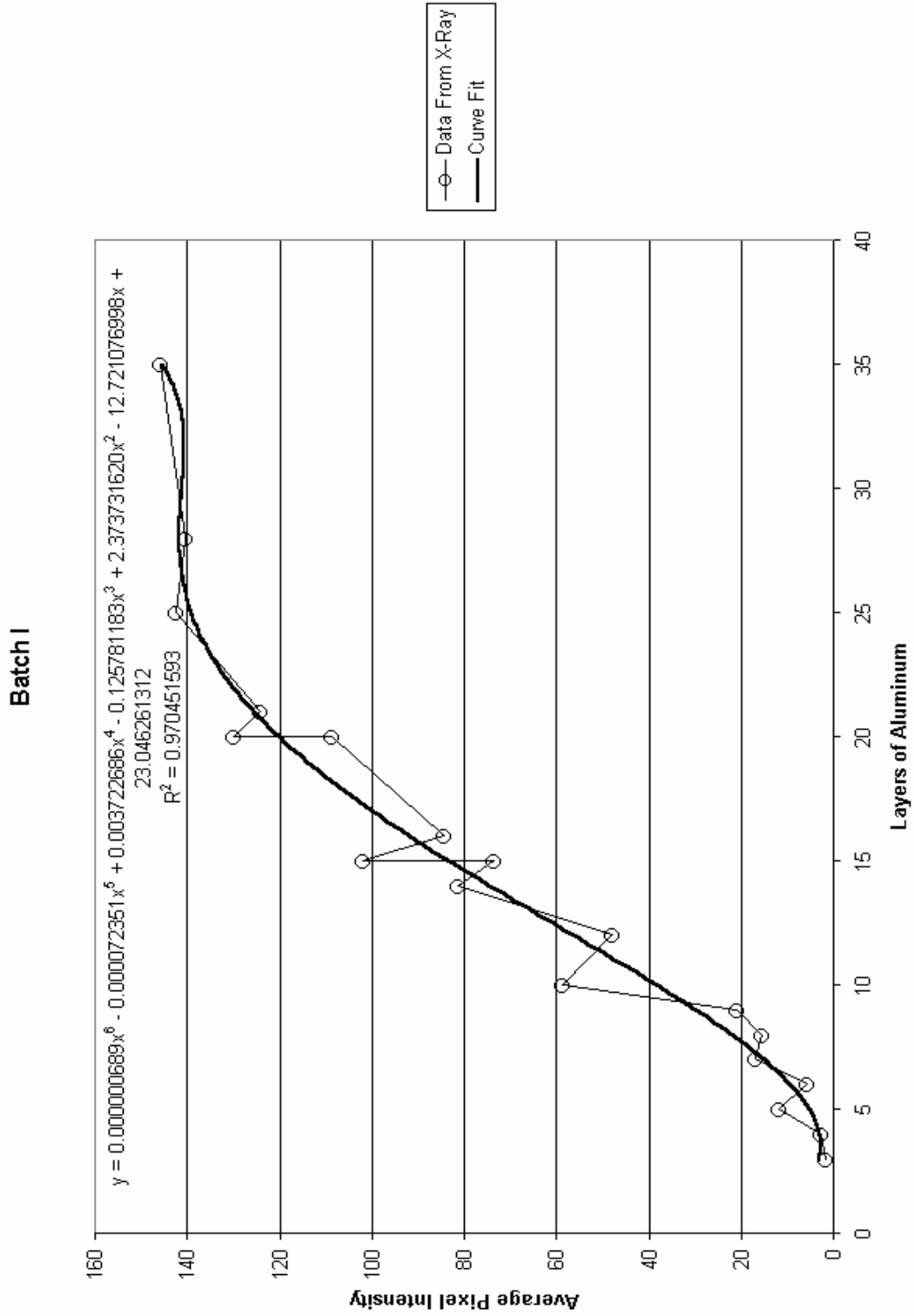


Fig 4.1 Calibration Curve for Batch I

Batch II

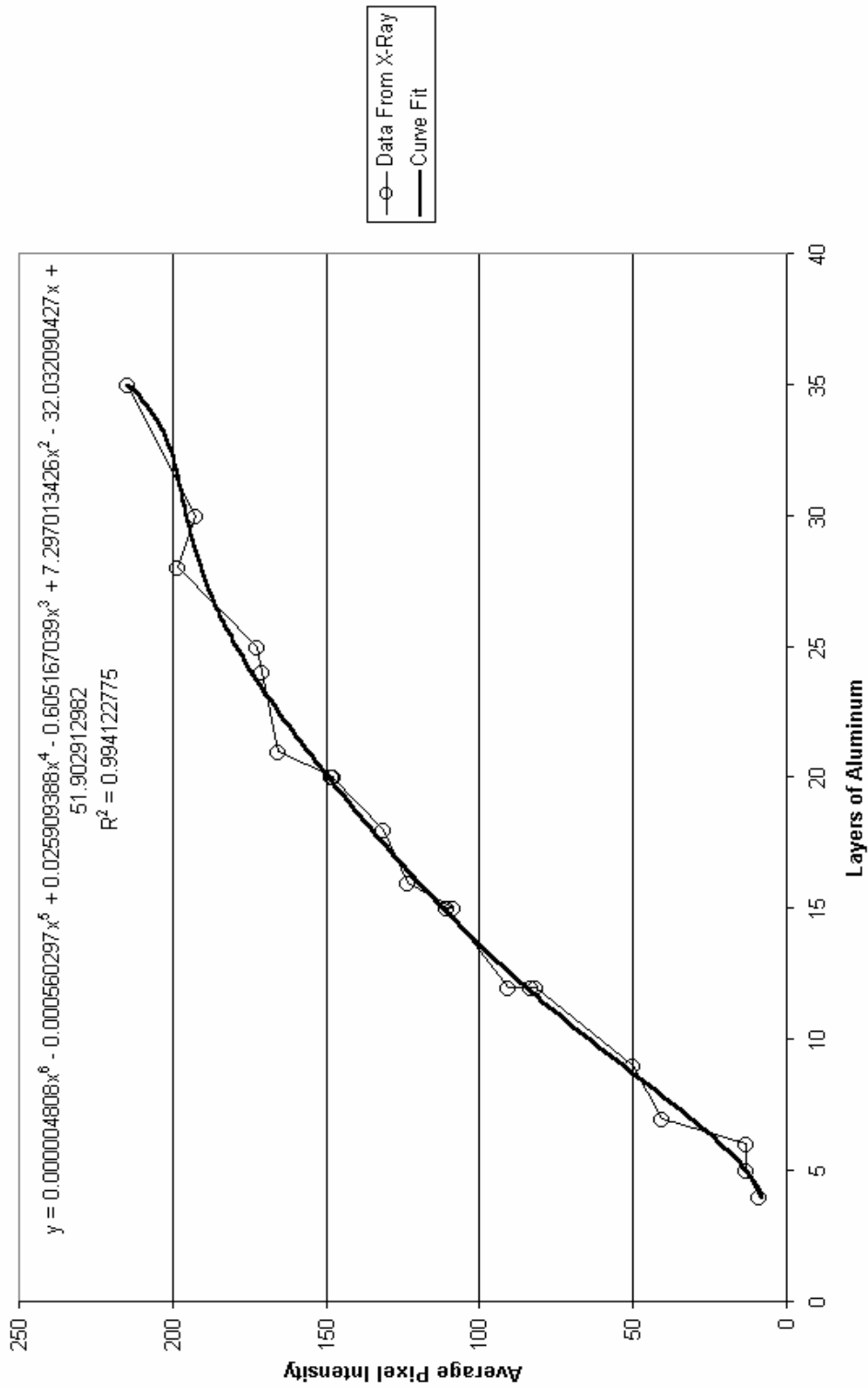


Fig 4.2 Calibration Curve for Batch II



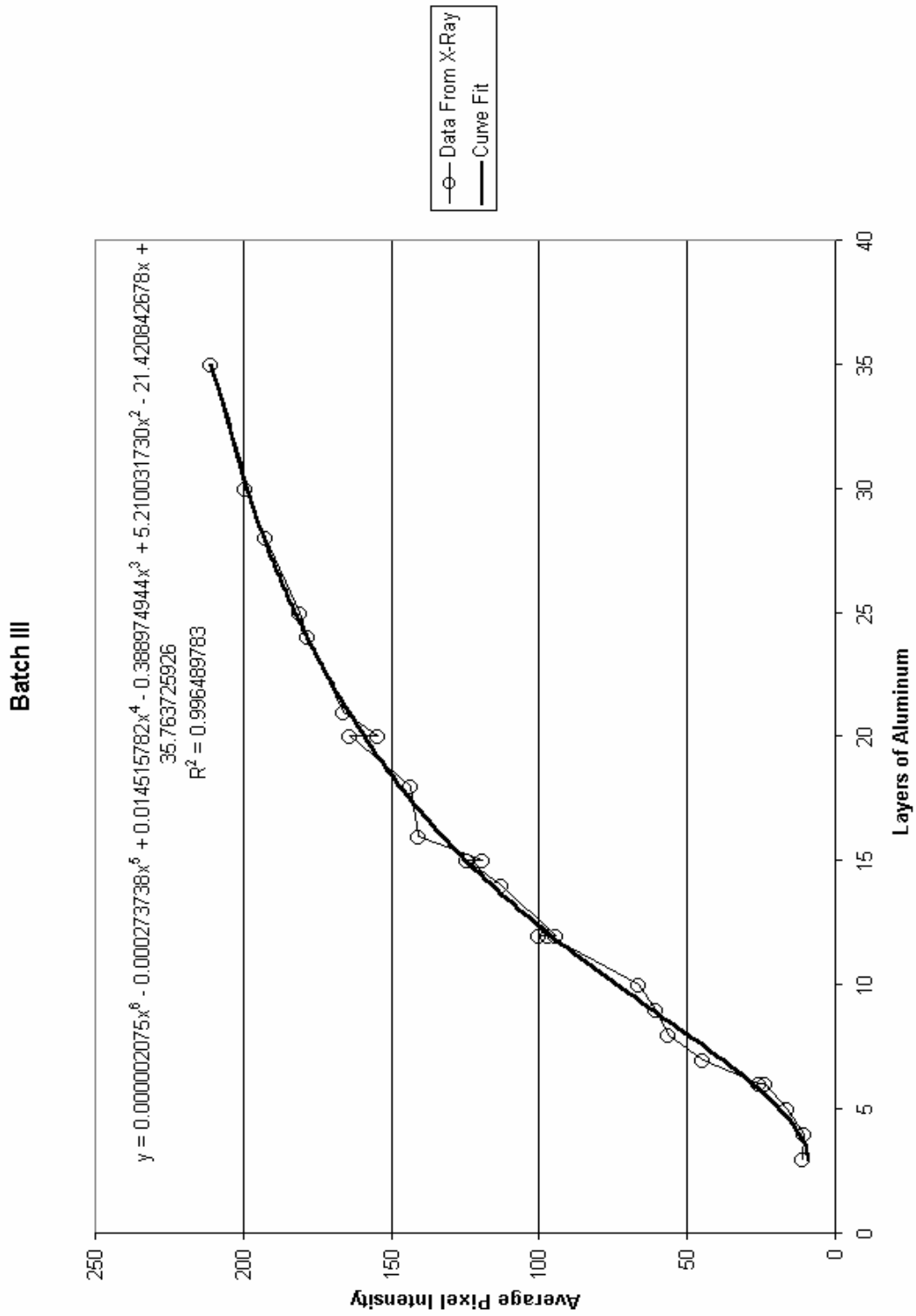


Fig 4.3 Calibration Curve for Batch III

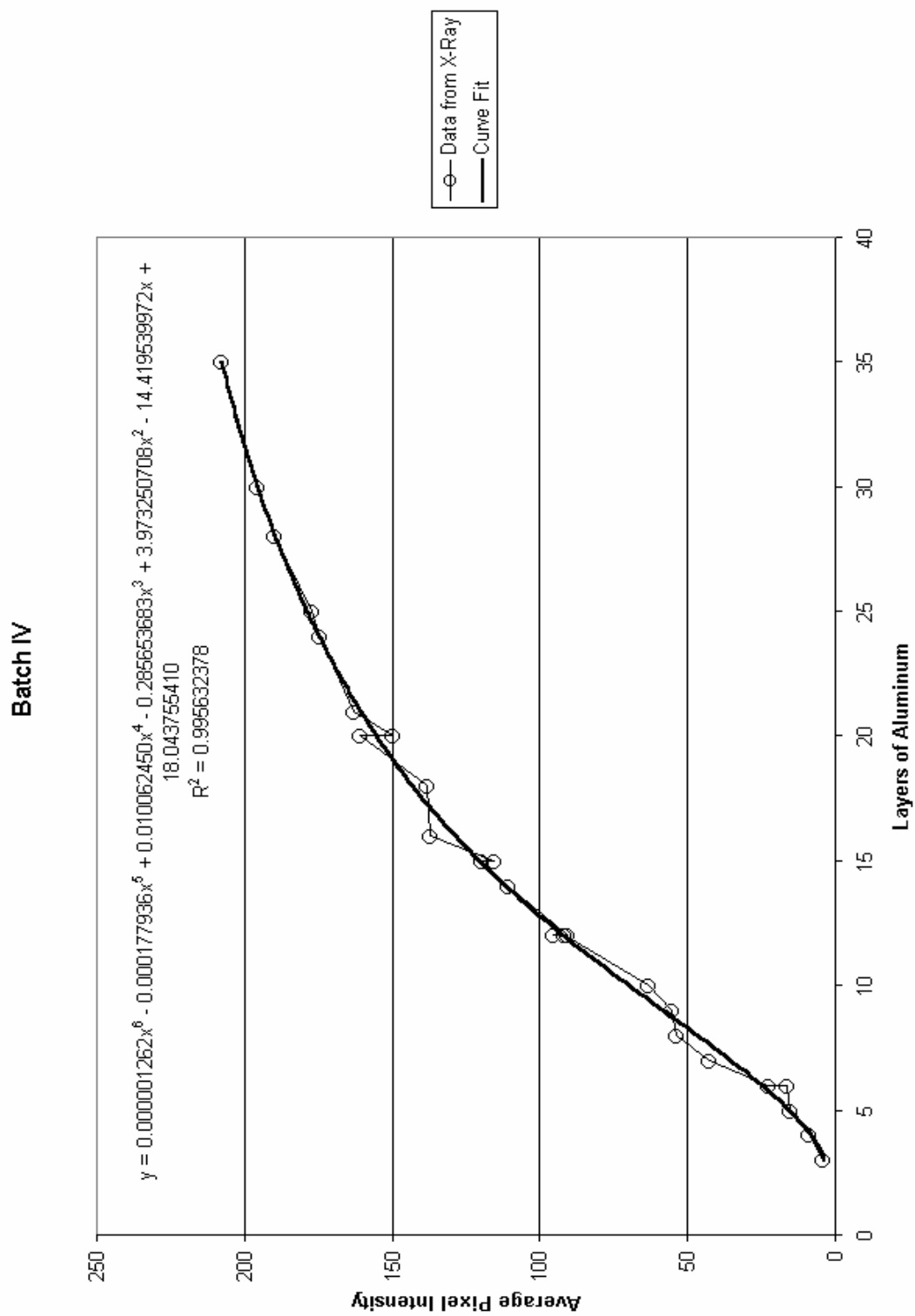


Fig 4.4 Calibration Curve for Batch IV

#### 4.5 pQCT Density Results

As pointed out in Chapter III, the data from pQCT scanning were provided from another source and were not generated as a part of this thesis research. The results are nevertheless included here for completeness (Table 4.7).

Table 4.7 Results from pQCT for Bone Mineral Density (BMD) Values.

	N	Trabecular Density (mg/cm <sup>3</sup> )
Total Group	108	206.35 ± 28.49
Batch I	19	223.68 ± 26.82
Batch II	39	191.59 ± 19.76
Batch III	21	202.88 ± 28.94
Batch IV	29	217.35 ± 29.48

#### 4.6 Results from Correlations

The main objective of this thesis is to correlate the mechanical properties to the density measures of the rat tibia. The mechanical properties, ultimate stress and elastic modulus, were correlated to trabecular density measured using pQCT and average intensity of the cancellous region calibrated using aluminum layer step-wedge. The results are presented in terms of coefficient of determination ( $r^2$ ) values. The rationale behind this is that  $r^2$  represents the strength of the correlation between the different measures of density and mechanical properties. Generally,  $r^2$  values are between 0 and +1.

Tables 4.8 through 4.13 list the various  $r^2$ ,  $b$  and  $P$  values for the correlations between density and mechanical properties. The  $b$  values presented in the table are the exponent for the power law. For Tables 4.8 and 4.9, the density used is the average intensity in aluminum layers for the entire cancellous bone compartment of the RPC specimen, and the mechanical properties are ultimate stress and elastic modulus, respectively. Similarly, Tables 4.10 and 4.11 present results for density as measured by pQCT, and Tables 4.12 and 4.13 use the average intensity in aluminum layers for the platen area only as the density measure. For all of these results (Tables 4.8 through 4.13), correlations were performed using two software packages: SigmaStat and TableCurve 2D.

A common feature of Tables 4.8 through 4.13 is that they all show the results according to each batch and also batches pooled together. Looking at batches individually gives an idea on the variation of correlations with specimen locations and methods followed. Also, this justifies the pooling of batches corresponding to variation in methods followed. Batch I and Batch II had a different specimen location method compared to Batch III and Batch IV, and Batch I had a different exposure time compared to the last three batches. Hence, in order to compare correlations between the various batches and also between various methods, correlations shown among batches and are also pooled together as all four batches, the last three batches, and the last two batches.

In Table 4.8, the  $r^2$  values for all four batches and Batch II from TableCurve 2D differ from that of SigmaStat, as the data are fitted using non-linear robust fit equation for TableCurve 2D. Normal distribution fit was not available for these data sets, as there were a few data points beyond  $\pm 3$  standard deviation (SD). Hence, there is a difference in the  $r^2$  values between the two softwares. Similarly, in Table 4.10 for Batch II, correlation coefficient is unavailable between ultimate stress and pQCT trabecular density using TableCurve 2D due to the presence of two data points that are outliers. TableCurve 2D defines outliers based on  $\pm 3$  SD, based upon least square assumption of normal distribution, or Gaussian errors. In Table 4.11, there is one point that is termed as an outlier and hence, there is no correlation coefficient  $r^2$  value between

elastic modulus and pQCT trabecular density. These data points were not removed to ensure that comparisons between groups could be performed.

Regardless of the softwares used, both linear and power law forms were fitted to the data points of all batches. Tables 4.12 and 4.13 show the correlation between the platen area density (in aluminum layers) and mechanical properties for the last two batches. This data is available only for Batch III and Batch IV of the BMR study owing to the time constraint and better specimen location methods followed.

In Table 4.8, P values for the correlations are mostly less than 0.001, which means that the confidence interval for this data set is more than 99%. For Batch I, SigmaStat shows a zero correlation, but TableCurve 2D gives a correlation coefficient of 0.17. The confidence interval for the Batch III is 96.5%. There is no difference in the correlation coefficient values for the linear correlations between the data from two softwares. The differences between the correlation values for the two softwares, SigmaStat and TableCurve 2D, for All Four Batches, Batch II, and Batch IV occur because of the presence of outlier values. The strongest correlations can be noted for Batch IV, which may be due to the specimen location improvements followed.

In Table 4.9, P values are 0.54 and 0.51 for Batch I and 0.20 and 0.18 for Batch III, which are well below the standard threshold value of 0.05 required for statistical significance. The  $r^2$  values are also extremely low, indicate very weak correlations. For the other batches, there is a confidence interval more than 99%. Comparing Tables 4.8 and 4.9, ultimate stress correlates stronger with average intensity than does elastic modulus, which has been shown in previous studies (Ulrich et al., 1999, Pothuaud, 2002). The  $r^2$  values are generally higher in Table 4.8, although not for all cases. There is no significant difference between the two different softwares for  $r^2$  values for linear and power law fit.

In Tables 4.10 and 4.11, correlations of mechanical properties with pQCT are presented. Correlation coefficients are lower, as there is a difference in the region of interest for the pQCT densities and the location of the RPC specimen. There is no significant difference in the  $r^2$  values for linear and power law fit for the data set in

Tables 4.10 and 4.11. As mentioned earlier, due to the presence of two outliers, there are no correlation coefficient values for Batch II of Table 4.10 and Batch III of Table 4.11.

Tables 4.12 and 4.13 list the  $r^2$ , P and b values for the last two batches for correlation between average intensity of the platen area and mechanical properties. It is interesting to note that there is a strong correlation between mechanical properties and the intensity for the area under the platen. There is no difference between the correlation coefficient from both softwares and P values confirm the strength of the correlations.

Because the last two batches had the most consistent and improved specimen preparation procedures, these results are considered the most reliable and important. The generally higher  $r^2$  values confirm this, and Fig 4.5 through 4.10 show selected plots of data correlated for these batches. Fig 4.5 shows the correlation for the last two batches between the average intensity in terms of aluminum layers and ultimate stress (MPa). Only the power law curves are shown, as it has been shown by previous studies that power law models are generally better for correlations of mechanical properties of cancellous bone (Currey, 1986). The center curve is the regression equation and the other two represent the 99% confidence intervals. Fig 4.6 shows the correlation between the average intensity in aluminum layers and elastic modulus (MPa) for the last two batches. Figs 4.7 and 4.8 are the correlation graphs between pQCT trabecular density and mechanical properties, ultimate stress and elastic modulus (MPa), for the last two batches. Fig 4.9 shows the correlation curves for the last two batches, between ultimate stress and aluminum layer average intensity for the platen area only. Similarly, Fig 4.10 shows the correlation curve between elastic modulus and aluminum layer average intensity for the platen area only, for the last two batches.

Table 4.8 List of  $r^2$  Values and P Values for Correlation Between Average Intensity and Ultimate Stress (b = power law exponent)

Average Intensity (Al. Layers) Vs. Ultimate Stress (MPa)	Power Law				Linear		
	SigmaStat		TableCurve 2D		SigmaStat		TableCurve 2D
	$r^2$	P	$r^2$	b	$r^2$	P	$r^2$
All Four Batches	0.2946	<0.001	0.2196*	1.66*	0.2807	<0.001	0.2807
Batch I	0	1	0.1708	2.35	0.1446	0.1084	0.1445
Last Three Batches	0.3543	<0.001	0.3543	2.12	0.3352	<0.001	0.3352
Batch II	0.3604	<0.001	0.3219&	4.21&	0.4195	<0.001	0.4195
Last Two Batches	0.3590	<0.001	0.3590	2.54	0.3315	<0.001	0.3315
Batch III	0.2126	0.035	0.2126	1.53	0.2239	0.03	0.2240
Batch IV	0.4539	<0.001	0.4183*	2.49*	0.4449	<0.001	0.4449

\* Non-linear Robust Fit Equation using Least Absolute Deviation method

& Non-linear Robust Fit Equation using Lorentzian Minimization method

Table 4.9 List of  $r^2$  Values and P Values for Correlation Between Average Intensity and Elastic Modulus (b = power law exponent)

Average Intensity (Al. Layers) Vs. Elastic Modulus (MPa)	Power Law				Linear		
	SigmaStat		TableCurve 2D		SigmaStat		TableCurve 2D
	$r^2$	P	$r^2$	b	$r^2$	P	$r^2$
All Four Batches	0.2657	<0.001	0.2657	1.87	0.2636	<0.001	0.2636
Batch I	0.0221	0.54	0.0246	0.73	0.0259	0.51	0.0259
Last Three Batches	0.4067	<0.001	0.4067	2.41	0.3858	<0.001	0.3857
Batch II	0.3740	<0.001	0.3740	2.72	0.4001	<0.001	0.4000
Last Two Batches	0.2604	<0.001	0.2674	2.53	0.2496	<0.001	0.2796
Batch III	0.0843	0.20	0.0859	1.23	0.0907	0.18	0.0907
Batch IV	0.4155	<0.001	0.4155	3.23	0.4282	<0.001	0.4283



Table 4.10 List of  $r^2$  Values and P Values for Correlations Between pQCT - Trabecular Density and Ultimate Stress (b = power law exponent)

Trabecular Density pQCT (mg/cm <sup>3</sup> ) Vs. Ultimate Stress (MPa)	Power Law				Linear		
	SigmaStat		TableCurve 2D		SigmaStat		TableCurve 2D
	$r^2$	P	$r^2$	b	$r^2$	P	$r^2$
All Four Batches	0.0492	0.021	0.04496	2.17	0.0592	0.011	0.0592
Batch I	0.0063	0.75	0.0063	0.44	0.0046	0.784	0.0046
Last Three Batches	0.0553	0.027	0.063	1.67	0.0663	0.015	0.0663
Batch II	0.1094	0.04	NA <sup>&amp;</sup>	NA <sup>&amp;</sup>	0.1620	0.011	0.1619
Last Two Batches	0.1692	0.003	0.176	2.32	0.1794	0.002	0.1794
Batch III	0.3034	0.01	0.3174	2.54	0.3095	0.009	0.3094
Batch IV	0.1133	0.074	0.128	2.19	0.1331	0.052	0.1330

<sup>&</sup> Contains two outlier values, which prevented correlation without removing these values

Table 4.11 List of  $r^2$  Values and P Values for Correlations Between pQCT - Trabecular Density and Elastic Modulus (b = power law exponent)

Trabecular Density pQCT (mg/cm <sup>3</sup> ) Vs. Elastic Modulus (MPa)	Power Law				Linear		
	SigmaStat		TableCurve 2D		SigmaStat		TableCurve 2D
	$r^2$	P	$r^2$	b	$r^2$	P	$r^2$
All Four Batches	0.0213	0.132	0.0213	0.96	0.0213	0.13	0.214
Batch I	0	1	0.0002	0.04	0.0016	0.8689	0.0016
Last Three Batches	0.0293	0.108	0.0306	1.24	0.0323	0.0917	0.0323
Batch II	0.1552	0.013	0.2718	5.65	0.2127	0.003	0.2126
Last Two Batches	0.0837	0.042	0.091	1.864	0.0962	0.03	0.096
Batch III	0.1840	0.06	NA <sup>&amp;</sup>	NA <sup>&amp;</sup>	0.2355	0.026	0.2355
Batch IV	0.0383	0.31	0.0417	1.36	0.0432	0.28	0.0431

<sup>&</sup> Contains one outlier value, which prevented correlation without omitting these values

Table 4.12 List of  $r^2$  Values and P Values for Platen Area Only for Correlation Between Average Intensity and Ultimate Stress (b = power law exponent)

Average Intensity (Al. Layers) Vs. Ultimate Stress (MPa)	Power Law				Linear		
	SigmaStat		TableCurve 2D		SigmaStat		TableCurve 2D
	$r^2$	P	$r^2$	b	$r^2$	P	$r^2$
Last Two Batches	0.3750	<0.001	0.3750	1.77	0.3704	<0.001	0.3703
Batch III	0.2739	0.015	0.2739	1.17	0.2853	0.013	0.2852
Batch IV	0.4537	<0.001	0.4537	2.22	0.4735	<0.001	0.4735

Table 4.13 List of  $r^2$  Values and P Values for Platen Area Only for Correlation Between Average Intensity and Elastic Modulus (b = power law exponent)

Average Intensity (Al. Layers) Vs. Elastic Modulus (MPa)	Power Law				Linear		
	SigmaStat		TableCurve 2D		SigmaStat		TableCurve 2D
	$r^2$	P	$r^2$	b	$r^2$	P	$r^2$
Last Two Batches	0.3154	<0.001	0.3154	1.87	0.3125	<0.001	0.3125
Batch III	0.1563	0.076	0.1563	1.18	0.1631	0.07	0.1631
Batch IV	0.4453	<0.001	0.4453	2.35	0.4826	<0.001	0.4825

# Last Two Batches - Average Intensity (AL) Vs. Ultimate Stress (MPa)

Rank 2 Eqn 8156 Power\_(a,b)  
 $r^2=0.35896623$  DF Adj  $r^2=0.3316882$  FitStdErr=0.69421859 Fstat=26.87905  
a=0.0041406807  
b=2.5357214

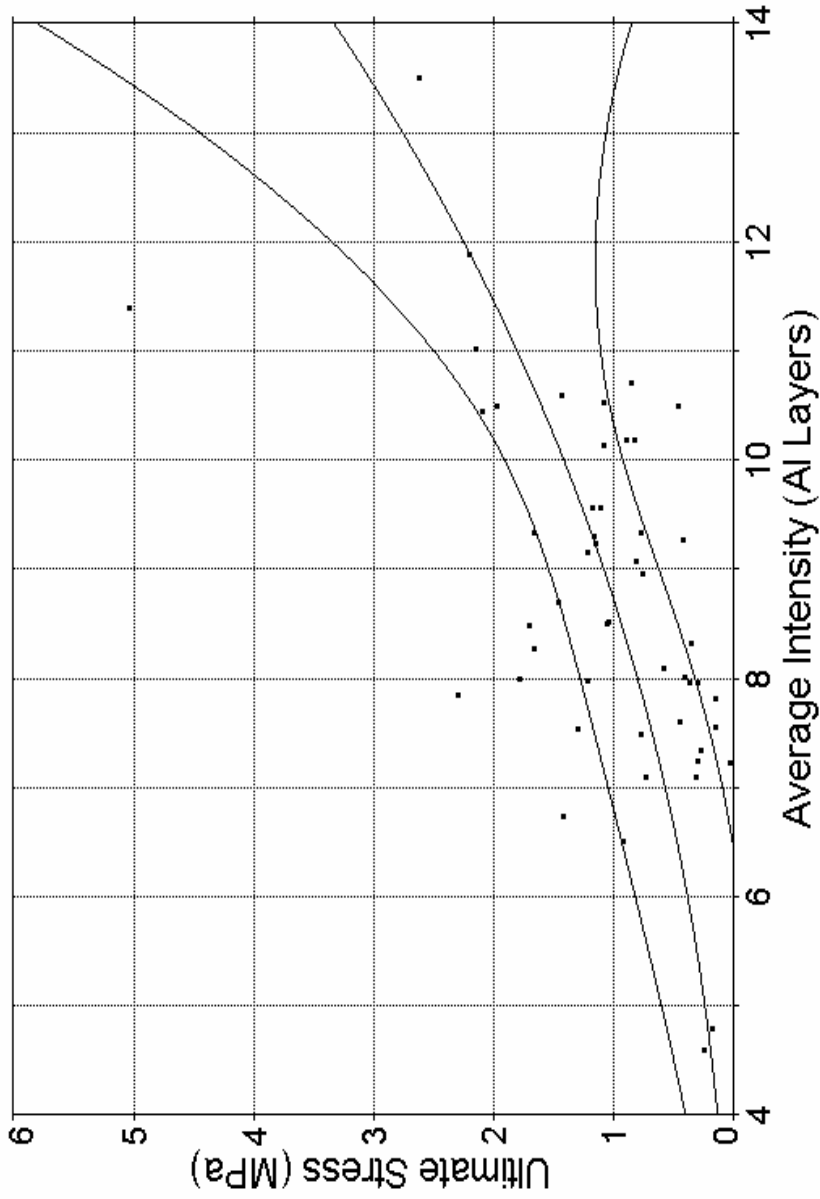


Fig. 4.5 Correlation Curve for the Last Two Batches (Power Law)  
Ultimate Stress (MPa) vs. Average Intensity (AL Layers)

# Last Two Batches- Average Intensity (AL) Vs. Elastic Modulus (MPa)

Rank 2 Eqn 8156 Power\_(a,b)

$r^2=0.26738627$  DF Adj  $r^2=0.23621121$  FitStdErr=34.036181 Fstat=17.518837

a=0.16594101

b=2.5280182

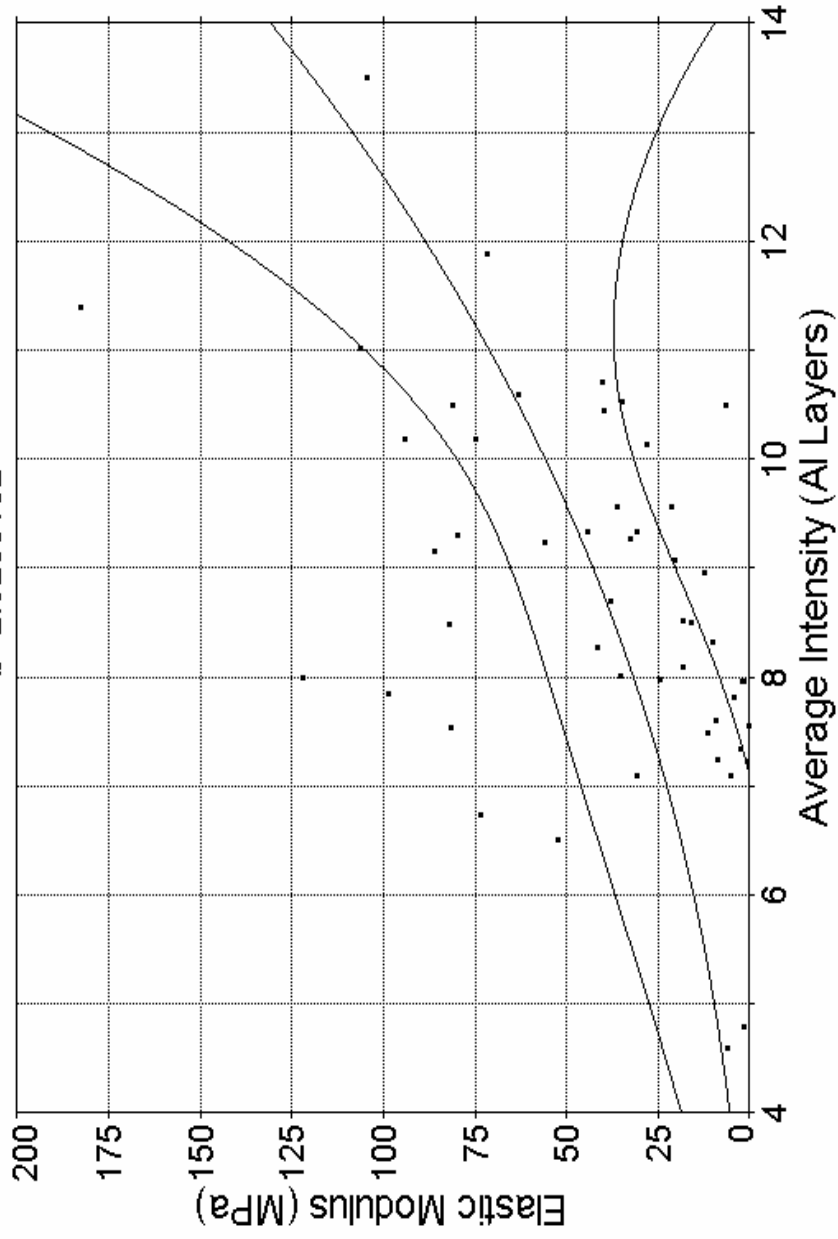


Fig 4.6 Correlation Curve for the Last Two Batches (Power Law)  
Elastic Modulus (MPa) vs. Average Intensity (AI Layers)

Last Two Batches - Trabecular Density pQCT Vs. Ultimate Stress (MPa)

Rank 13 Eqn 8001 Power Law(a,b)  
 $r^2=0.17592316$  DF Adj  $r^2=0.14085606$  FitStdErr=0.78711763 Fstat=10.246995  
 $a=4.4116803e-06$   
 $b=2.3148803$

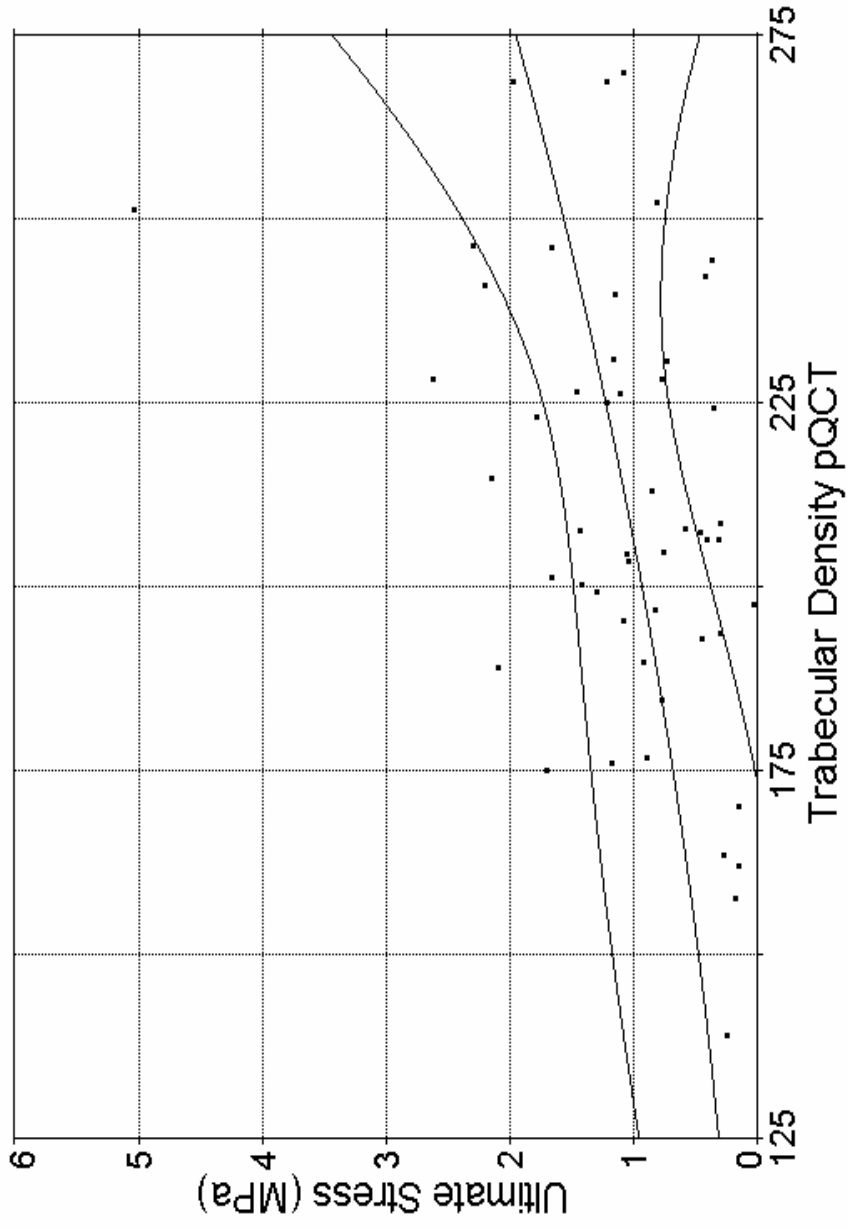


Fig 4.7 Correlation Curve for the Last Two Batches (Power Law)  
 Ultimate Stress (MPa) vs. Trabecular Density pQCT

# Last Two Batches - Trabecular Density pQCT Vs. Elastic Modulus (MPa)

$r^2=0.091123996$  DF Adj  $r^2=0.052448421$  FitStdErr=37.91016 Fstat=4.8124846  
 Rank 16 Eqn 8156 Power\_(a,b)  
 $a=0.001958635$   
 $b=1.8648625$

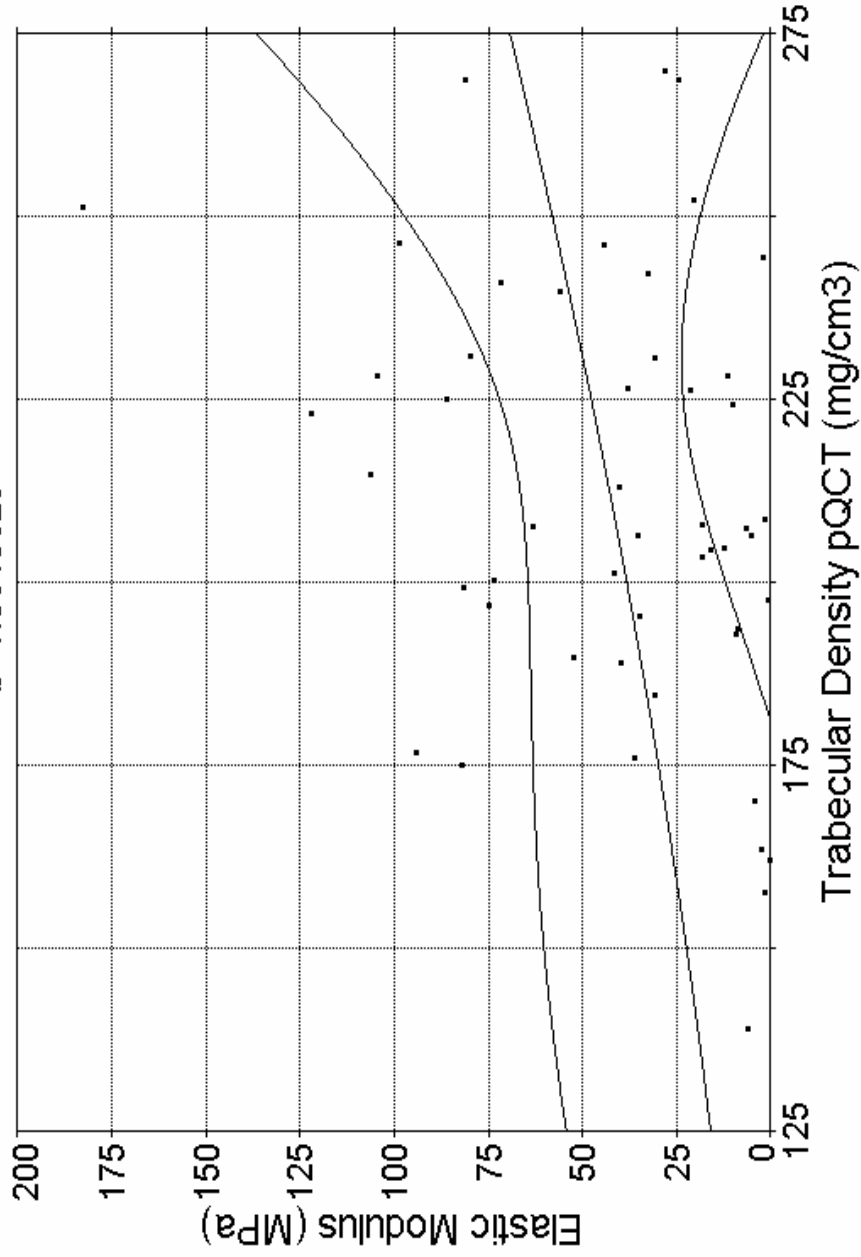


Fig 4.8 Correlation Curve for the Last Two Batches (Power Law)  
Elastic Modulus (MPa) vs. Trabecular Density pQCT

### Last Two Batches - Average Intensity (Al Layers) Vs. Ultimate Stress (MPa)

Rank 2 Eqn 8156 Power\_(a,b)  
 $r^2=0.37498564$  DF Adj  $r^2=0.34838928$  FitStdErr=0.68511135 Fstat=28.798235  
 $a=0.039209233$   
 $b=1.7739924$

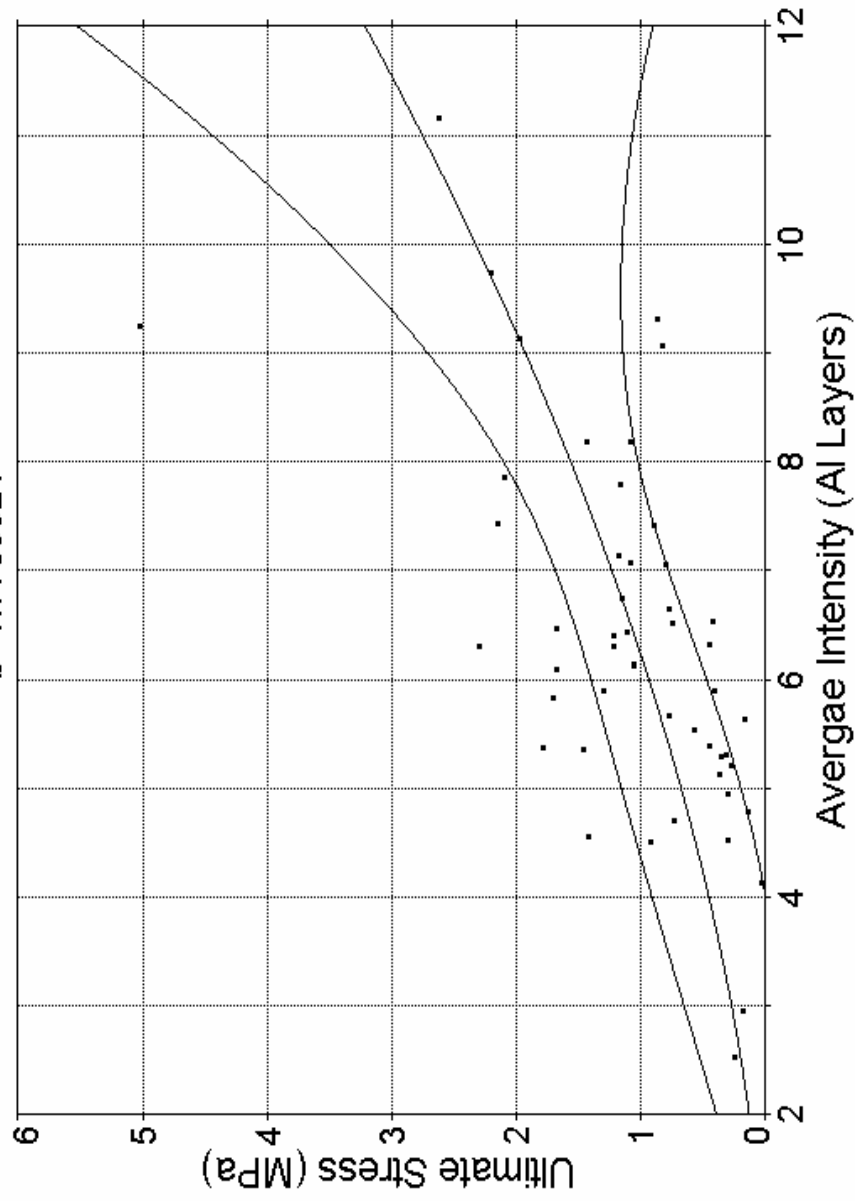


Fig 4.9 Correlation Curve for the Last Two Batches, Platen Area Only (Power Law)  
 Ultimate Stress (MPa) vs. Average Intensity (Al. Layers)



# Last Two Batches - Average Intensity (Al Layers) Vs. Elastic Modulus (MPa)

Rank 4 Eqn 8156 Power\_(a,b)  
 $r^2=0.31542286$  DF Adj  $r^2=0.28629192$  FitStdErr=32.900998 Fstat=22.116277  
a=1.2729131  
b=1.8739442

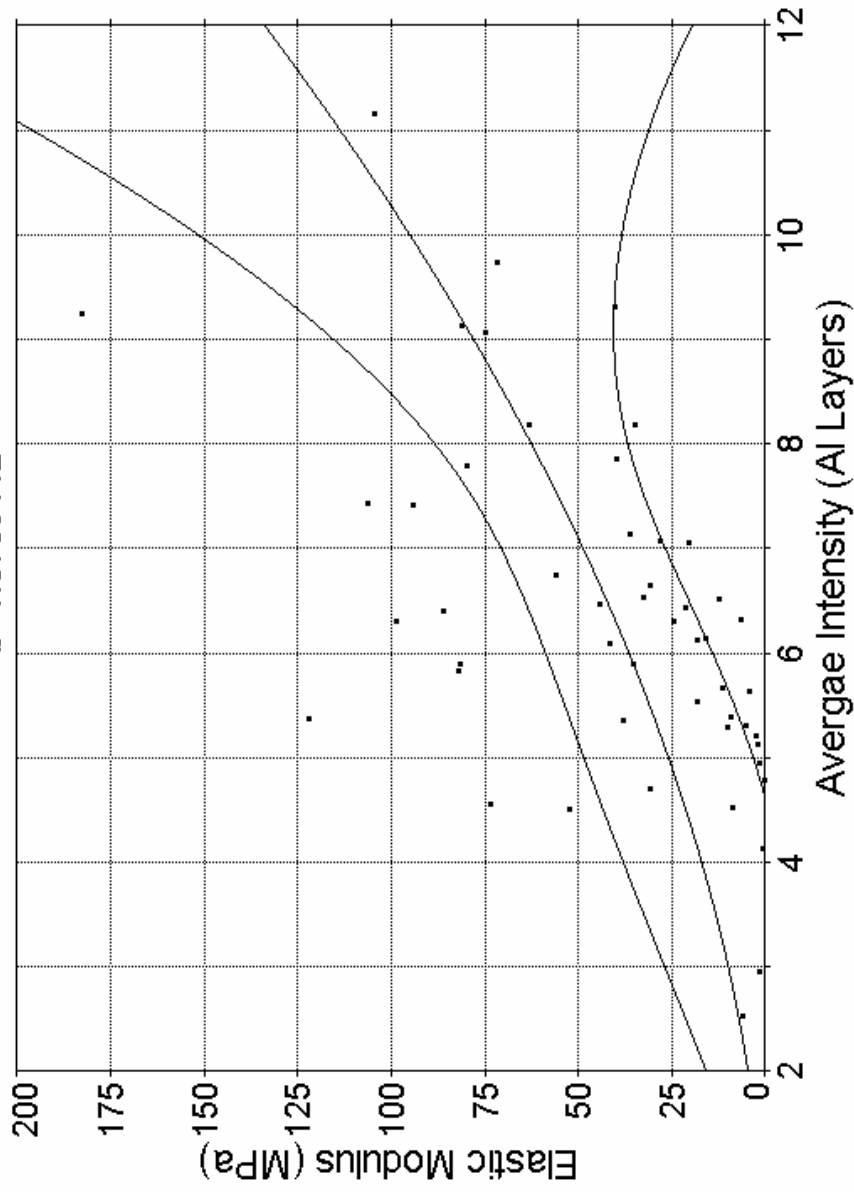


Fig 4.10 Correlation Curve for the Last Two Batches, Platen Area Only (Power Law)  
Elastic Modulus (MPa) vs. Average Intensity (Al. Layers)

## **CHAPTER V**

### **DISCUSSION**

#### **5.1 Introduction**

This chapter will discuss the effectiveness of the new methods and the rationale behind this thesis. The results from correlation of the mechanical properties will be discussed in detail. The purpose of this thesis was to determine the relationship between mechanical properties of the rat bone determined the reduced platen compression test with various density measures like pQCT and radiography techniques. This thesis also deals with improving methods for the location of the specimen for RPC testing, and aluminum step-wedge preparation and analysis. The results will be discussed in terms of their rationale, effectiveness in meeting the objectives, and broader impact.

#### **5.2 Specimen Location**

Specimen location is one of the most important steps of the reduced platen compression testing. Cancellous bone is a very diverse material and it is important to test the largest percentage of the available tissue in order to obtain a truly representative response. Specimens located too far from the growth plate offer only a minimal amount of cancellous bone. Locations too near the growth plate contain primary spongiosa, which is not true mature cancellous bone. Also, it is necessary to have specimens that do not contain any growth plate.

The radiographs of the proximal tibia were studied to pick the best location for specimens. The ideal specimen location is distal to the growth plate, but not too close and not too far from it. It has been shown in previous experiments that an anterior view of the radiograph is suited best for specimen location (Rogers, 2002). Attempting to use the procedure for specimen location devised by Rogers (2002) for batches III and IV suggested that the reference landmarks (lateral meniscus tubercles)

would not be effective for these bones so a new, hopefully improved and more universal, method was developed. The details were presented previously in section 3.5 (pg. 23-26). Briefly, the new procedure began by sketching a reference line through the growth plate. A second line was then drawn parallel to the reference line at a distance of 1.75 mm. 1.75 mm was chosen, as the specimens were well clear of the growth plate and they also had good cancellous bone for RPC testing. After selecting the location of the specimen, a line was sketched along the proximal end of the tibia, tangent to the “highest” intercondylar tubercles. While cutting the specimen, the long axis of the tibia should be aligned perpendicular to the blade of the cutting saw. But, this is very difficult, as the tibia is not straight along the diaphysis. Care should be taken while cutting to see to that the growth plate is parallel to the face of the blade.

The above method was adopted to prepare and test specimens from batches III and IV of the bone muscle recovery study. Following the new procedure for the last two batches tested, there were only two specimens with growth plate in a total of fifty. By contrast, of the 58 specimens in the first two batches, 8 were noted to have some growth plate present. Hence, 1.75 mm from the growth plate was determined to be the best distance for the location of specimens for RPC testing.

### **5.3 Radiography Technique**

Aluminum step-wedges were used for radiographic technique analysis of the reduced platen compression specimens. The rationale behind the usage of aluminum step-wedges was to standardize radiographically based density measures to factor out potential differences in film, exposure details, and processing procedures. Previous studies have shown that average intensity of cancellous and cortical bone for rat specimens lies between 3 to 35 layers of the aluminum step-wedge (Luthringer, 2001). Table 4.5 (pg. 46) shows that the average aluminum layers for cancellous bone was 7.11 for all the batches and Figures 4.1, 4.2, 4.3 and 4.4 show that there is a slight difference between the curves calibrated for the four different batches. One of the major discrepancies between the four groups is that the last three have a different radiograph

exposure time from the first batch. This is most likely one of the major reasons for the differences that occur between the groups. Also, the first two batches have a different set of aluminum step-wedges from the last two groups.

#### **5.4 Correlations**

The purpose of performing a correlation study of mechanical properties and density measures is to quantify the importance and significance of relationships between the variables. Similar correlations are the focus of many past and continuing research studies because of clinical interest in understanding the predictive value of the density measures done for post-menopausal women and in bone loss studies done during weightlessness (space flight) for estimating the mechanical strength of cancellous bone. P values for correlations represent the probability of being wrong in concluding that there is a true association between the variables. The smaller the P values the greater the probability that one variable can be used to predict the other. Traditionally, when the value of P is less than 0.05, it is concluded that one variable can be reasonably predicted in terms of the other. It is encouraging that the P values in Tables 4.8 through 4.13 are generally quite low for most cases. The strength of the correlation is indicated by the  $r^2$  value. It should be recalled that the numerical value for the  $r^2$  quantifies the proportion of the variation in one quantity that can be explained by the variation in the other quantity being correlated (Metcalf, 1994). For example,  $r^2$  value of 0.63 means that 63% of the variation in one quantity is due to the variation in the other. In this sense, the results in Tables 4.8 through 4.13 are not as encouraging. The maximum value is 0.48 and many are less than 0.30.

Comparing results from Tables 4.8 through 4.13, it can be seen that mechanical properties correlate more strongly with aluminum layer average intensity than with pQCT density. One of the reasons for the weak correlations with pQCT density could be the difference between RPC specimen location and density measurement location. For mechanical testing, the average distance from the tibial plateau to the top (proximal surface) of the tested specimen is  $3.67 \pm 0.35$  mm, which

also means that the average distance to the distal end of the tested specimen is  $5.67 \pm 0.35$  mm. For pQCT density measurements, however, serial scans were taken at 5, 5.5 and 6-mm distal to the tibial plateau and the values were averaged from all three slices. Each scan slice was 0.5 mm thick and centered at these three locations. Thus, the full region scanned by pQCT was from 4.45 mm to 6.25 mm from the tibial plateau. Hence, there is a variation between the specimen location for mechanical testing and pQCT density measurements, although there is also a considerable overlap in these regions as well (roughly 1 mm or half the RPC specimen thickness).

The results also show that correlations are generally stronger (higher  $r^2$  values) for aluminum layer intensities analyzed for the platen area only compared to those for the entire region of cancellous bone. Considering Tables 4.12 and 4.13 for the platen area only, Batch III seems to be a little weak in correlation compared to Batch IV and both batches together. It should be noted that there were at least three different people involved in cutting the specimens for this batch, which could have resulted in some inconsistency in cutting procedures.

Correlation results from the first batch of the BMR study vary significantly from the rest of the batches because of numerous differences between the testing methods followed. Exposure time for radiographs was 100 seconds for Batch I and 80 seconds for the last three batches. Cutting procedures followed for the first two batches were different from those of the last two batches. For the first two batches, the first cut distance was measured from above the lateral intercondylar tubercle of the proximal end of the tibia to a line drawn below the growth plate of the specimen. For the last two batches, the method specified in section 3.6 was followed.

Correlations of mechanical property with densities were performed using both power law and linear fit equations. Currey (1986) has shown that power law models are better for bone both statistically and for mechanistic reasons. The results shown in Tables 4.8 through 4.13 do not show significant differences between the power law and linear fit model in most instances. Morgan et al. (2003) have pointed out in their recent article, however, that studies for which specimen densities do not span a wide range

typically yield similar correlations for linear and power law models. Also, Hvid et al. (1989) compared linear and power law correlations for mechanical properties of cylindrical specimens from the proximal tibia of cadaver knees. They conducted both destructive and non-destructive tests and determined densities two ways: (1) by physically measuring, and (2) by QCT. A total of 100 samples were tested and analyzed, and  $r^2$  values were higher for the power law than linear models but not dramatically so. Specifically, for elastic modulus and apparent ash density,  $r^2$  was 0.66 for power law and 0.60 for linear. For ultimate stress,  $r^2$  was 0.82 for the power law and 0.72 for linear. Ebbesen et al. (1999) have also compared power law and linear correlations, but it should be noted that they tested vertebral bodies ( $n = 101$ ) that included both cancellous and cortical bone components. Results for correlating stress and BMD gave  $r^2$  values of 0.75 for power law and 0.71 for linear for BMD by DEXA. They also measured BMD by QCT and pQCT. For QCT the results were the opposite, with  $r^2$  values of 0.64 for power law and a higher value of 0.75 for linear. For pQCT,  $r^2$  was 0.86 for both power law and linear. In this context, the present results are not atypical.

Generally, exponent  $b$  of the power law varies between 1 and 3 (Carter, 1977). When compared with the results obtained for this study, it is noted that this is true for all the power law correlations performed, except for Batch II (Table 4.8) between ultimate stress and average intensity in terms of aluminum layers. One of the major reasons for this aberration is the presence of outliers in the data set. Non-linear robust fit equation method was followed for this batch, as the data set contains values that were beyond  $\pm 3$  SD. Also, it should be noted that, when the outlier was removed, the  $r^2$ ,  $P$  value and  $b$  fitted the pattern set by the other data points. The outliers were not removed from the data set, however, so as to facilitate comparison between groups and between the combination of batches. It should be noted that when the batches were pooled together, the influence of the outlier decreased significantly. It is also useful to compare the values for the exponent  $b$  in the current research with those found in the other studies. The values in Chapter IV can be summarized as follows:

Table 5.1 Ranges of Exponent b

	Ultimate Stress	Elastic Modulus
Aluminum Layers (Cancellous bone)	1.53 to 4.21	1.87 to 3.23
pQCT	1.67 to 2.54	1.86 to 5.65
Aluminum Layers (Platen Area)	1.17 to 2.22	1.18 to 2.35

The study by Morgan et al. (2003) reported b values ranging from 1.49 to 2.18 for elastic modulus (ultimate stress was not determined). Ebbesen et al. (1999) did not report elastic modulus but found values of b of 2.00 for correlating stress with BMD by DEXA and 0.62 for QCT and 1.44 for pQCT. Langton et al. (1996) studied specimens from the calcaneus of cadavers and measured apparent density physically. They found b values of 2.92 for correlating with ultimate stress ( $r^2 = 0.88$ ) and 3.13 for correlating with elastic modulus ( $r^2 = 0.89$ ). The present results compare quite favorably with these findings from other studies, despite numerous differences in experimental details. This is particularly true if we consider the results for Batches III and IV combined for aluminum layer intensity of the platen area only (Table 5.1), which are the most consistent and reliable results.

A final consideration is to compare correlations for ultimate stress and elastic modulus. Reviewing Tables 4.8 through 4.13, ultimate stress generally correlates better (i.e., higher  $r^2$  values) with the density measures than does elastic modulus. One of the reasons is that elastic modulus is dependant on the direction of testing and the mechanical properties dependant on the metaphyseal type and the donor of the bones. It should also be noted that the compression testing is confined compression and hence a lot of issues arise in terms of how true these elastic properties are with regard to the boundary conditions. Also, Gibson (1985) has shown that the spread of data for elastic

modulus is larger because of the variability inherent in the Young's modulus of the cell wall of the bone, and the varying strain rates during testing. Previous studies (Gibson, 1985) have shown that use of confining ring testing results in the data being higher than that which would be measured in an unconfined uniaxial test by a factor of one-third. Furthermore, for the study mentioned previously by Hvid et al. (1989), the  $r^2$  values were higher for ultimate stress compared to elastic modulus (0.78-0.82 vs. 0.60-0.66, respectively). Majumdar et al. (1998) conducted only linear correlations and measured BMD by QCT for 94 cadaver specimens (calcaneus, distal femur, proximal femur, and vertebrae). They found  $r^2$  values of 0.56 for ultimate stress and 0.34 for elastic modulus. Thus, the findings in the present research are generally consistent with most previous studies.



## CHAPTER VI

### CONCLUSIONS AND RECOMMENDATIONS

#### 6.1 Conclusions

In this study, existing methods for reduced platen compression testing of rodent proximal tibia were improved. Improvements have led to better specimen preparations and more accurate location of RPC specimens that have consistent dimensions. This study also deals with correlation of mechanical properties to the various density measures for the proximal tibia.

The specimen location for the reduced platen testing of the proximal tibia metaphysis was improved by using the growth plate as a plane of reference. Using the radiograph, a line was sketched through the growth plate and another at a distance of 1.75 mm below the growth plate and parallel to it. Precise RPC specimens can be prepared by aligning the highest ridges of the tibial plateau of the proximal tibia with the saw blade and proper gripping of the specimen.

Platen sizing of the specimens was improved by using the endocortical circle methods. Using the radiographs of the specimens, circles were sketched on the cancellous region of the specimen and the diameters were noted. This circle is termed as the endocortical circle, as it just encircles the cancellous region, without touching the cortical shell. For platen sizing, 69% of the diameter was used. Diameter of the platens were deliberately chosen smaller than the endocortical circle, so as to reduce errors including testing of cortical shell during the reduced platen compression. Such errors would alter the data drastically.

Correlations of mechanical properties of the proximal tibia to the average intensity in terms of aluminum layers resulted in some interesting findings. Strong correlation was noted between ultimate stress of the proximal tibia to the average pixel intensity by radiograph. Elastic modulus correlated best with the last batch tested in the bone muscle recovery study and weakly with the first batch. The last two batches yielded

the best results for correlations because of improved specimen preparation methods and platen sizing. There were only two specimens in fifty that had growth plate, compared to eight in ninety-nine of the first two batches. Mechanical properties correlated strongly with average intensity of the tested region, i.e. with the average aluminum layer intensity of the 69% of the endocortical circle diameter.

Trabecular density of the peripheral quantitative computed tomography (pQCT) correlates weakly with the mechanical properties. One of the reasons for this could be that pQCT measurements are made at a lower site than the specimen tested. However, ultimate stress correlates to some degree with the last two batches tested. This suggests that specimen location for the last two batches have improved with the changes made. Elastic modulus correlations with trabecular density are weaker compared to the ultimate stress. It correlates best with the second and the third batch and has no correlation with the first batch.

## **6.2 Recommendations**

A few minor enhancements can be done to fine tune the reduced platen compression testing methods. Specimen location can likely be further improved by adapting a method of judging the location and end of the growth plate by external means so as to reduce the time taken in trying to judge the radiograph of the specimen. Sketching lines parallel to the growth plate at a distance of 1.75 mm is error-prone, as it has to be done manually and judgement of location of the lines varies with the user. Also, handling of the bones during cutting plays an important role in the accuracy of the final RPC specimen. Due to the curved nature of the proximal tibia, handling of the bones should be done with great care. As much as possible, it might help if the same person does the entire cutting of the bones or at least the same procedure is followed for every specimen cut.

Correct selection of platen size for the reduced platen compression testing is essential for best results. Current methods require tracing the endocortical circle on the radiograph of the specimen, measuring the diameter and choosing a platen, which is 69%

of the actual endocortical circle diameter. This is followed by visual examination, to ensure that no portion of the platen touches the cortical shell. With better equipment like a magnifying glass, the diameter may be able to be increased up to 75% of the endocortical circle, which would increase the amount of cancellous bone tested. Increasing the size of the diameter further also increases the risk of testing the connecting tissue in between the cortical shell and cancellous bone, and testing the cortical shell accidentally.

Density measurements made using pQCT should be done at the same location as that as the RPC specimen. This increases the probability of better correlations with mechanical properties.

Other issues that can be addressed include incorporating custom sized platen for the RPC testing. Preliminary studies have shown that this may give better results than using round platen for testing. Also, consistency in the procedures followed will lead to better results. This study has shown that the best exposure time for average intensity using aluminum layers is 80 seconds.

## REFERENCES

- Bay B.K., 1995. Texture correlation: a method for the measurement of detailed strain distributions within trabecular bone. *Journal of Orthopaedic Research* 13, 258-267.
- Bloomfield, S.A, Allen, M.R., Hogan, H.A., Delp, M.D., 2002. Site- and compartment-specific changes in bone with hindlimb unloading in mature adult rats. *Bone* 31, 149-157.
- Brodt, M.D., Ellis, C.B., Taniguchi, J., Silva, M.J., 2001. Accuracy of bone density and area measurements from pQCT. 47<sup>th</sup> Annual Meeting, Orthopedic Research Society, Feb 2001, San Francisco, CA.
- Bronzino, J.D., Jaron, D., Neuman, M.R., Onaral, B., Webster, J., 1995. *The Biomedical Engineering Handbook*. CRC Press, Boca Raton, FL.
- Carter, D.R., Hayes, W.C., 1976. Bone compressive strength: the influence of density and strain rate. *Science* 194, 1174-1175.
- Carter, D.R., Hayes, W.C., 1977. The compressive behavior of the bone as a two-phase porous structure. *Journal of Bone and Joint Surgery* 59A, 954-962.
- Ciarelli M.J., Goldstein S.A., Kuhn J.L., Cody D.D., Brown M.B., 1991. Evaluation of orthogonal mechanical properties and density of human trabecular bone from the major metaphyseal regions with materials testing and computed tomography. *Journal of Orthopaedic Research* 9, 674-682.
- Cowin, S.C., 1989. *Bone Mechanics*. CRC Press, Boca Raton, FL.
- Cowin, S.C., 2001. *Bone Mechanics Handbook*, 2<sup>nd</sup> edition. CRC Press, Boca Raton, FL.
- Cummings, S.R., Cosman, F., Jamal, S.A., 2002. *Osteoporosis – An evidence-based guide to prevention and management*. American College of Physicians, Philadelphia, PA.
- Currey, J.D., 1969. The mechanical consequences of variation in the mineral content of bone. *Journal of Biomechanics* 2, 1-11.
- Currey, J.D., 1986. Power law models for the mechanical properties of cancellous bone. *Engineering in Medicine* 15, 153-154.
- Currey, J.D., 2002. *Bones: Structure and Mechanics*. Princeton University Press, NJ.

- Ebbesen, E.N., Thomsen, J.S., Beck-Nielsen, H., Nepper-Rasmussen, H.J., Mosekilde, Li., 1999. Lumbar vertebral body compressive strength evaluated by dual-energy X-ray absorptiometry, quantitative computed tomography and ashing. *Bone* 25, 713-724.
- Engesaeter, L.B., Ekeland, A., Langeland, N., 1978. Methods for testing the mechanical properties of the rat femur. *Acta Orthopaedica Scandinavica* 49, 512-518.
- Fyhrie, D.P., Vashishth, D., 2000. Bone stiffness predicts strength similar for human vertebral cancellous bone in compression and for cortical bone in tension. *Bone* 26, 169-173.
- Galante, J., Rostoker, W., Ray, R. D., 1970. Physical properties of trabecular bone. *Calcified Tissue Research* 5, 236-246.
- Gray, H., 1977. *Gray's Anatomy*. Grammercy Books, New York.
- Gibson, L.J., 1985. The mechanical behavior of cancellous bone. *Journal of Biomechanics* 18, 317-328.
- Goulet, R.W., Goldstein, S.A., Ciarelli, M.J., Kuhn, J.L., Brown, M.B., Feldkamp, L.A., 1994. The relationship between the structural and orthogonal compressive properties of trabecular bone. *Journal of Biomechanics* 27, 375-389.
- Harms, K. (2000). Reduced platen compression test verification. Graduate research assignment, Dr. Harry Hogan, Texas A&M University, College Station.
- Hernandez, C.J., Beaupre, G.S., Keller, T.S. and Carter, D.R., 2001. The influence of bone volume fraction and ash fraction on bone strength and modulus. *Bone* 29, 74-78.
- Hodgkinson, R., Currey, J., 1990. The effect of variation in structure on the Young's modulus of cancellous bone: a comparison of human and non-human material. *Proc of Institute of Mechanical Engineers* 204, 115-121.
- Hvid, I., Bentzen, S.M., Linde, F., Mosekilde, L., Pongsoipetch, B., 1989. X-ray quantitative tomography: the relations to physical properties of proximal tibial trabecular bone specimens. *Journal of Biomechanics*, 22, 837-844.
- Keller, T.S., 1994. Predicting the compressive mechanical behavior of bone. *Journal of Biomechanics* 27, 1159-1168.
- Keaveny, T.M., 1997. Mechanistic approaches to analysis of trabecular bone. *Forma* 12, 267-275.

- Keaveny, T.M., Pinilla, T.P., Crawford, R.P., Kopperdahl, D.L., Lou, A., 1997. Systematic and random errors in compression testing of trabecular bone. *Journal of Orthopaedic Research* 15, 101–110.
- Langton, C.M., Njeh, C.F., Hodgkinson, R., Currey, J.D., 1996. Prediction of mechanical properties of the human calcaneus by broadband ultrasonic attenuation. *Bone* 18, 495-503.
- Luthringer, K., 2001. Correlation study between the mechanical properties and the pixel density of the left femur from the ovariectomized rats. Honors independent research, Texas A&M University, College Station.
- Marcus, R., Feldman, D., Kelsey, J., 1996. *Osteoporosis*. Academic Press, San Diego, CA.
- Majumdar, S., Kothari, M., Augat, P., Newitt, D.C., Link, T.M., Lin, J.C., Lang, T., Lu, Y., Genant, H.K., 1996. High resolution magnetic resonance imaging: three-dimensional trabecular bone architecture and biomechanical properties. *Bone* 22, 445-454.
- Martin, R.B., Burr, D.B., 1989. *Structure, Function and Adaptation of Compact Bone*. Raven Press, New York.
- Martin, R.B., Burr, D.B., Sharkey, N.A., 1998. *Skeletal Tissue Mechanics*. Springer-Verlag Publishing, New York.
- McElhaney, J.H., 1966. Dynamic response of bone and muscle tissue. *Journal of Applied Physiology* 21, 1231-1236.
- Metcalf, A.V., 1994. *Statistics in Engineering*. Chapman & Hall, Great Britain, UK.
- Morey-Holton, E.R., Globus, R.K., 1998. Hindlimb unloading of growing rats: a model for predicting skeletal changes during space flight. *Bone* 22 (5), 83S-88S.
- Morgan, E.F., Bayraktar, H.H., Keaveny, T.M., 2003. Trabecular bone modulus – density relationships depend on anatomic site. *Journal of Biomechanics* 36, 897-904.
- Muller, R., Gerber, S.C., Hayes, W.C., 1998. Micro-compression: a novel technique for the nondestructive assessment of local bone failure. *Technology and Health Care* 6, 433–444.

- Nicholson, P.H.F., Cheng, X.G., Lowet, G., Boonen, S., Davie, M.W.J., Dequeker, J., Van der Perre, G., 1997. Structural and material mechanical properties of human vertebral cancellous bone. *Medical Engineering and Physics* 19, 729-737.
- Osteogenesis Imperfecta Foundation – Home Page: Online statement; Available at <Http://www.oif.org/BoneStruct> Accessed: 'Feb 8, 2003'.
- Patten, B.M., Carlson, B.M., 1974. *Foundations of Embryology*. McGraw-Hill, New York.
- Pelker, R.R., Friedlander, G.E., Punjabi, M.M., Markham, T., Moen, C.J., 1984. Effects of freezing and freeze drying on the biomechanical properties of rat bone. *Journal of Orthopedic Research* 1, 405-411.
- Pothuau, L., Rietbergen, B.V., Mosekilde, L., Beuf, O., Levitz, P., Benhamou, C.L., Majumdar, S., 2002. Combination of topological parameters and bone volume fraction better predicts the mechanical properties of trabecular bone. *Journal of Biomechanics* 35, 1091-1099.
- Rice, J.C., Cowin, S.C., Bowman, J.A. (1988). On the dependence of the elasticity and strength of the cancellous bone on apparent density. *Journal of Biomechanics*, 21, 155-168.
- Rogers, W.E., 2002. *Methods and modeling for the reduced platen compression of cancellous bone in the rodent proximal tibia*. M.S. Thesis, Texas A&M University, College Station.
- Ruhmann, S.P., 1998. *Methods for testing the strength of cancellous bone and tested method effects on cortical bone in the ovariectomized rat*. M.S. Thesis, Texas A&M University, College Station.
- Siegel, I.M., 1998. *All About Bone: An Owner's Manual*. Demos Medical Publishing, Inc., New York.
- Ulrich, D., VanRietbergen, B., Laib, A., Rügsegger, P., 1999. The ability of three-dimensional structural indices to reflect mechanical aspects of trabecular bone. *Bone* 25, 55-60.
- VanAudsal, T., Liao, D.W., Bloebaum, R.D., Hoffmann, A.A., 2001. Radiographic determination of bone density in the proximal human tibia. 47<sup>th</sup> Annual Meeting, Orthopedic Research Society, Feb 2001, San Francisco, CA.
- Vaughan, J., 1975. *The Physiology of Bone*, 2<sup>nd</sup> Edition. Oxford University Press, New York.

Vaughan, J., 1981. *The Physiology of Bone*, 3<sup>rd</sup> Edition. Oxford University Press, New York.

Weiss, L., 1983. *Histology. Cell and Tissue Biology*. Elsevier Biomedical, New York.

White, T.D., 2000. *Human Osteology*. Academic Press, San Diego, CA.

Yates, A.J., Ross, P.D., Lydick, E., Epstein, R.S., 1995. Radiographic absorptiometry in the diagnosis of osteoporosis. *American Journal of Medicine* 98(2A), 41S-47S.



## **APPENDIX I**

### **VALUES GENERATED FOR CALIBRATION CURVES PIXELS TO ALUMINUM LAYER DENSITY**

<b>Batch I</b>	
<b>Layers Of Aluminum</b>	<b>Equation Generated Pixel Intensity</b>
3	3.13
4	2.97
5	5.17
6	9.30
7	14.97
8	21.85
9	29.65
10	38.11
11	46.99
12	56.11
13	65.28
14	74.35
15	83.18
16	91.65
17	99.66
18	107.12
19	113.94
20	120.07
21	125.46
22	130.06
23	133.87
24	136.87
25	139.10
26	140.60
27	141.44
28	141.72
29	141.58
30	141.21
31	140.82
32	140.71
33	141.19
34	142.69
35	145.67

<b>Batch II</b>	
<b>Layers Of Aluminum</b>	<b>Equation Generated Pixel Intensity</b>
3	7.11
4	7.87
5	13.04
6	21.13
7	31.02
8	41.83
9	52.97
10	63.99
11	74.63
12	84.75
13	94.30
14	103.29
15	111.76
16	119.81
17	127.50
18	134.90
19	142.06
20	148.99
21	155.70
22	162.13
23	168.22
24	173.89
25	179.03
26	183.57
27	187.44
28	190.61
29	193.13
30	195.16
31	196.96
32	198.97
33	201.83
34	206.41
35	213.89

<b>Batch III</b>	
<b>Layers Of Aluminum</b>	<b>Equation Generated Pixel Intensity</b>
3	9.00
4	11.99
5	18.54
6	27.56
7	38.19
8	49.71
9	61.60
10	73.44
11	84.94
12	95.89
13	106.17
14	115.73
15	124.55
16	132.64
17	140.06
18	146.87
19	153.14
20	158.92
21	164.29
22	169.28
23	173.95
24	178.31
25	182.38
26	186.16
27	189.66
28	192.87
29	195.80
30	198.47
31	200.92
32	203.23
33	205.53
34	208.01
35	210.94

<b>Batch IV</b>	
<b>Layers Of Aluminum</b>	<b>Equation Generated Pixel Intensity</b>
3	3.60
4	8.05
5	15.32
6	24.58
7	35.13
8	46.44
9	58.04
10	69.61
11	80.89
12	91.69
13	101.91
14	111.46
15	120.32
16	128.49
17	136.01
18	142.91
19	149.25
20	155.09
21	160.48
22	165.48
23	170.15
24	174.50
25	178.59
26	182.43
27	186.03
28	189.40
29	192.55
30	195.47
31	198.18
32	200.69
33	203.04
34	205.28
35	207.51

**APPENDIX II**

**CORRELATION CURVES**

## All Four Batches - Average Intensity (AL) Vs. Ultimate Stress

Rank 15 Eqn 8156 Power\_(a,b)  
 $r^2=0.21955853$  DF Adj  $r^2=0.20469298$  FitStdErr=1.1450445 Fstat=29.820564  
 $a=0.01895195$   
 $b=1.6646755$

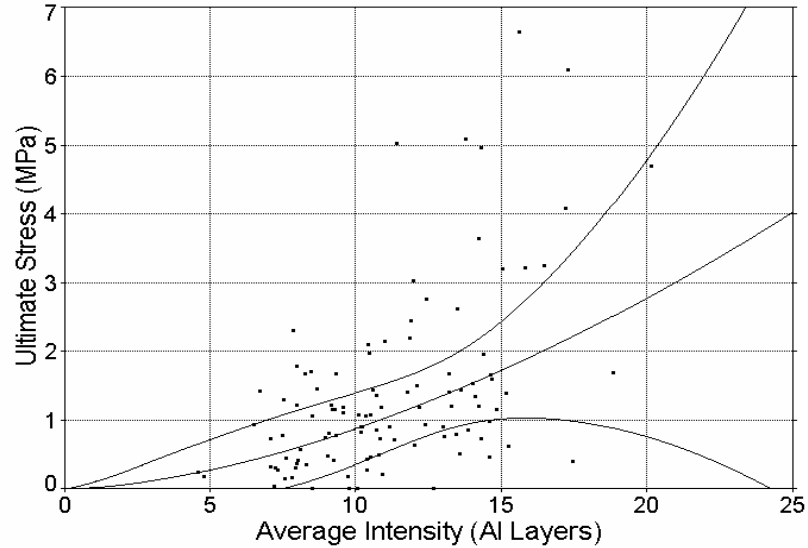


Fig A.1 Correlation Curve for all four batches – Power Law

## All Four Batches - Average Intensity (AL) Vs. Ultimate Stress

Rank 7 Eqn 1  $y=a+bx$   
 $r^2=0.28048481$  DF Adj  $r^2=0.26677976$  FitStdErr=1.0994416 Fstat=41.321422  
 $a=-1.103568$   
 $b=0.22247317$

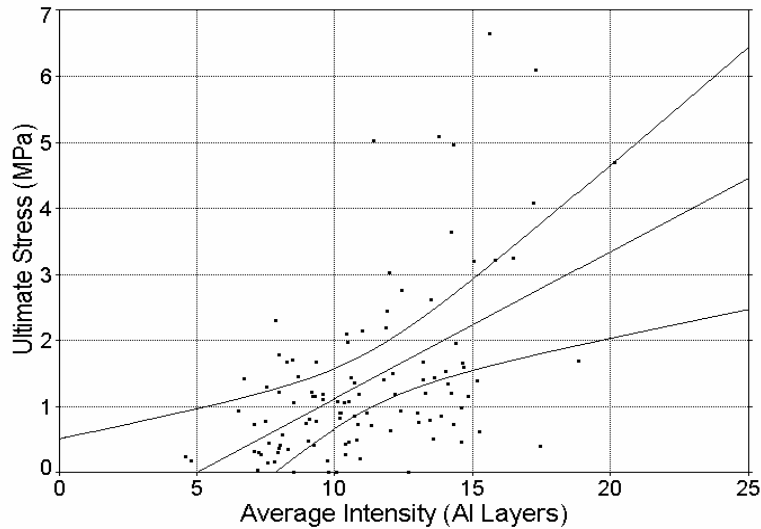


Fig A.2 Correlation Curve for all four batches – Linear Fit

First Batch - Average Intensity (AL Layers) Vs. Ultimate Stress (MPa)

Rank 7 Eqn 8156 Power\_(a,b)  
 $r^2=0.17084776$  DF Adj  $r^2=0.067203728$  FitStdErr=1.1731871 Fstat=3.5028693  
 $a=0.0030544857$   
 $b=2.3507168$

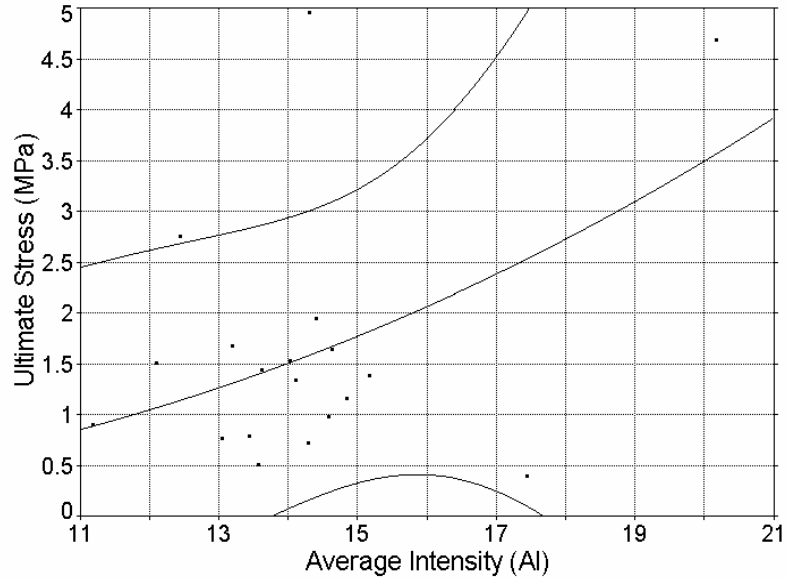


Fig A.3 Correlation Curve for the Batch I – Power Law

First Batch - Average Intensity (AL Layers) Vs. Ultimate Stress (MPa)

Rank 11 Eqn 1  $y=a+bx$   
 $r^2=0.14453147$  DF Adj  $r^2=0.037597906$  FitStdErr=1.1916595 Fstat=2.8721513  
 $a=-1.8452393$   
 $b=0.24462258$

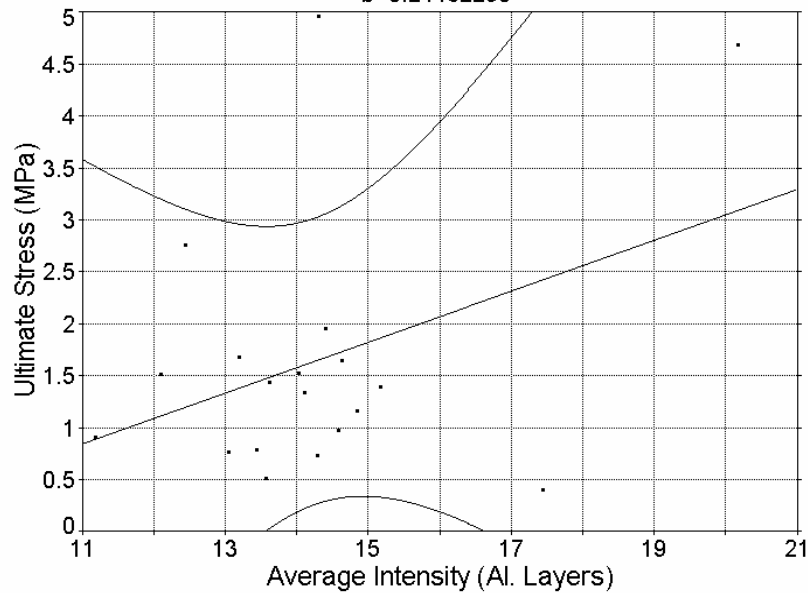


Fig A.4 Correlation Curve for the Batch I – Linear Fit

Last Three Batches - Average Intensity (AI Layers) Vs. Ultimate Stress (MPa)

Rank 3 Eqn 8156 Power\_(a,b)  
 $r^2=0.35434011$  DF Adj  $r^2=0.33932476$  FitStdErr=1.0493513 Fstat=47.745864  
 $a=0.0082857321$   
 $b=2.1198254$

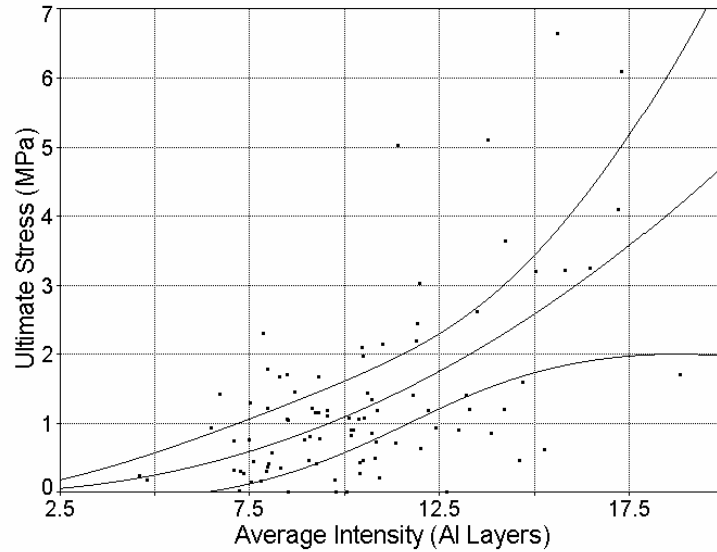


Fig A.5 Correlation Curve for the last three batches – Power Law

Last Three Batches - Average Intensity (AI Layers) Vs. Ultimate Stress (MPa)

Rank 8 Eqn 1  $y=a+bx$   
 $r^2=0.33521572$  DF Adj  $r^2=0.31975562$  FitStdErr=1.0647787 Fstat=43.86952  
 $a=1.4364947$   
 $b=0.26289747$

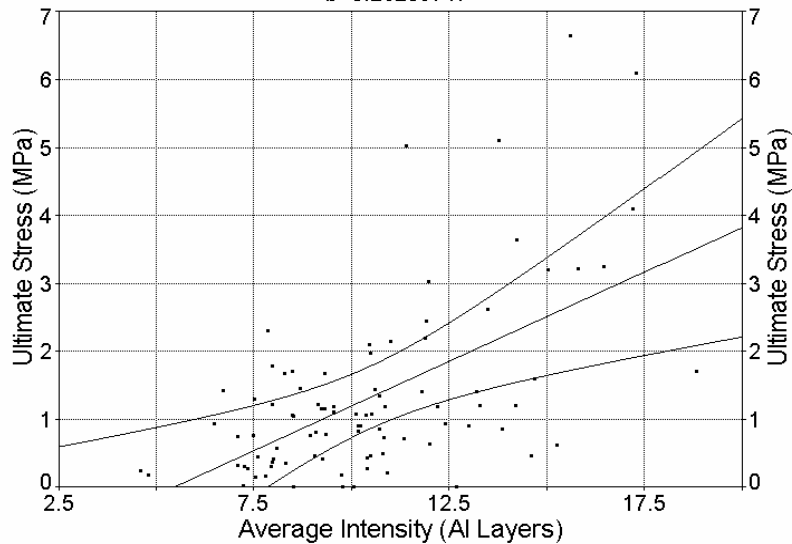


Fig A.6 Correlation Curve for the last three batches – Linear Fit

Summer Batch - Average Intensity(Al. Layer) Vs. Ultimate Stress

Eqn 8001 Power Law(a,b)

$r^2=0.32190365$  DF Adj  $r^2=0.28423163$  FitStdErr=1.3957132 Fstat=17.564518  
 $a=2.504451e-05$   
 $b=4.2116448$

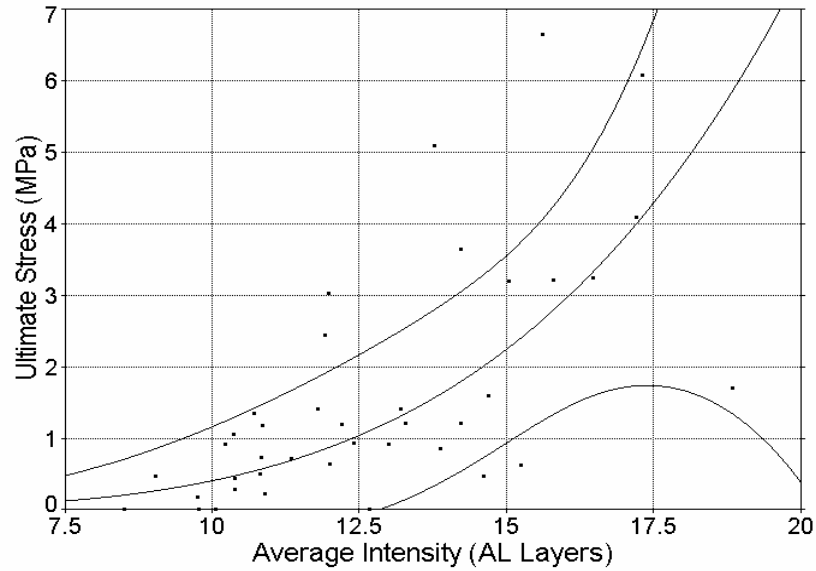


Fig A.7 Correlation Curve for the Batch II – Power Law  
 (Lorentzian Minimization Method)

Summer Batch - Average Intensity(Al. Layer) Vs. Ultimate Stress (MPa)

Rank 3 Eqn 1  $y=a+bx$

$r^2=0.41955569$  DF Adj  $r^2=0.38730879$  FitStdErr=1.2913108 Fstat=26.744272  
 $a=-3.8783691$   
 $b=0.43225717$

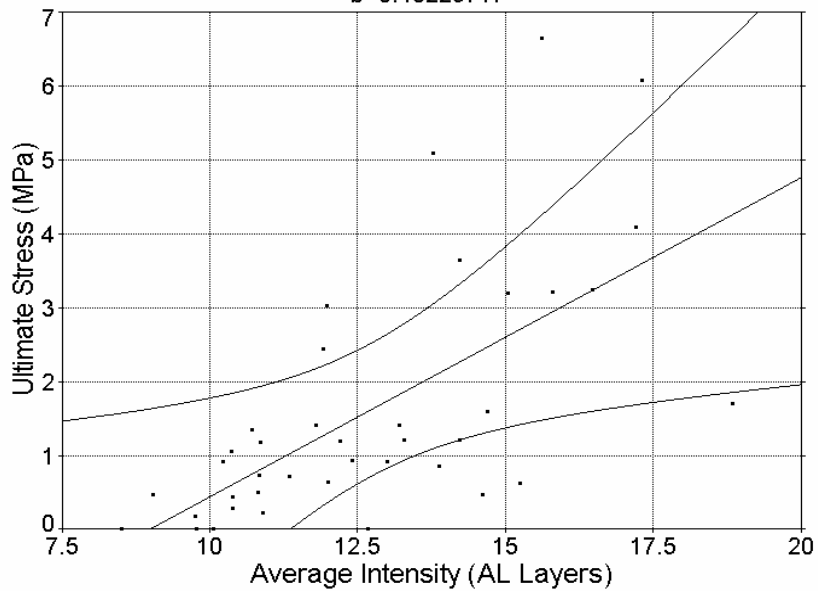


Fig A.8 Correlation Curve for the Batch II – Linear Fit



Last Two Batches - Average Intensity(Al. Layer) Vs. Ultimate Stress (MPa)

Rank 9 Eqn 1  $y=a+bx$   
 $r^2=0.33154734$  DF Adj  $r^2=0.30310254$  FitStdErr=0.70891001 Fstat=23.807628  
 $a=-1.4811925$   
 $b=0.29384797$

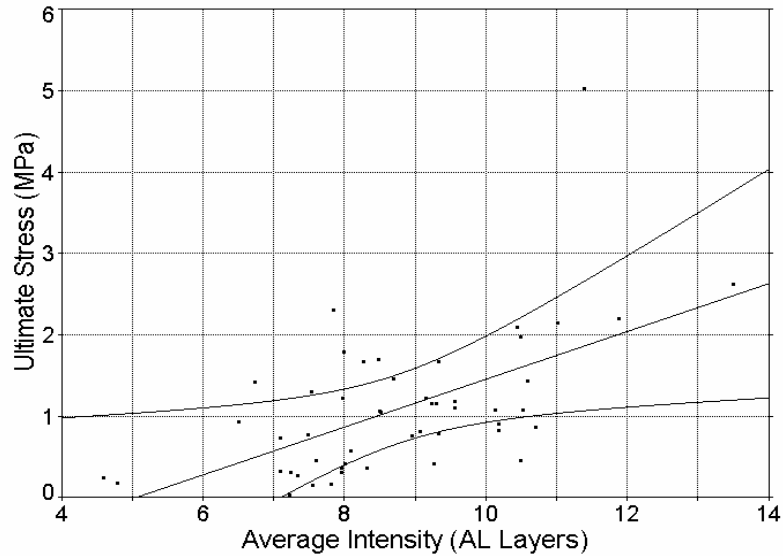


Fig A.9 Correlation Curve for the Last Two Batches – Linear Fit

Third Batch - Average Intensity(Al. Layer) Vs. Ultimate Stress (MPa)

Rank 16 Eqn 8001 Power Law(a,b)  
 $r^2=0.2126474$  DF Adj  $r^2=0.12516378$  FitStdErr=0.58509602 Fstat=5.131501  
 $a=0.042074379$   
 $b=1.5325321$

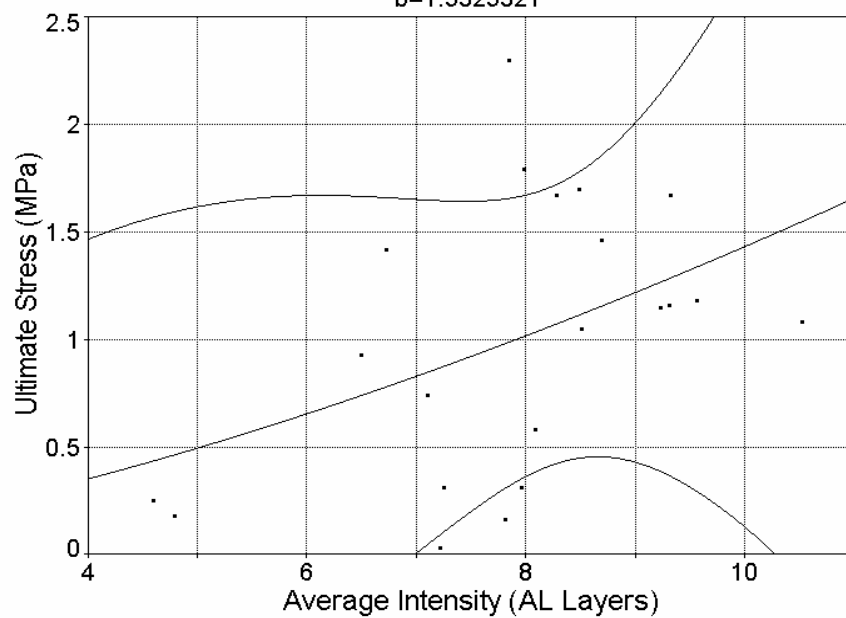


Fig A.10 Correlation Curve for the Batch III – Power Law

Third Batch - Average Intensity (Al. Layer) Vs. Ultimate Stress (MPa)

Rank 12 Eqn 1  $y=a+bx$   
 $r^2=0.22396444$  DF Adj  $r^2=0.13773826$  FitStdErr=0.58087586 Fstat=5.483414  
 $a=-0.64433704$   
 $b=0.20895542$

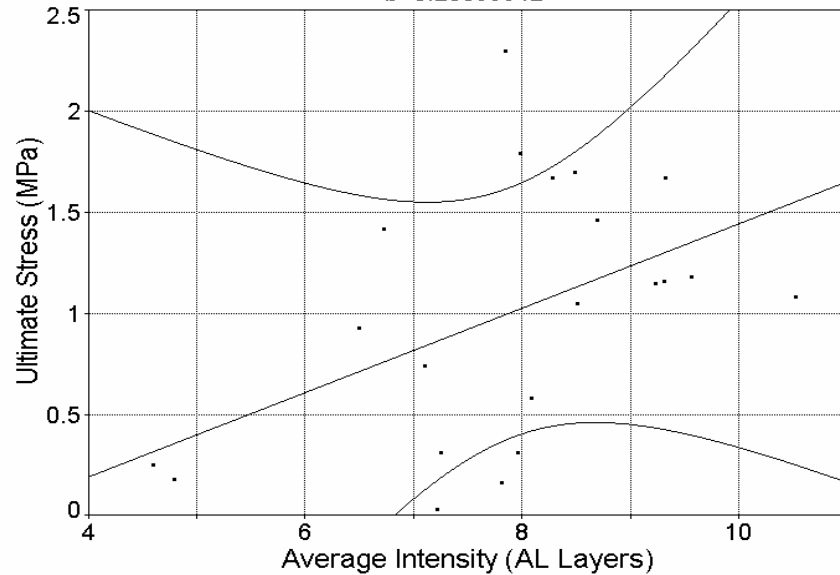


Fig A.11 Correlation Curve for the Batch III – Linear Fit

Fourth Batch - Average Intensity (AL) Vs. Ultimate Stress

Rank 14 Eqn 8156 Power\_(a,b)  
 $r^2=0.41829591$  DF Adj  $r^2=0.37354944$  FitStdErr=0.77061907 Fstat=19.415352  
 $a=0.0040311531$   
 $b=2.488525$

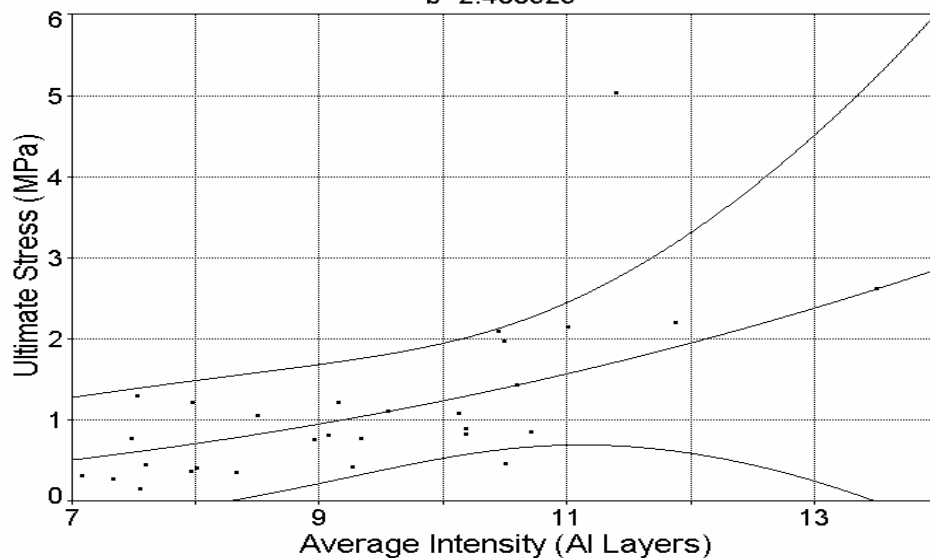


Fig A.12 Correlation Curve for the Batch IV – Power Law  
 (Least Absolute Deviation)

Fourth Batch - Average Intensity(Al. Layer) Vs. Ultimate Stress (MPa)

Rank 7 Eqn 1  $y=a+bx$   
 $r^2=0.44487538$  DF Adj  $r^2=0.40217348$  FitStdErr=0.75280751 Fstat=21.637727  
 $a=-2.7802999$   
 $b=0.41958978$

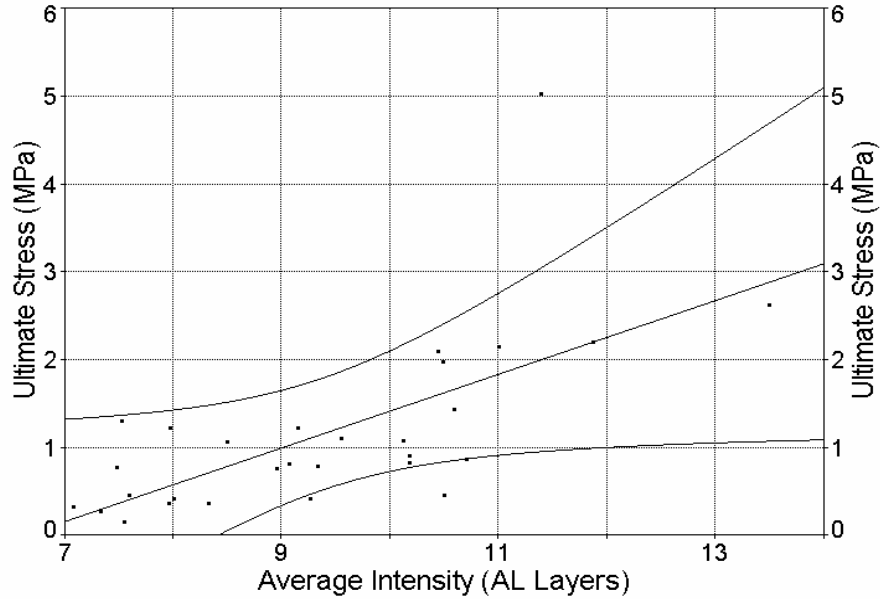


Fig A.13 Correlation Curve for the Batch IV – Linear Fit

All Four Batches - Average Intensity (AL) Vs. Elastic Modulus (MPa)

Rank 3 Eqn 8156 Power\_(a,b)  
 $r^2=0.2656726$  DF Adj  $r^2=0.25168541$  FitStdErr=53.427086 Fstat=38.349782  
 $a=0.64138075$   
 $b=1.8667931$

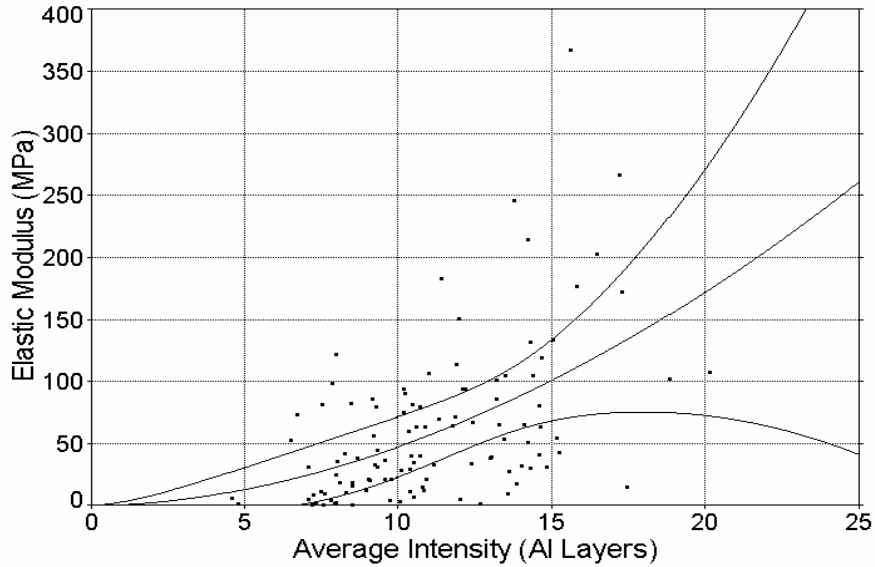


Fig A.14 Correlation Curve for all Batch IV – Power Law

## All Four Batches - Average Intensity (AL) Vs. Elastic Modulus (MPa)

Rank 5 Eqn 1  $y=a+bx$   
 $r^2=0.26361148$  DF Adj  $r^2=0.24958504$  FitStdErr=53.502013 Fstat=37.945754  
 $a=-54.623356$   
 $b=10.374557$

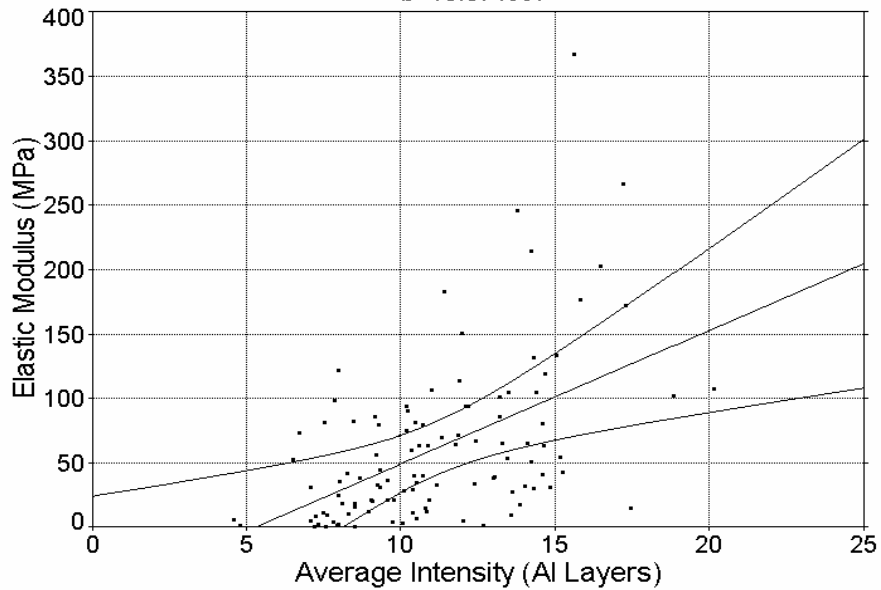


Fig A.15 Correlation Curve for all four batches – Linear Fit

## Initial Batch - Average Intensity (AL) Vs. Elastic Modulus (MPa)

Rank 11 Eqn 8001 Power Law(a,b)  
 $r^2=0.024557535$  DF Adj  $r^2=0$  FitStdErr=34.952447 Fstat=0.42798844  
 $a=8.6122317$   
 $b=0.72541077$

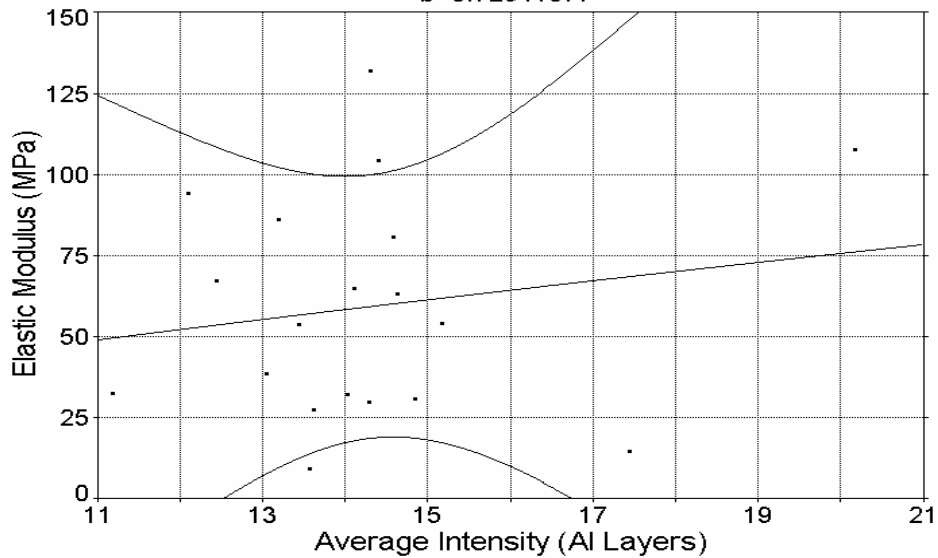


Fig A.16 Correlation Curve for the Batch I – Power Law

Initial Batch - Average Intensity (AL) Vs. Elastic Modulus (MPa)

Rank 8 Eqn 1  $y=a+bx$   
 $r^2=0.025894055$  DF Adj  $r^2=0$  FitStdErr=34.928494 Fstat=0.45190048  
 $a=18.574791$   
 $b=2.844081$

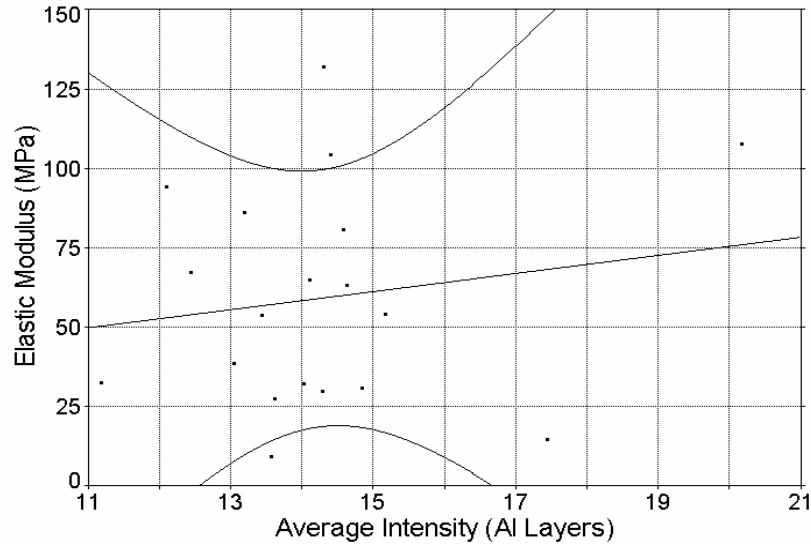


Fig A.17 Correlation Curve for the Batch I –Linear Fit

Last Three Batches- Average Intensity (AL) Vs. Elastic Modulus (MPa)

Rank 2 Eqn 8156 Power\_(a,b)  
 $r^2=0.40667521$  DF Adj  $r^2=0.39287695$  FitStdErr=51.616389 Fstat=59.631324  
 $a=0.19141572$   
 $b=2.4062261$

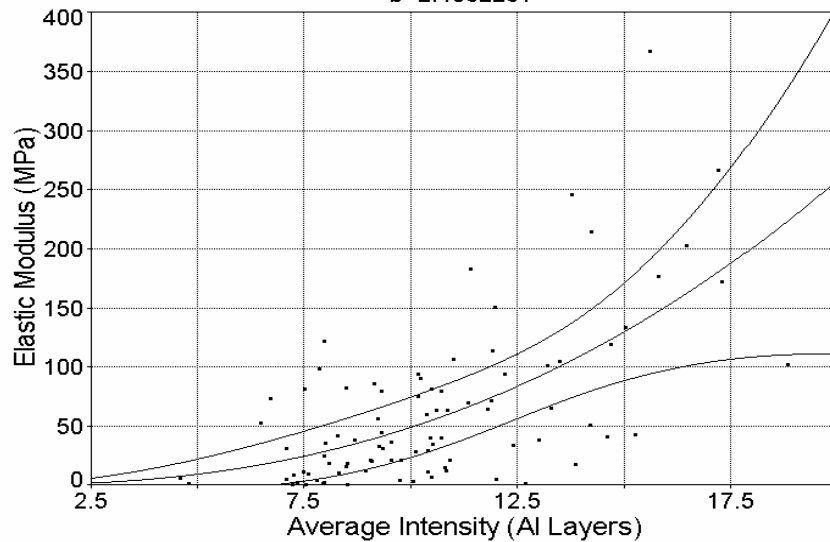


Fig A.18 Correlation Curve for the last three batches –Power Law

Last Three Batches- Average Intensity (AL) Vs. Elastic Modulus (MPa)

Rank 9 Eqn 1  $y=a+bx$   
 $r^2=0.38573549$  DF Adj  $r^2=0.37145027$  FitStdErr=52.519318 Fstat=54.632796  
 $a=-90.297763$   
 $b=14.470762$

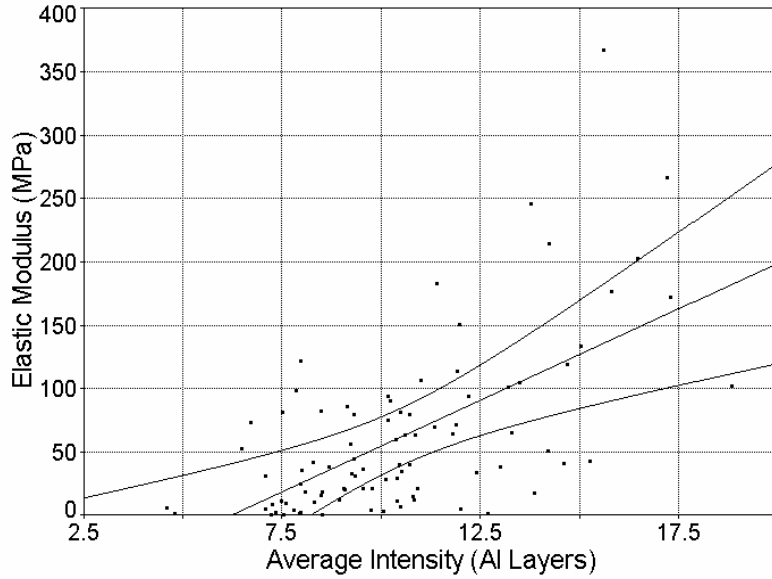


Fig A.19 Correlation Curve for the last three batches –Linear Fit

Summer Batch - Average Intensity (AL) Vs. Elastic Modulus (MPa)

Rank 18 Eqn 8001 Power Law(a,b)  
 $r^2=0.37396126$  DF Adj  $r^2=0.33918133$  FitStdErr=68.280953 Fstat=22.101774  
 $a=0.079336202$   
 $b=2.7211912$

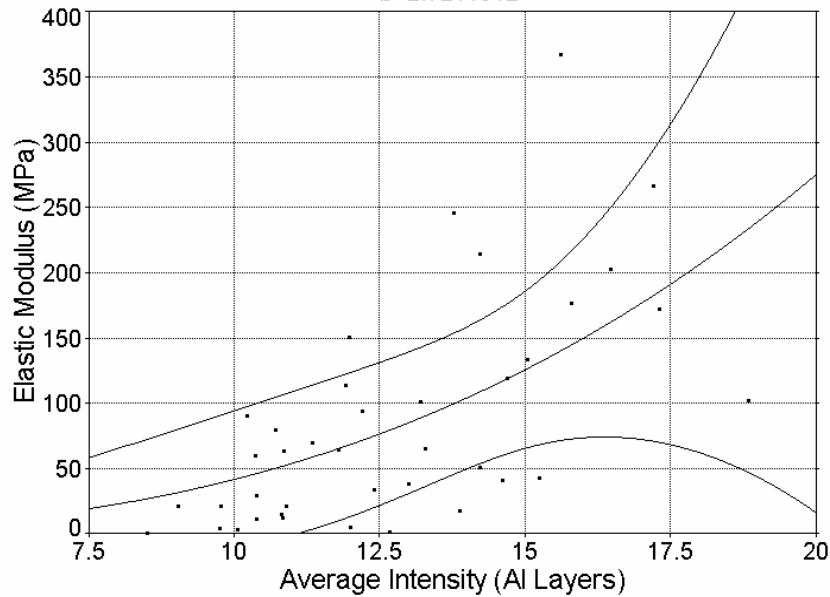


Fig A.20 Correlation Curve for the Batch II –Power Law

Summer Batch - Average Intensity (AL) Vs. Elastic Modulus (MPa)

Rank 5 Eqn 1  $y=a+bx$   
 $r^2=0.40001382$  DF Adj  $r^2=0.36668125$  FitStdErr=66.845103 Fstat=24.668087  
 $a=-187.85218$   
 $b=21.489849$

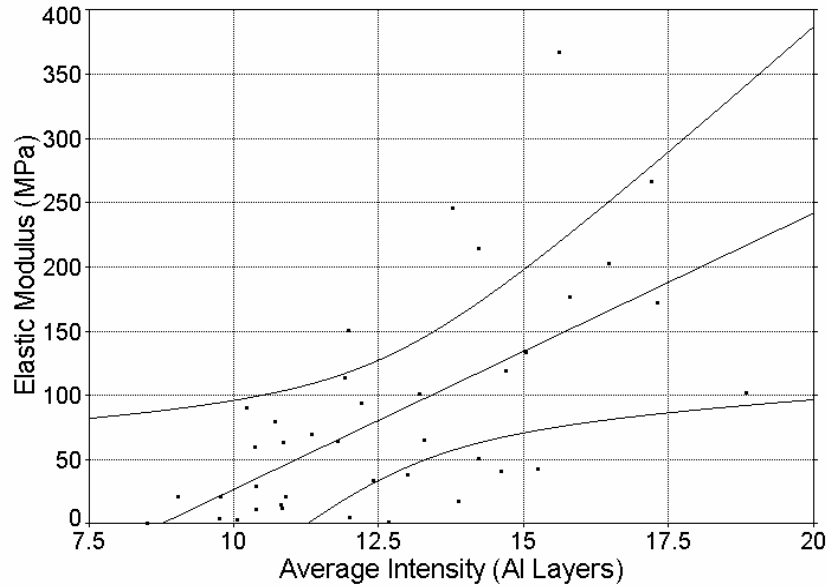


Fig A.21 Correlation Curve for the Batch II –Linear Fit

Last Two Batches- Average Intensity (AL) Vs. Elastic Modulus (MPa)

Rank 9 Eqn 1  $y=a+bx$   
 $r^2=0.24964399$  DF Adj  $r^2=0.21771394$  FitStdErr=34.445856 Fstat=15.969634  
 $a=-59.463043$   
 $b=11.693863$

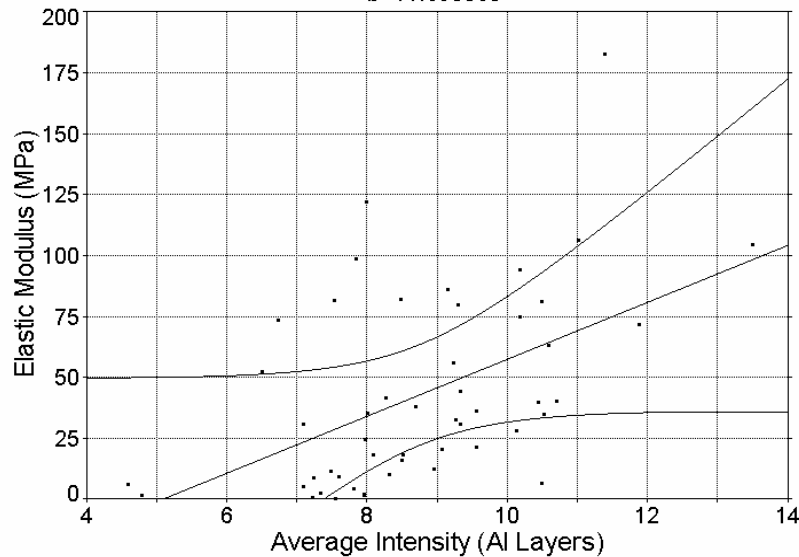


Fig A.22 Correlation Curve for the last two batches –Linear Fit

Third Batch - Average Intensity (AL) Vs. Elastic Modulus (MPa)

Rank 15 Eqn 8001 Power Law(a,b)  
 $r^2=0.08597983$  DF Adj  $r^2=0$  FitStdErr=34.029212 Fstat=1.7872874  
 $a=3.2067928$   
 $b=1.2275971$

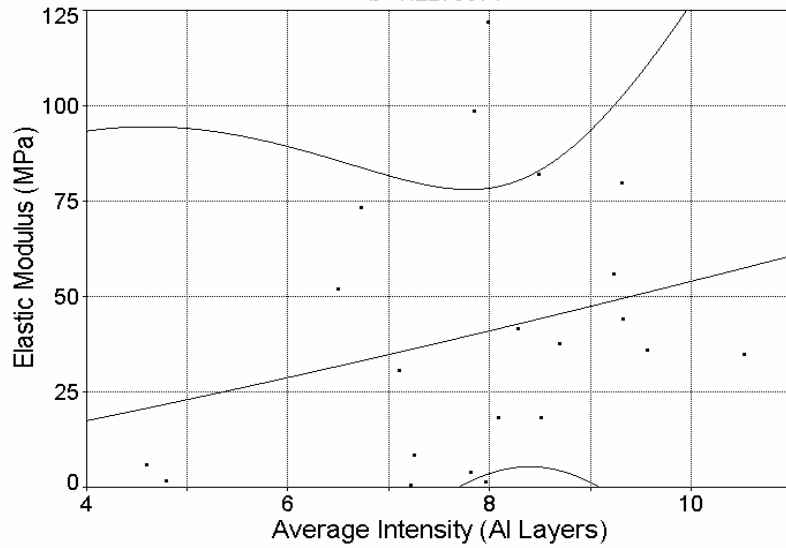


Fig A.23 Correlation Curve for the Batch III –Power Law

Third Batch - Average Intensity (AL) Vs. Elastic Modulus (MPa)

Rank 13 Eqn 1  $y=a+bx$   
 $r^2=0.090704543$  DF Adj  $r^2=0$  FitStdErr=33.941147 Fstat=1.8952985  
 $a=-16.221715$   
 $b=7.1781102$

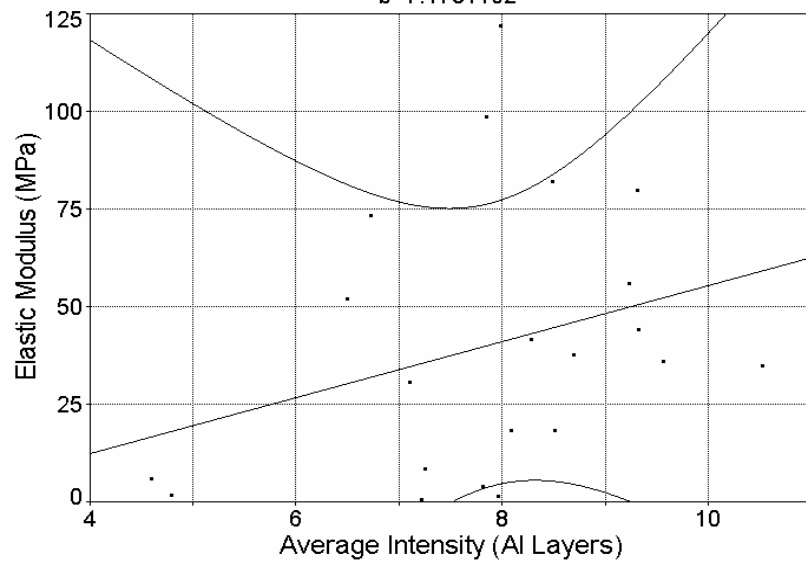


Fig A.24 Correlation Curve for the Batch III –Linear Fit



Fourth Batch - Average Intensity (AL) Vs. Elastic Modulus (MPa)

Rank 13 Eqn 8156 Power\_(a,b)  
 $r^2=0.41546248$  DF Adj  $r^2=0.37049805$  FitStdErr=33.428444 Fstat=19.190362  
 $a=0.029912624$   
 $b=3.2317986$

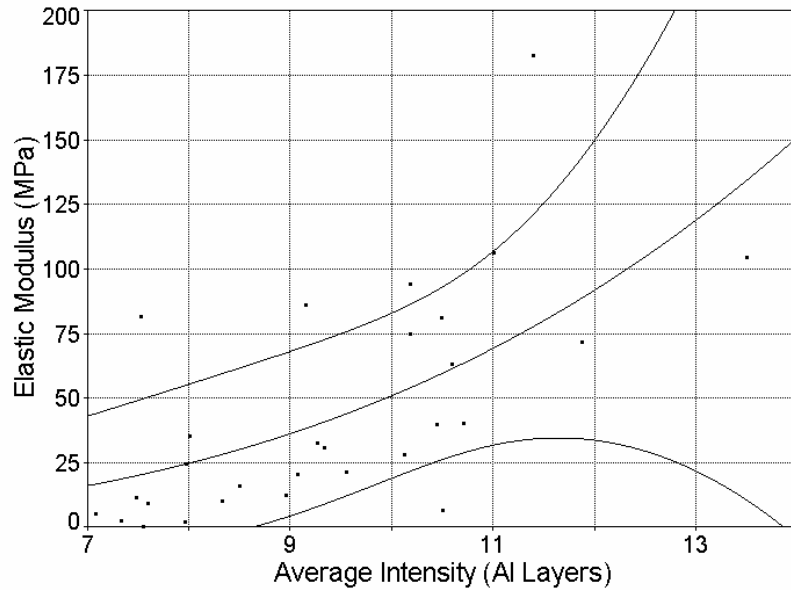


Fig A.25 Correlation Curve for the Batch IV –Power Law

Fourth Batch - Average Intensity (AL) Vs. Elastic Modulus (MPa)

Rank 5 Eqn 1  $y=a+bx$   
 $r^2=0.42829347$  DF Adj  $r^2=0.38431605$  FitStdErr=33.059519 Fstat=20.227028  
 $a=-122.32992$   
 $b=17.815487$

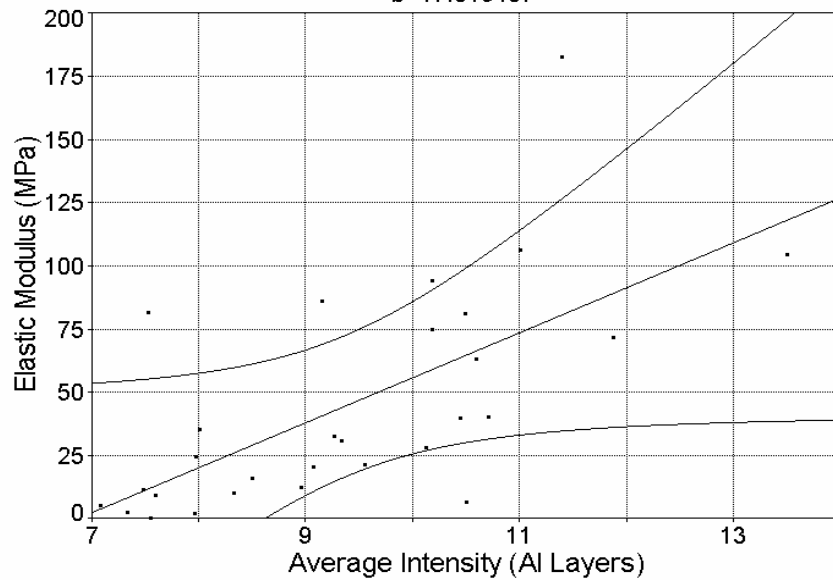


Fig A.26 Correlation Curve for the Batch IV –Linear Fit

All Four Batches - Trabecular Density pQCT Vs. Ultimate Stress (MPa)

Rank 22 Eqn 8156 Power\_(a,b)  
 $r^2=0.044957692$  DF Adj  $r^2=0.02676641$  FitStdErr=1.2670731 Fstat=4.9898474  
 $a=1.2272151e-05$   
 $b=2.1712468$

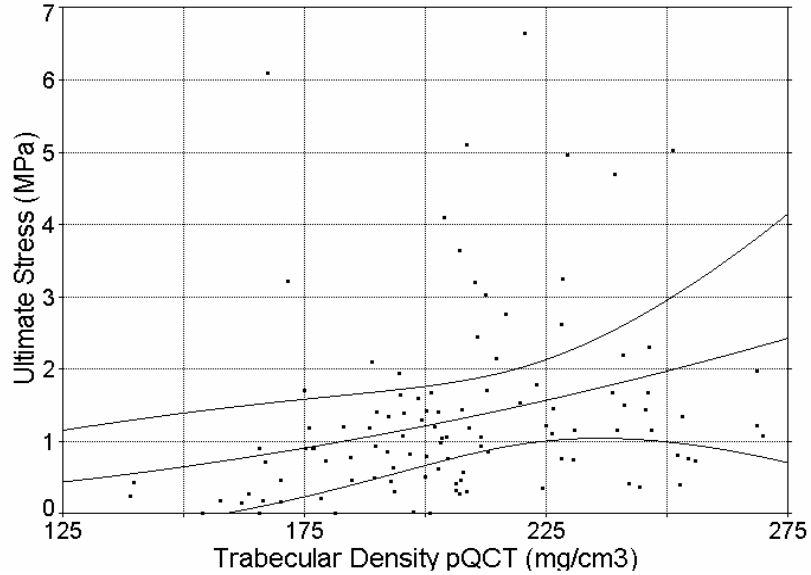


Fig A.27 Correlation Curve for all four batches –Power Law

All Four Batches - Trabecular Density pQCT Vs. Ultimate Stress (MPa)

Rank 13 Eqn 1  $y=a+bx$   
 $r^2=0.059236646$  DF Adj  $r^2=0.041317344$  FitStdErr=1.2575654 Fstat=6.6744569  
 $a=-0.89878556$   
 $b=0.01102496$

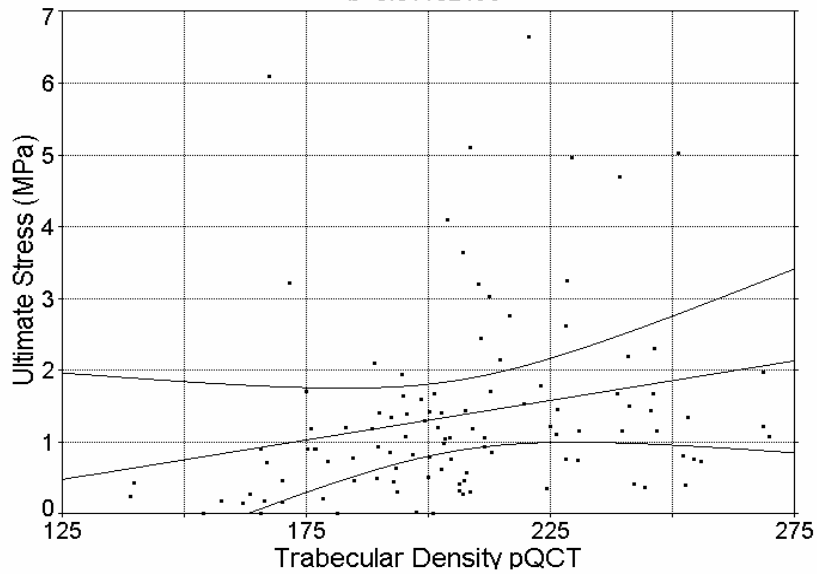


Fig A.28 Correlation Curve for all four batches –Linear Fit

Initial Batch - Trabecular Density pQCT Vs. Ultimate Stress (MPa)

Rank 11 Eqn 8001 Power Law(a,b)  
 $r^2=0.0062589443$  DF Adj  $r^2=0$  FitStdErr=1.28436 Fstat=0.10707221  
 $a=0.15378606$   
 $b=0.43781516$

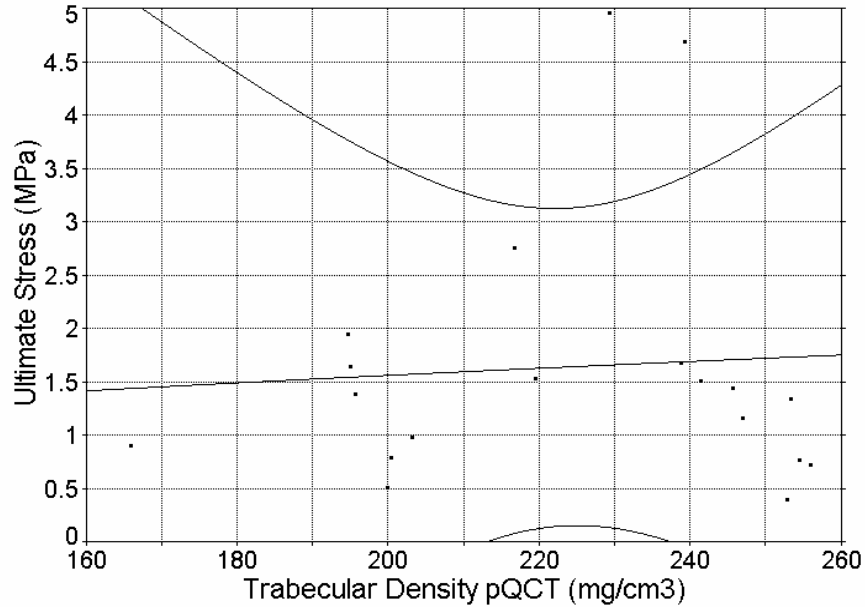


Fig A.29 Correlation Curve for the Batch I –Power Law

Initial Batch - Trabecular Density pQCT Vs. Ultimate Stress (MPa)

Rank 15 Eqn 1  $y=a+bx$   
 $r^2=0.0045643247$  DF Adj  $r^2=0$  FitStdErr=1.2854546 Fstat=0.077949305  
 $a=0.93401524$   
 $b=0.0031538736$

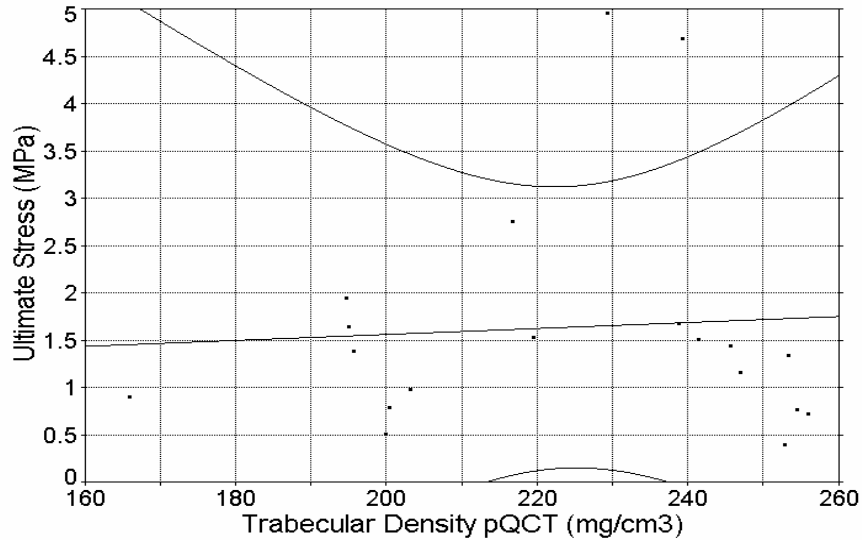


Fig A.30 Correlation Curve for the Batch I –Linear Fit

Last Three Batches- Trabecular Density pQCT Vs. Ultimate Stress (MPa)

Rank 16 Eqn 8001 Power Law(a,b)  
 $r^2=0.062785389$  DF Adj  $r^2=0.0409897$  FitStdErr=1.2642661 Fstat=5.8282583  
 $a=0.00018284634$   
 $b=1.6714798$

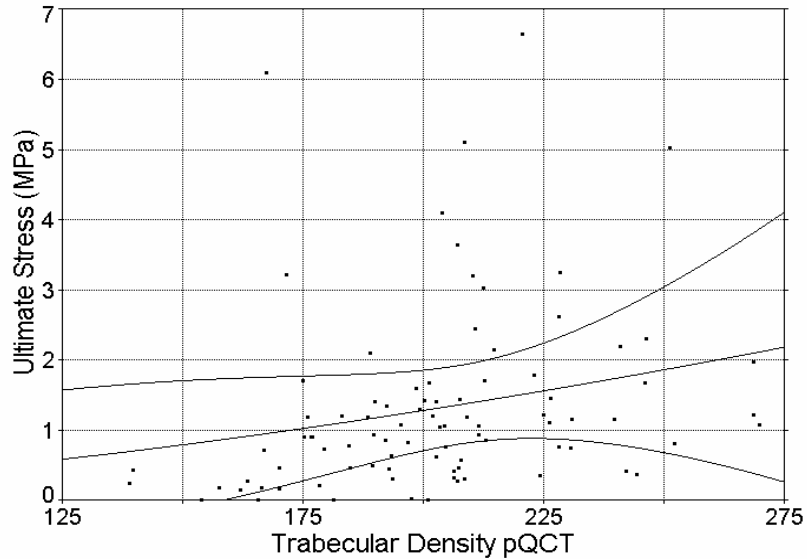


Fig A.31 Correlation Curve for the last three batches –Power Law

Last Three Batches- Trabecular Density pQCT Vs. Ultimate Stress (MPa)

Rank 13 Eqn 1  $y=a+bx$   
 $r^2=0.066256742$  DF Adj  $r^2=0.044541783$  FitStdErr=1.2619226 Fstat=6.1733636  
 $a=-1.1353306$   
 $b=0.012116168$

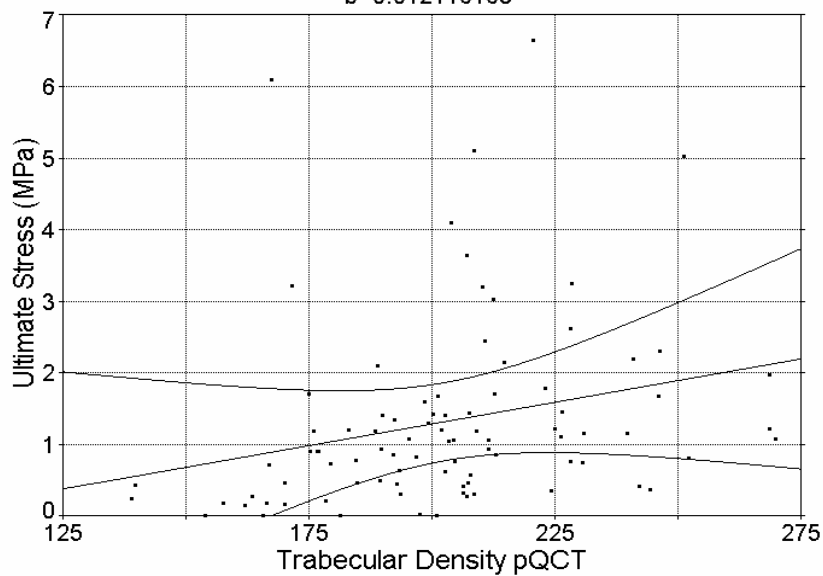


Fig A.32 Correlation Curve for the last three batches –Linear Fit

## Third Batch - Trabecular Density pQCT Vs. Ultimate Stress (MPa)

Rank 3 Eqn 8001 Power Law(a,b)  
 $r^2=0.31745195$  DF Adj  $r^2=0.24161327$  FitStdErr=0.54476492 Fstat=8.8368679  
 $a=1.3412358e-06$   
 $b=2.5403451$

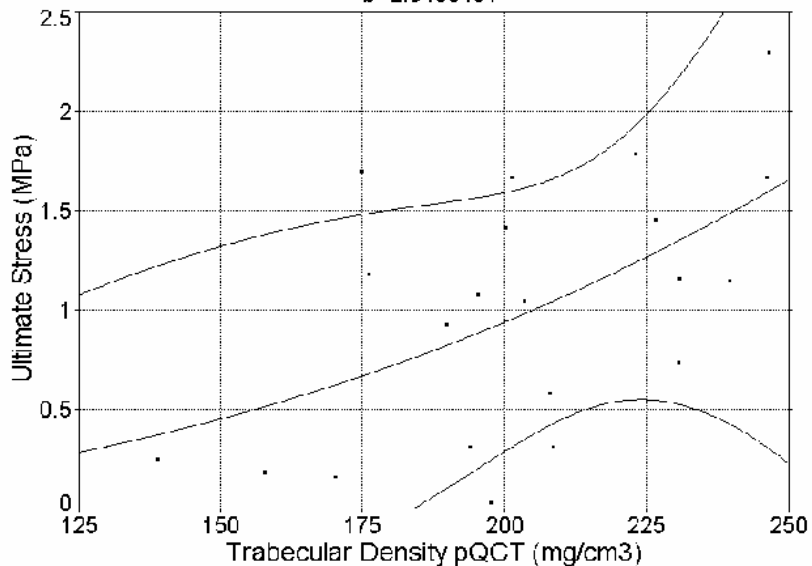


Fig A.33 Correlation Curve for the Batch II –Power Law

## Second Batch - Trabecular Density pQCT Vs. Ultimate Stress (MPa)

Rank 7 Eqn 1  $y=a+bx$   
 $r^2=0.16198165$  DF Adj  $r^2=0.11542508$  FitStdErr=1.551591 Fstat=7.1517779  
 $a=-4.9132502$   
 $b=0.034067861$

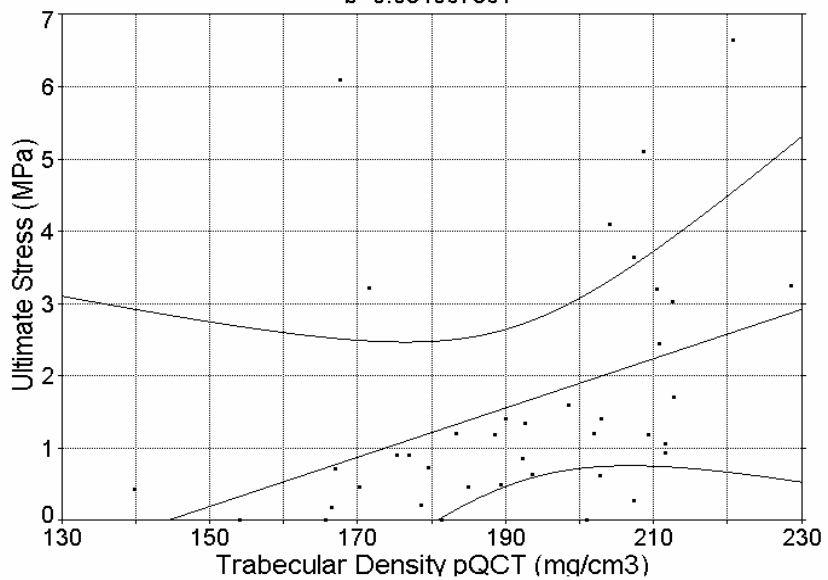


Fig A.34 Correlation Curve for the Batch II –Linear Fit

Last Two Batches - Trabecular Density pQCT Vs. Ultimate Stress (MPa)

Rank 2 Eqn 1  $y=a+bx$   
 $r^2=0.17940689$  DF Adj  $r^2=0.14448803$  FitStdErr=0.78545212 Fstat=10.494276  
 $a=-1.4824737$   
 $b=0.012179771$

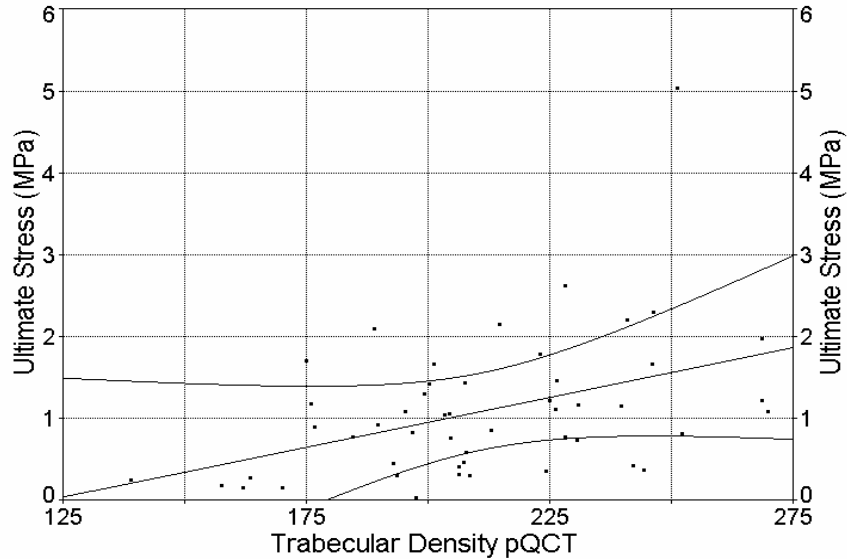


Fig A.35 Correlation Curve for the last two batches –Linear Fit

Third Batch - Trabecular Density pQCT Vs. Ultimate Stress (MPa)

Rank 8 Eqn 1  $y=a+bx$   
 $r^2=0.30942642$  DF Adj  $r^2=0.23269602$  FitStdErr=0.54795828 Fstat=8.5133606  
 $a=-1.5000806$   
 $b=0.01235077$

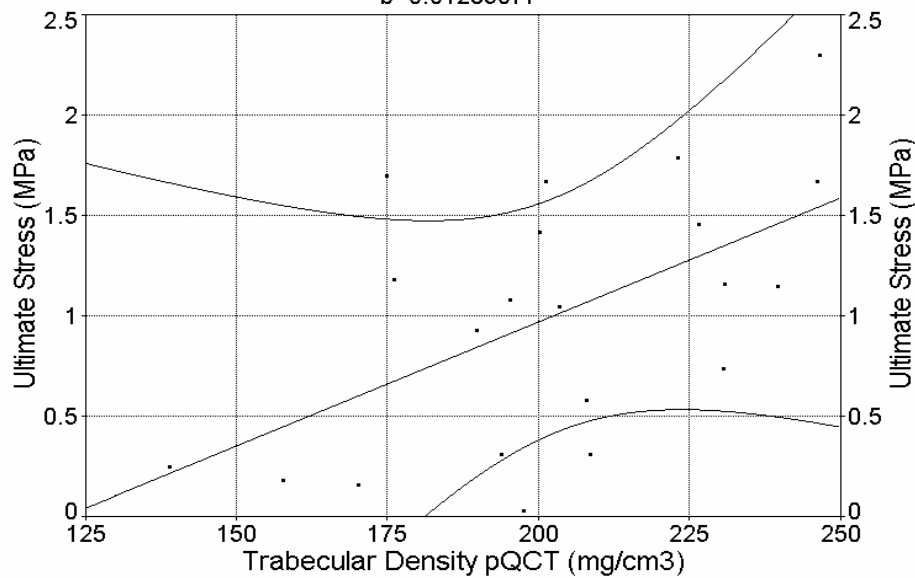


Fig A.36 Correlation Curve for the Batch III –Linear Fit

Fall Batch - Trabecular Density pQCT Vs. Ultimate Stress (MPa)

Rank 18 Eqn 8001 Power Law(a,b)

$r^2=0.12812162$  DF Adj  $r^2=0.061054049$  FitStdErr=0.94344514 Fstat=3.9676218

$a=8.5117196e-06$

$b=2.1920618$

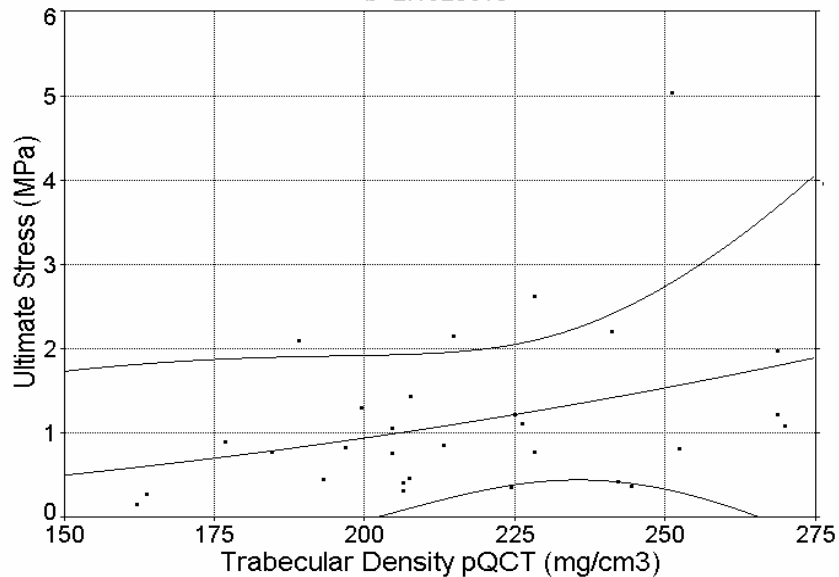


Fig A.37 Correlation Curve for the Batch IV –Power Law

Fourth Batch - Trabecular Density pQCT Vs. Ultimate Stress (MPa)

Rank 13 Eqn 1  $y=a+bx$

$r^2=0.13304486$  DF Adj  $r^2=0.066356004$  FitStdErr=0.94077769 Fstat=4.14348

$a=-1.5156028$

$b=0.012275267$

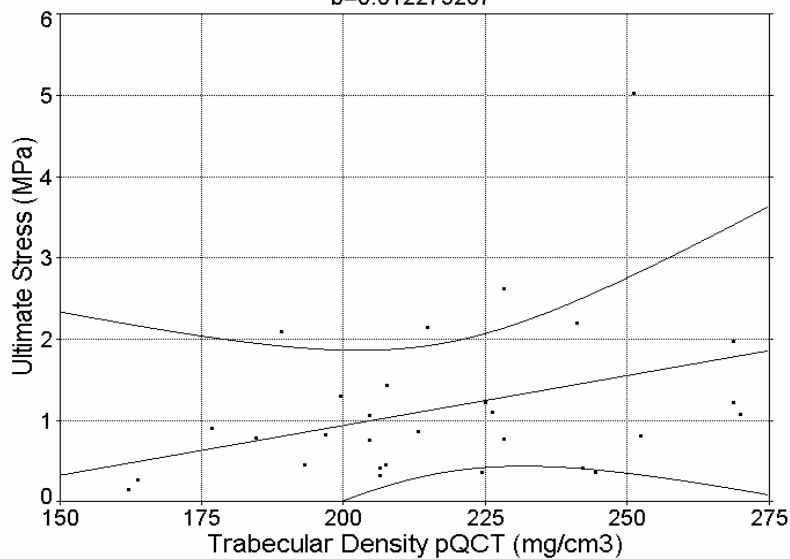


Fig A.38 Correlation Curve for the Batch IV –Linear Fit

## All Four Batches - Trabecular Density pQCT Vs. Elastic Modulus (MPa)

Rank 14 Eqn 8001 Power Law(a,b)  
 $r^2=0.021289233$  DF Adj  $r^2=0.0026471231$  FitStdErr=61.679921 Fstat=2.3057463  
 $a=0.36924837$   
 $b=0.95880127$

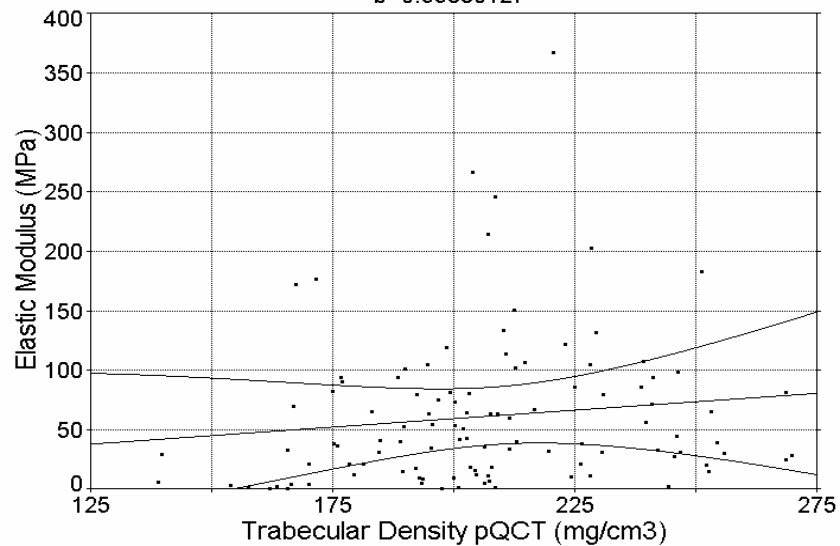


Fig A.39 Correlation Curve for all four batches –Power Law

## All Four Batches - Trabecular Density pQCT Vs. Elastic Modulus (MPa)

Rank 13 Eqn 1  $y=a+bx$   
 $r^2=0.021356821$  DF Adj  $r^2=0.0027159986$  FitStdErr=61.677791 Fstat=2.3132262  
 $a=-4.6694797$   
 $b=0.31832911$

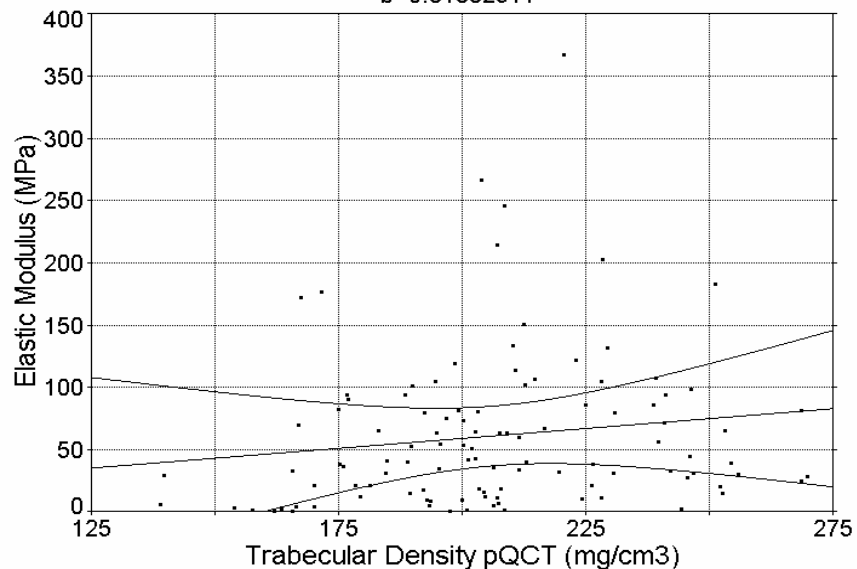


Fig A.40 Correlation Curve for all four batches –Linear Fit



Initial Batch - Trabecular Density pQCT Vs. Elastic Modulus (MPa)

Rank 17 Eqn 8001 Power Law(a,b)  
 $r^2=0.00022765139$  DF Adj  $r^2=0$  FitStdErr=35.385662 Fstat=0.0038709549  
 $a=75.807866$   
 $b=-0.046249724$

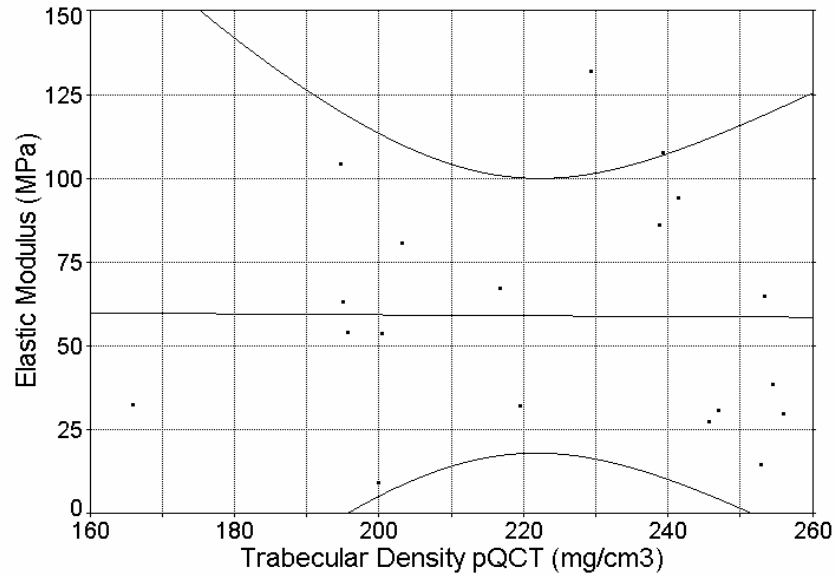


Fig A.41 Correlation Curve for the Batch I –Power Law

Initial Batch - Trabecular Density pQCT Vs. Elastic Modulus (MPa)

Rank 8 Eqn 1  $y=a+bx$   
 $r^2=0.0016488749$  DF Adj  $r^2=0$  FitStdErr=35.360501 Fstat=0.02807717  
 $a=70.736194$   
 $b=-0.052068669$

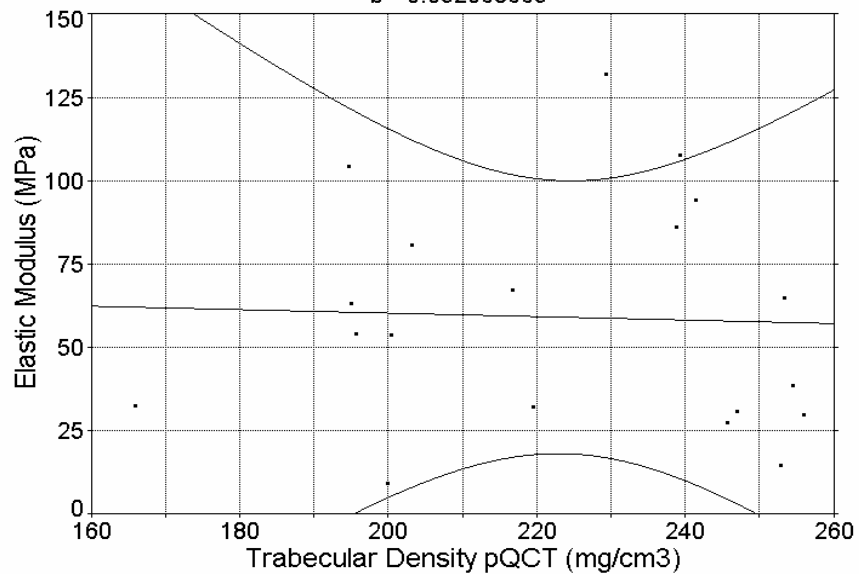


Fig A.42 Correlation Curve for the Batch I –Linear Fit

## Last Three Batches - Trabecular Density pQCT Vs. Elastic Modulus (MPa)

Rank 15 Eqn 8001 Power Law(a,b)  
 $r^2=0.030620198$  DF Adj  $r^2=0.0080764813$  FitStdErr=65.97636 Fstat=2.7481047  
 $a=0.082820816$   
 $b=1.2444191$

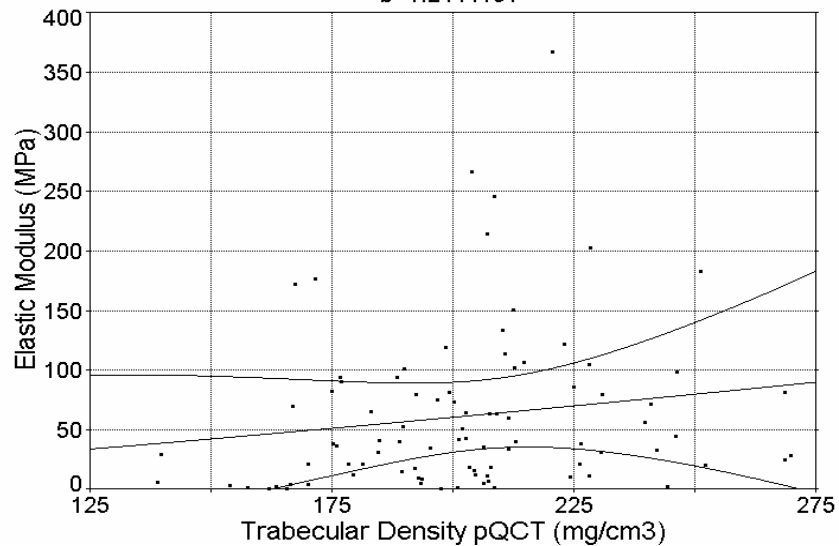


Fig A.43 Correlation Curve for the last three batches –Power Law

## Last Three Batches - Trabecular Density pQCT Vs. Elastic Modulus (MPa)

Rank 13 Eqn 1  $y=a+bx$   
 $r^2=0.032343317$  DF Adj  $r^2=0.0098396732$  FitStdErr=65.917696 Fstat=2.9079204  
 $a=-26.596735$   
 $b=0.4343751$

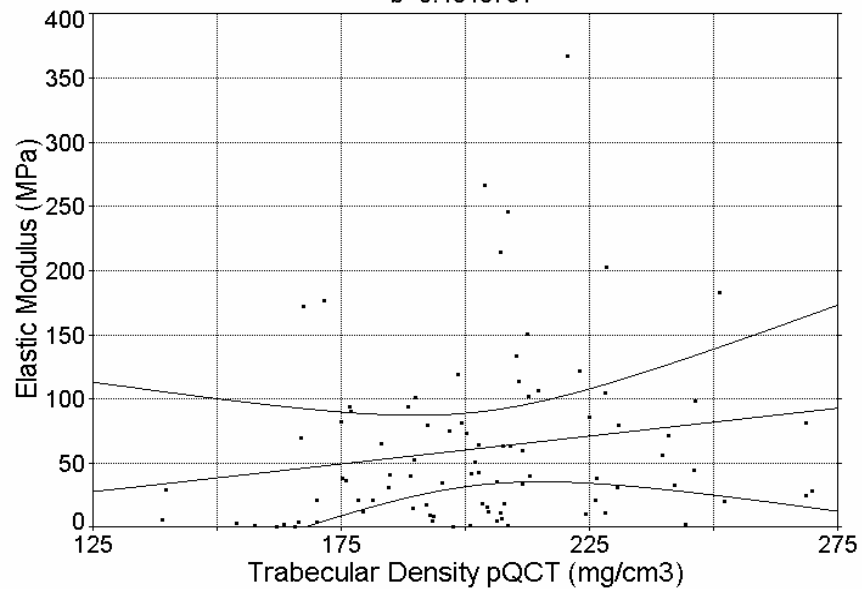


Fig A.44 Correlation Curve for the last three batches –Linear Fit

Summer Batch - Trabecular Density pQCT Vs. Elastic Modulus (MPa)

Rank 2 Eqn 8156 Power\_(a,b)  
 $r^2=0.27180083$  DF Adj  $r^2=0.23134532$  FitStdErr=73.641744 Fstat=13.810275  
 $a=9.7824745e-12$   
 $b=5.6465796$

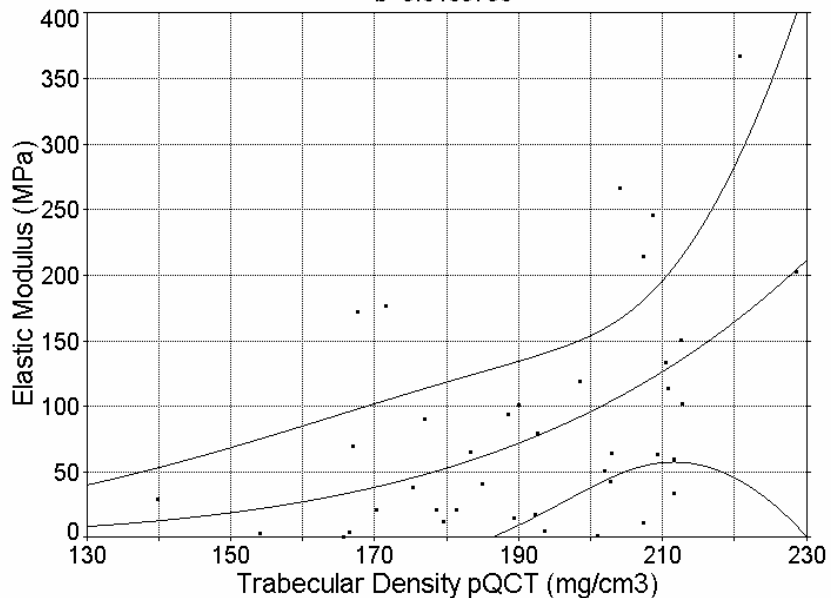


Fig A.45 Correlation Curve for the Batch II –Linear Fit

Summer Batch - Trabecular Density pQCT Vs. Elastic Modulus (MPa)

Rank 10 Eqn 1  $y=a+bx$   
 $r^2=0.21265972$  DF Adj  $r^2=0.16891859$  FitStdErr=76.573802 Fstat=9.9936581  
 $a=295.58793$   
 $b=1.9874813$

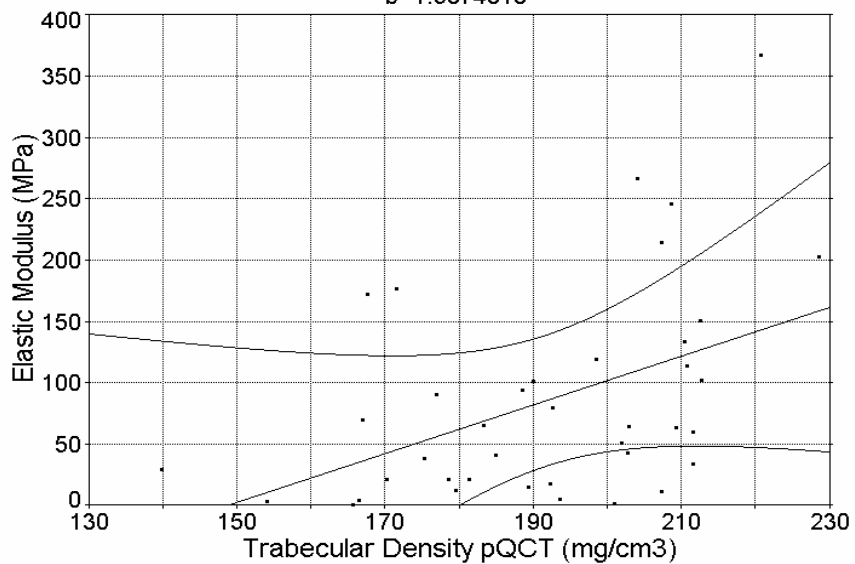


Fig A.46 Correlation Curve for the Batch II –Linear Fit

## Last Two Batches - Trabecular Density pQCT Vs. Elastic Modulus (MPa)

Rank 13 Eqn 1  $y=a+bx$   
 $r^2=0.096179527$  DF Adj  $r^2=0.057719081$  FitStdErr=37.804577 Fstat=5.1078919  
 $a=-43.517261$   
 $b=0.40898595$

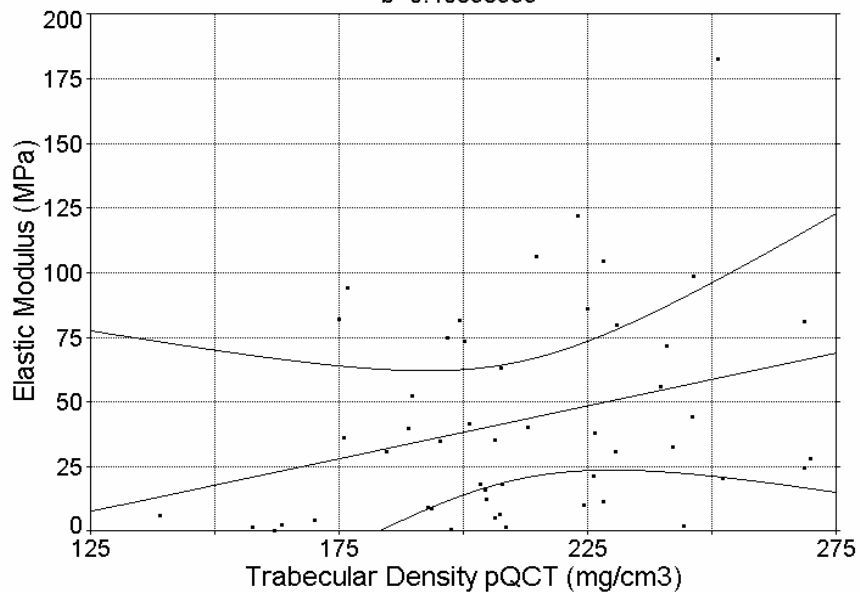


Fig A.47 Correlation Curve for the last two batches –Linear Fit

## Third Batch - Trabecular Density pQCT Vs. Elastic Modulus (MPa)

Rank 7 Eqn 1  $y=a+bx$   
 $r^2=0.23550928$  DF Adj  $r^2=0.15056586$  FitStdErr=31.121471 Fstat=5.8531466  
 $a=-77.544089$   
 $b=0.58163542$

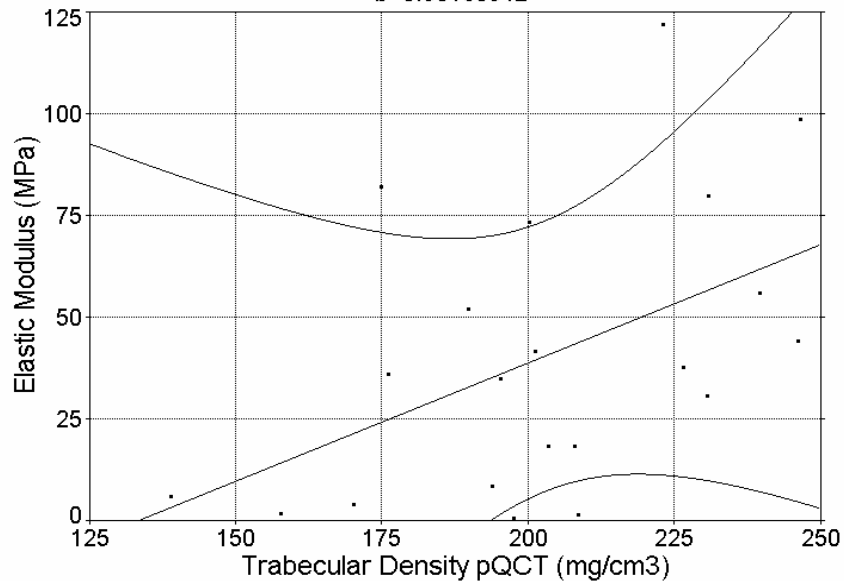


Fig A.48 Correlation Curve for the Batch III –Linear Fit

## Fall Batch - Trabecular Density pQCT Vs. Elastic Modulus (MPa)

Rank 16 Eqn 8001 Power Law(a,b)  
 $r^2=0.041749402$  DF Adj  $r^2=0$  FitStdErr=42.800566 Fstat=1.1763456  
 $a=0.029981881$   
 $b=1.3572109$

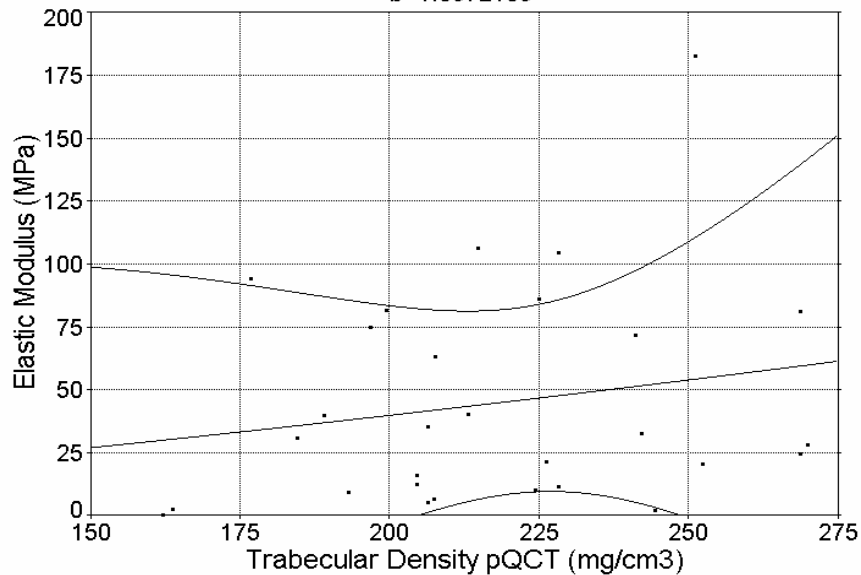


Fig A.49 Correlation Curve for the Batch IV –Power Law

## Fall Batch - Trabecular Density pQCT Vs. Elastic Modulus (MPa)

Rank 14 Eqn 1  $y=a+bx$   
 $r^2=0.043176436$  DF Adj  $r^2=0$  FitStdErr=42.768684 Fstat=1.2183686  
 $a=-21.120608$   
 $b=0.30260532$

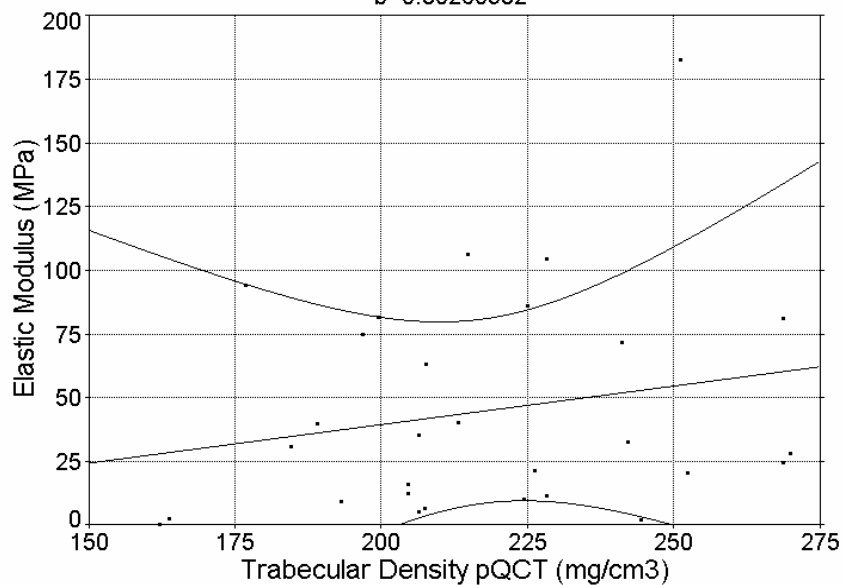


Fig A.50 Correlation Curve for the Batch IV –Linear Fit

Last Two Batches - Average Intensity (AI Layers) Vs. Ultimate Stress (MPa)

Rank 6 Eqn 1  $y=a+bx$   
 $r^2=0.37034604$  DF Adj  $r^2=0.34355225$  FitStdErr=0.68764951 Fstat=28.232348  
 $a=-0.86852206$   
 $b=0.30813554$

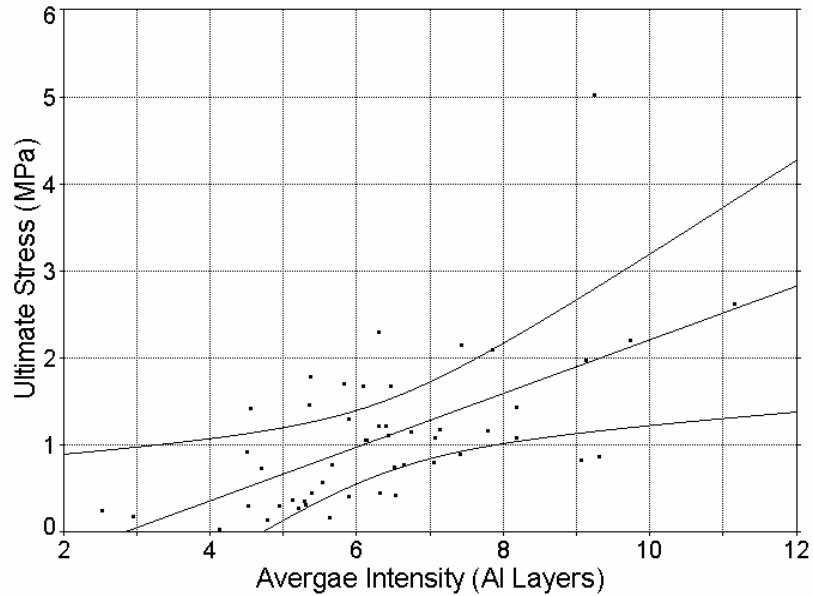


Fig A.51 Correlation Curve for the last two batches –Linear Fit

Third Batch - Average Intensity (AI Layers) Vs. Ultimate Stress (MPa)

Rank 13 Eqn 8001 Power Law(a,b)  
 $r^2=0.27386661$  DF Adj  $r^2=0.19318513$  FitStdErr=0.56278092 Fstat=7.1659915  
 $a=0.13836535$   
 $b=1.1668079$

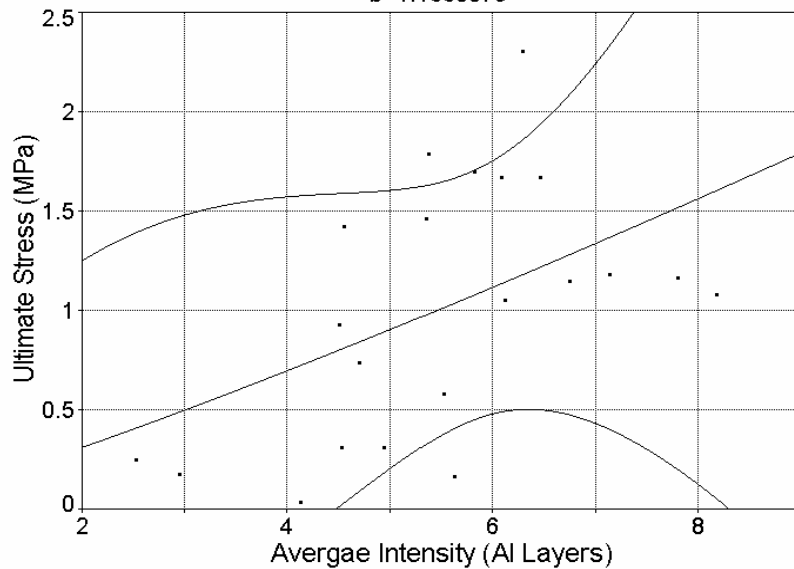


Fig A.52 Correlation Curve for the Batch III –Power Law

## Third Batch - Average Intensity (Al Layers) Vs. Ultimate Stress (MPa)

Rank 11 Eqn 1  $y=a+bx$   
 $r^2=0.28523279$  DF Adj  $r^2=0.20581421$  FitStdErr=0.55835894 Fstat=7.582081  
 $a=-0.32761602$   
 $b=0.24270192$

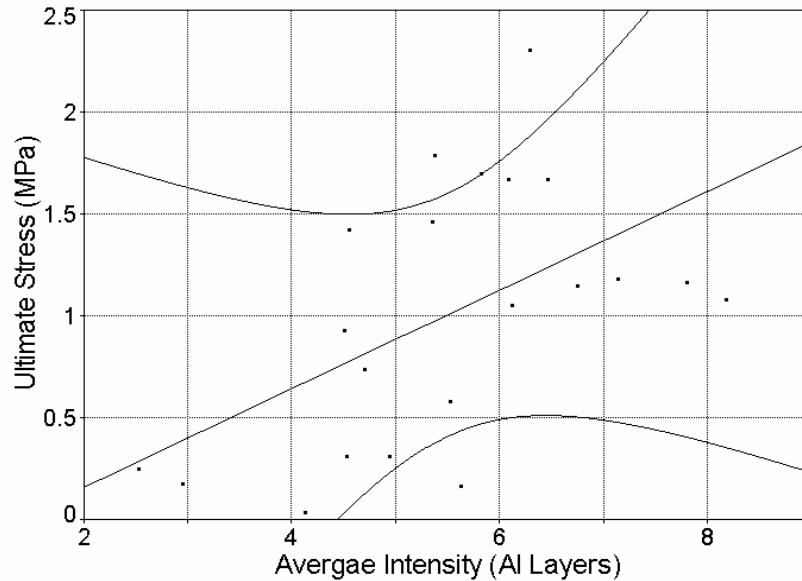


Fig A.53 Correlation Curve for the Batch III –Linear Fit

## Fourth Batch - Average Intensity (Al Layers) Vs. Ultimate Stress (MPa)

Rank 15 Eqn 8156 Power\_(a,b)  
 $r^2=0.45367102$  DF Adj  $r^2=0.41164571$  FitStdErr=0.74596895 Fstat=22.420772  
 $a=0.014678019$   
 $b=2.2172555$

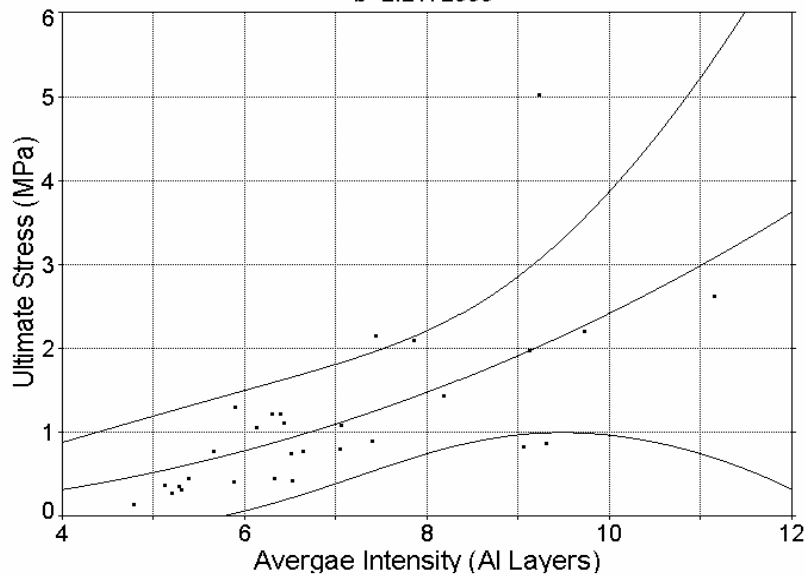


Fig A.54 Correlation Curve for the Batch IV –Power Law

Fourth Batch - Average Intensity (Al Layers) Vs. Ultimate Stress (MPa)

Rank 7 Eqn 1  $y=a+bx$   
 $r^2=0.47345164$  DF Adj  $r^2=0.43294792$  FitStdErr=0.73234002 Fstat=24.277341  
 $a=-1.78632$   
 $b=0.42075675$

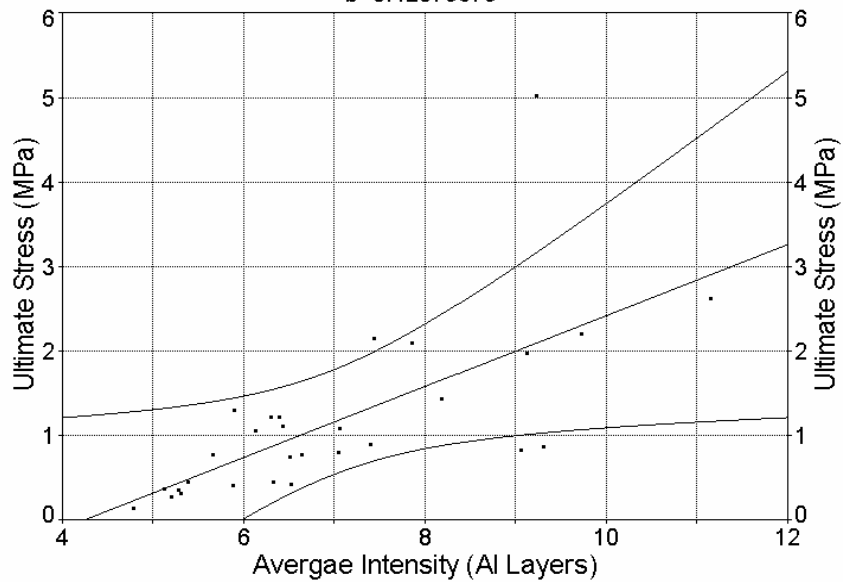


Fig A.55 Correlation Curve for the Batch IV –Linear Fit

Last Two Batches - Average Intensity (Al Layers) Vs. Elastic Modulus (MPa)

Rank 7 Eqn 1  $y=a+bx$   
 $r^2=0.31252347$  DF Adj  $r^2=0.28326914$  FitStdErr=32.970597 Fstat=21.820565  
 $a=-39.715216$   
 $b=12.988559$

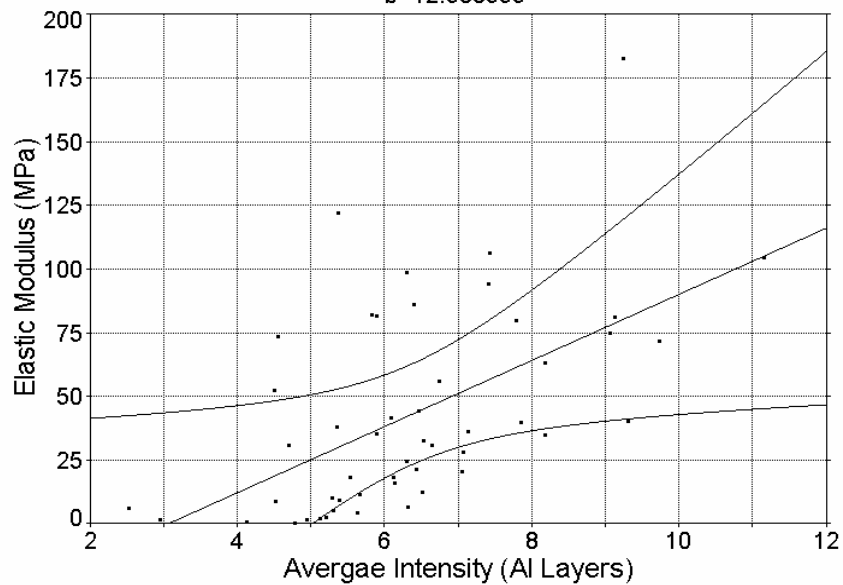


Fig A.56 Correlation Curve for the last two batches –Linear Fit



## Third Batch - Average Intensity (AI Layers) Vs. Elastic Modulus (MPa)

Rank 13 Eqn 8156 Power\_(a,b)  
 $r^2=0.15628803$  DF Adj  $r^2=0.06254225$  FitStdErr=32.693898 Fstat=3.5195334  
 $a=5.3953671$   
 $b=1.1842767$

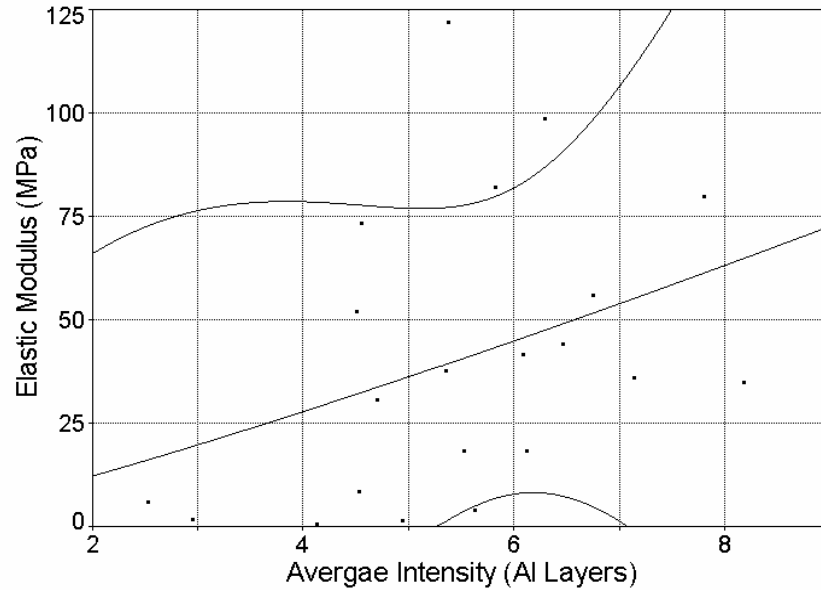


Fig A.57 Correlation Curve for the Batch III –Power Law

## Third Batch - Average Intensity (AI Layers) Vs. Elastic Modulus (MPa)

Rank 12 Eqn 1  $y=a+bx$   
 $r^2=0.16312945$  DF Adj  $r^2=0.070143836$  FitStdErr=32.561075 Fstat=3.7036309  
 $a=-13.918935$   
 $b=9.8918634$

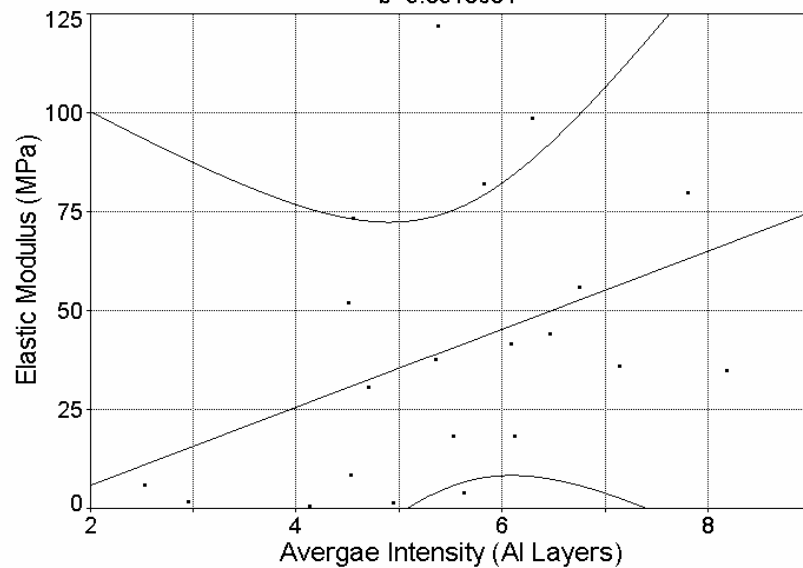


Fig A.58 Correlation Curve for the Batch III –Linear Fit

## Fourth Batch - Average Intensity (AI Layers) Vs. Elastic Modulus (MPa)

Rank 18 Eqn 8156 Power\_(a,b)  
 $r^2=0.44526341$  DF Adj  $r^2=0.40259136$  FitStdErr=32.564745 Fstat=21.671749  
 $a=0.44013591$   
 $b=2.3492275$

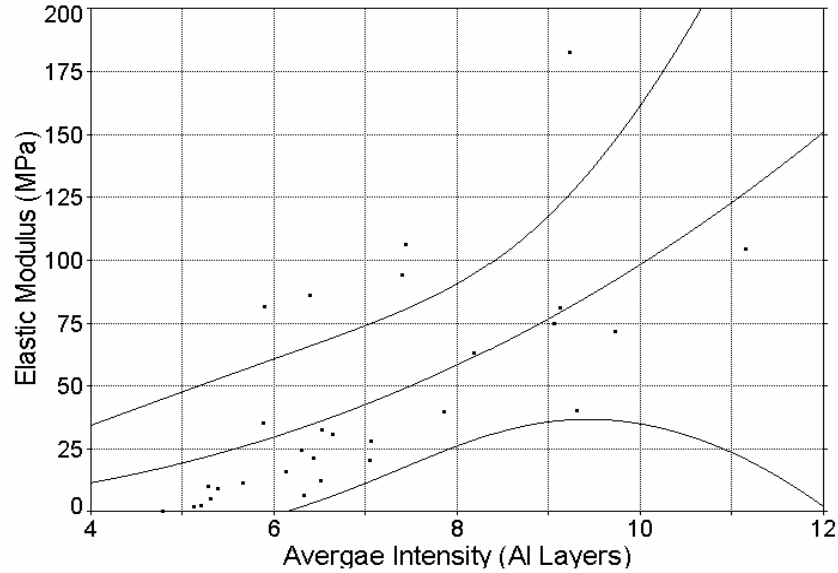


Fig A.59 Correlation Curve for the Batch IV –Power Law

## Fourth Batch - Average Intensity (AI Layers) Vs. Elastic Modulus (MPa)

Rank 10 Eqn 1  $y=a+bx$   
 $r^2=0.48254278$  DF Adj  $r^2=0.44273837$  FitStdErr=31.45151 Fstat=25.178226  
 $a=-83.879328$   
 $b=18.402288$

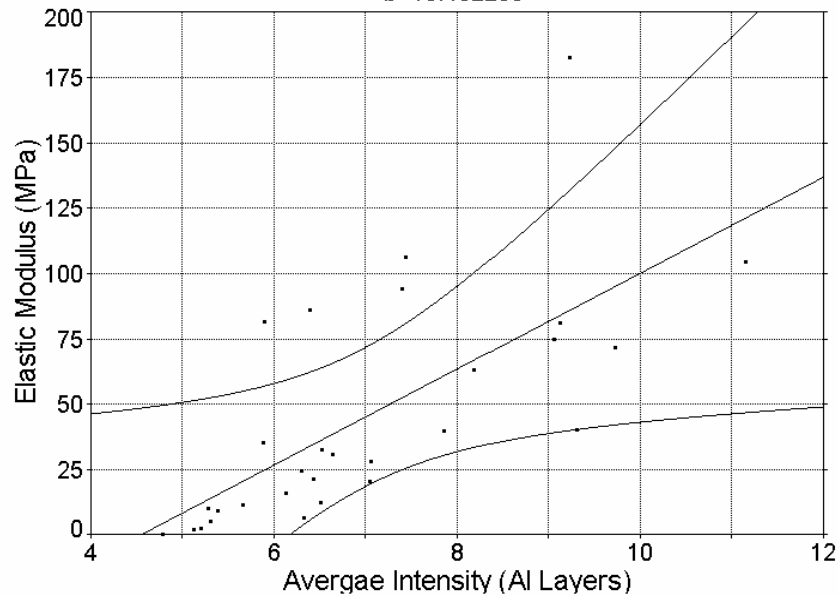


Fig A.60 Correlation Curve for the Batch IV –Linear Fit

## VITA

Ramya Ramaswamy was born in Tamil Nadu, India on May 24 1979 to Ramaswamy and Shantha. Ramya spent her entire childhood in Coimbatore and attended Avila Convent Matriculation Higher Secondary School, from which she graduated in May of 1996. Ramya studied mechanical engineering at Sri Ramakrishna Engineering College as an undergraduate and received her B.E in May of 2000. Ramya began her graduate studies at Texas A&M University in the Fall of 2000. She joined Dr. Hogan and his team of “bone-breakers” in the Fall of 2001. In December 2003, Ramya received her M.S. in mechanical engineering. At this point, she hopes to find gainful employment in the field of mechanical engineering. Ramya’s future goals include getting her M.B.A. from a reputable university and helping her father in his business in India. Ramya’s permanent address is as follows:

Ramya Ramaswamy  
28 Bharathi Park First Cross  
Coimbatore – 641011  
Tamil Nadu, India  
(979) 575-1211  
ramya\_ramaswamy@hotmail.com